THERMAL ENHANCEMENT IN A MICROCHANNEL HEAT SINK USING PASSIVE METHODS

NAVIN RAJA KUPPUSAMY

FACULTY OF ENGINEERING
UNIVERSITY OF MALAYA
KUALA LUMPUR

2016

THERMAL ENHANCEMENT IN A MICROCHANNEL HEAT SINK USING PASSIVE METHODS

NAVIN RAJA KUPPUSAMY

THESIS SUBMITTED IN FULFILMENT OF THE REQUIREMENTS FOR THE DEGREE OF DOCTOR OF PHILOSOPHY

FACULTY OF ENGINEERING
UNIVERSITY OF MALAYA
KUALA LUMPUR

2016

UNIVERSITY OF MALAYA

ORIGINAL LITERARY WORK DECLARATION

Name of Candidate: **Navin Raja Kuppusamy**

Registration/Matric No: **KHA 130114**

Name of Degree: **Doctor of Philosophy**

Title of Project Paper/Research Report/Dissertation/Thesis ("this Work"):

Thermal Enhancement in a Micro Channel Heat Sink Using Passive Methods

Field of Study:

Heat Transfer

I do solemnly and sincerely declare that:

(1) I am the sole author/writer of this Work;
(2) This Work is original;
(3) Any use of any work in which copyright exists was done by way of fair dealing and for permitted purposes and any excerpt or extract from, or reference to or reproduction of any copyright work has been disclosed expressly and sufficiently and the title of the Work and its authorship have been acknowledged in this Work;
(4) I do not have any actual knowledge nor do I ought reasonably to know that the making of this work constitutes an infringement of any copyright work;
(5) I hereby assign all and every rights in the copyright to this Work to the University of Malaya ("UM"), who henceforth shall be owner of the copyright in this Work and that any reproduction or use in any form or by any means whatsoever is prohibited without the written consent of UM having been first had and obtained;
(6) I am fully aware that if in the course of making this Work I have infringed any copyright whether intentionally or otherwise, I may be subject to legal action or any other action as may be determined by UM.

Candidate's Signature Date: 1st September 2016

Subscribed and solemnly declared before,

Witness's Signature Date: 1st September 2016

Name:

Designation:

ABSTRACT

The present work focuses on enhancing the thermal performance of the microchannel heat sink (MCHS) using the passive method. Computational domain of the single channel was selected from the physical model of the MCHS for the numerical simulation. The basic geometry of the computational domain was taken from the geometry of the MCHS from existing literatures. This model was validated with the available analytical correlation and existing numerical results.

Five types of passive enhancements were studied in this study. Those methods are; (1) secondary channel, (2) micromixer, (3) constrictions, (4) re-entrant obstruction and (5) cavities. The fluid flow and heat transfer characteristics of all these MCHS were numerically investigated in a laminar and steady state condition at a constant heat flux. The effect of the geometrical parameter on the thermal and pressure loss was studied at different flow configurations. The results showed that passive enhancements of the MCHS significantly improved compared to the simple MCHS.

There were a few highlights that were also gathered from this study. Firstly, the performance of secondary flow and micromixer is immensely good where heat transfer increased up to 1.43 times compare to simple MCHS. Furthermore, the pressure drop associated with this enhancement was in fact lower than the simple MCHS (0.97 times that of simple MCHS). Secondly, although constrictions and the re-entrant obstruction improved the performance of the MHCS by 2.25 and 1.2 respectively, the pressure loss associated with this enhancement was substantially high. Finally, the convection heat transfer in the MCHS with cavities improved considerably up to 1.63 with a negligible pressure drop.

It was also found that the performance of the MCHS was greatly dependent on the geometrical parameters of passive enhancement except for the constrictions and re-

entrant obstructions. Such improvement attributes to the increase of the heat transfer area and the repetitive development of the boundary layers. Besides that, the passive enhancement also enhanced the fluid mixing. For instance, the large and intense vortices observed in the cavities, the micromixers and secondary channels resulted in chaotic advection that ultimately improved the convection heat transfer. Similarly, the Eddy effect in the MCHS with constriction also improved the heat transfer. The jet and throttling effect, as well as the fluid acceleration that the fluid experienced after passing the modified section also contributed to the enhancement of heat transfer with some pressure drop penalty.

The overall result of the present work shows that the MCHS with passive enhancement has a high potential and is feasible to be implemented in practical applications.

ABSTRAK

Kajian ini memberi tumpuan pada peningkatan prestasi saluran penyikir haba mikro (MCHS) menggunakan kaedah pasif. Satu saluran telah dipilih dari model fizikal untuk simulasi. Geometri asas untuk domain simulasi diambil dari geometri MCHS yang sedia ada. Model ini disahkan dengan korelasi yang sedia ada.

Lima jenis kaedah peningkatan pasif telah digunakan untuk meningkatkan prestasi pemindahan haba MCHS. Kaedah tersebut adalah; (1) aliran pendua, (2) pengadun mikro, (3) penyempitan bersiri, (4) halangan jenis masuk-semula dan (5) kaviti. Kadar dan tahap pemindahan haba dan aliran cecair dalam kesemua MCHS ini dikaji dalam keadaan laminar dan kadar haba yang tetap. Kesan parameter geometri ke atas prestasi terma dan keupayaan aliran dianalisa pada konfigurasi aliran yang berbeza. Hasil kajian menunjukkan bahawa penggunaan kaedah pasif dalam MCHS menunjukan peningkatan prestasi terma yang ketara berbanding dengan MCHS biasa.

Terdapat beberapa perkara yang perlu dititikberatkan dalam keputusan daripada kajian ini. Pertama, peningkatan haba hasil daripada aliran pendua dan pengadun mikro adalah amat baik dan penurunan tekanan cecair adalah sebaliknya lebih rendah daripada MCHS biasa. Kedua, walaupun kaedah penyempitan dan halangan jenis masuk-semula telah meningkatkan prestasi MHCS sehingga 2.25 dan 1.2, kehilangan tekanan berikutan peningkatan ini adalah amat tinggi. Akhirnya, pemindahan haba dalam MCHS dengan kaviti didapati bertambah baik sehigga 1.63 dengan penurunan tekanan yang boleh diabaikan.

Ia juga mendapati bahawa prestasi MCHS adalah bergantung kepada parameter geometri peningkatan pasif kecuali bagi kaedah penyempitan dan halangan jenis masuk-semula. Penambahbaikan sebgini adalah kerana sebab-sebab berikut; meningkatkan

kawasan pemindahan haba dan pembentukan lapisan aliran yang berulang-ulang. Selain itu, peningkatan pasif juga telah meningkatkan pencampuran cecair. Sebagai contoh, pusaran besar dan sengit dalam kaviti, pengadun mikro dan saliran pendua telah mempertingkatkan pencampuran cecair. Begitu juga dengan kesan Eddy dalam saluran dengan penyemptian bersiri. Kesan pecutan dan pendikitan yang cecair alami selepas melepasi tempat ini turut menyumbang kepada peningkatan kadar pemindahan haba dengan kejatuhan tekanan cecair.

Secara keseluruhannya, hasil penyelidikan ini menunjukkan bahawa MCHS dengan peningkatan pasif mempunyai potensi yang tinggi dan sesuai digunakan dalam aplikasi praktikal.

ACKNOWLEDGEMENTS

Firstly, I would like to express my sincere gratitude to my advisor Dr. Nik Nazri Nik Ghazali for his continuous support of my Ph.D study and related research, for his patience, motivation, and immense knowledge. His guidance helped me all throughout the duration of carrying out this research and the writing of this thesis. I could not have imagined having a better advisor and mentor for my PhD study.

Special thanks to my ex-supervisor Prof. Saidur Rahman, who accepted me as his student and research assistant when I joined University Malaya. He is currently serving as Chair Professor at King Fahd University of Petroleum & Minerals (KFUPM). He has also been a great inspiration among students in our group for his achievements.

Sincere thanks to Dr. Azuddin Bin Mamat and Mr. Md. Abu Omar Bin Awang, my secondary supervisors for their insightful comments and encouragement in my research. They have also highlighted some critical issues in my research that incented me to widen my research from various perspectives. In particular, Dr. Azuddin Bin Mamat was also very helpful in developing the experimental rig and fabricating the microchannel heat sink.. On the other hand, Mr. Md Abu Omar Bin Awang guided me on the mathematical foundations. His guidance in research was highly valuable, especially on the theory validation and journal publications. I am immensely grateful to work with such highly knowledgeable and cooperative advisors. Without their precious support, it would be impossible for me to conduct this research.

I would like to make a special mention to Dr. Hussein A Mohammed for enlightening me with the first glance of this research area during my Master degree. I thank my fellow lab mates for creating a competitive environment that nudged me to work harder and complete my PhD on time. Last but not the least, I would like to thank my family; my parents and to my sisters for supporting me spiritually throughout the writing of this thesis and my life in general.

TABLE OF CONTENTS

LIST OF FIGURES

LIST OF TABLES

LIST OF SYMBOLS AND ABBREVIATIONS

A	:	solid-fluid interface area
c_p	:	heat capacity (J/kg·K)
D_1	:	Direction 1
D_2	:	Direction 2
D_c	:	hydraulic Diameter (μm)
f	:	friction factor
f/f_0	:	friction factor ratio compared to simple channel
G	:	volume flow rate (m^3/s)
h	:	heat transfer coefficient ($W/m^2 \cdot K$)
H	:	height of micro channel heat sink (mm)
k	:	thermal conductivity (W/m·K)
L	:	length of micro channel heat sink (mm)
$\dot{m}$	:	mass flow rate (kg/s)
MCHS	:	micro channel heat sink
n	:	local coordinate normal to the wall
Nu	:	Nusselt Number
Nu/Nu_0	:	Nusselt Number ratio compared to simple channel
ΔP	:	pressure drop (Pa)
q	:	heat flux (W/m^2)
T	:	temperature (K)
u, v, w	:	velocity components (m/s)
T	:	temperature (K)
W_c	:	width of the channel in micro channel heat sink (mm)
W	:	total width of micro channel heat sink (mm)

x,y,z : Cartesian coordinates

Greek Symbols

α : dimensionless flow coefficient

η : overall thermal enhancement

ρ : density (kg/m^3)

μ : viscosity (Pa·s)

τ : wall shear stress (N)

Subscripts

bf : base fluid

f : fluid

in : inlet

out : outlet

s : solid

CHAPTER 1: INTRODUCTION

1.1 Background

1.1.1 Revolution of Integrated Circuit

Semiconductor industry has significantly developed to become one of the prominent industries in the world. Latest developments in semiconductor elements have distinctly intensified its processing speed and also allowed their sizes to be compacted. The continual evolution and development of the semiconductor industry is mainly due to the exponential rise in the density of transistors in solid-state integrated circuits.

1.1.2 Moore's Law

The scaling of transistors on integrated circuit was observed by Moore's Law which principally conjectures that the number of transistors on a chip doubles every 18 months (Moore, 1998).

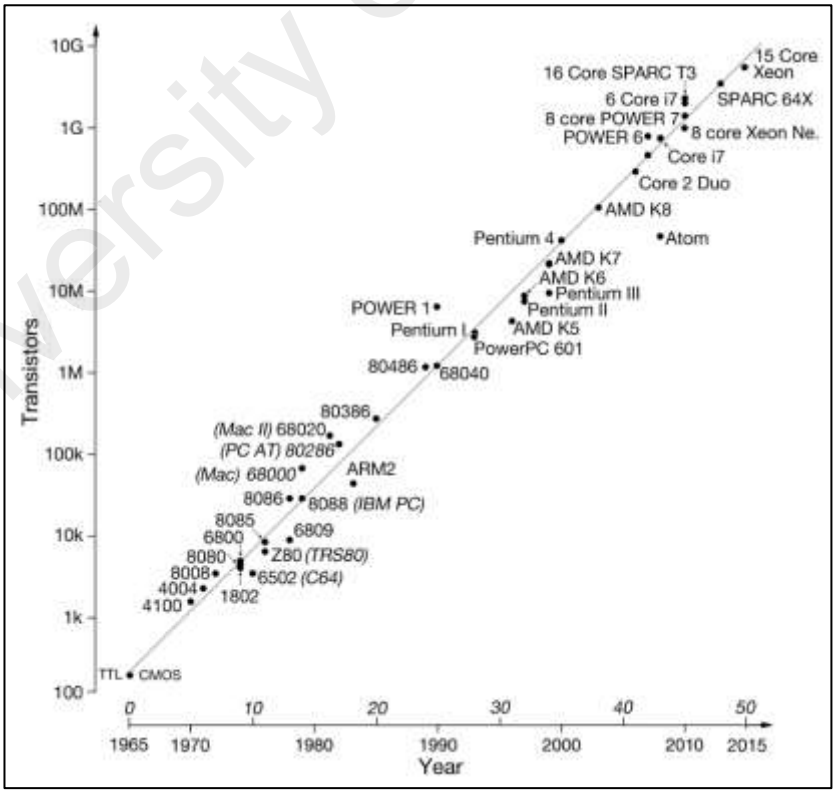

Figure 1.1: Moore's Law with time.

1.1.3 Heat Dissipation from the Integrated Circuit

While energy is consumed in charging and discharging the capacitances of the circuit, a large amount of heat is generated due to the current flow between the power supply to the ground. Additionally, in integrated circuits, many layers of interconnects generate heat due to Joule heating. Such non-uniformity tends to diminish the effectiveness of thermal management solutions (Torresola et al., 2005). This heat dissipation has long been recognized as a potential issue that may limit information processing. The heat density of innumerable electronic devices is increasing as ever and it is expected the devices will necessitate cooling performance of almost 100 W/cm^2 (Yuki & Suzuki, 2011).

1.1.4 Thermal Management of Integrated Circuit

The need of develop heat removal methods to maintain the microprocessor at desired temperature while dissipating a highly non-uniform power is called thermal demand. Ideally, the temperature of a CPU has to be maintained below 80ºC in order to maintain its reliability and to sustain its life expectancy (Abouali & Baghernezhad, 2010). It has to be also noted that such temperature has to be maintained by virtue of advanced and cost-effective cooling approaches with high heat transfer rate under high heat flux settings.

This fact has gotten enormous interest of scientific community where many researchers have taken serious efforts to conduct extensive studies to augment the cooling capability of the MCHS (Adams, Abdel-Khalik, Jeter, & Qureshi, 1998; Fedorov & Viskanta, 2000; Judy, Maynes, & Webb, 2002; R. H. Liu et al., 2000; Mohiuddin Mala & Li, 1999; Peng & Peterson, 1996; Phillips, 1988; Qu, Mala, & Li, 2000; Rahman & Gui, 1993; Sobhan & Garimella, 2001; Weisberg, Bau, & Zemel, 1992; B. Xu, Ooti, Wong, & Choi, 2000). Numbers of innovative technologies has been

developed over the past decades to meet the growth of thermal management demand that resulted from increasing performance of semiconductor devices such as microprocessors (Garimella, 2005, 2006; Lasance & Simons, 2005; Torresola et al., 2005).

1.1.5 Micro channel Heat Sink

Cooling methods for electronic devices have transformed from forced-air cooling to forced-liquid cooling due to the growth in the heat density. Micro channel heat sink (MCHS) is typically used for the liquid cooling of electronic devices where cooling fluid is series of channels that have small hydraulic diameter and high aspect ratio. It has become the most imperative cooling device due to its attributes of having a high heat transfer coefficient, an extended heat transfer area and its compactness that makes it apt for the cooling of microelectronics (Hadjiconstantinou & Simek, 2002; Judy et al., 2002; Satish G Kandlikar, 2002; Satish G Kandlikar, Steinke, & Balasubramanian, 2002; Qu & Mudawar, 2002a, 2002b; Ryu, Choi, & Kim, 2002). In addition, microchannel can enhance the local heat transfer rate greatly due to the channel-narrowing effect and this can solve the issue of non-uniform heat distribution.

Two-phase cooling seems to have high potential of cooling that includes fluid suspended with solid particles (i.e. nanofluids) and flow boiling. While the former has higher thermal potential as a result of increased thermal conductivity (T.-C. Hung, Yan, Wang, & Chang, 2012; Y.-H. Hung, Teng, Teng, & Chen, 2012; Jang & Choi, 2006; Kalteh, Abbassi, Saffar-Avval, & Harting, 2011), the latter has a potentially higher heat removal capacity due to the latent heat of vaporization (Sui, Teo, Lee, Chew, & Shu, 2010). However, this method involves lots of complication such as sedimentation in the solid-fluid solution and saturation temperature, condensation, nucleation, site activation,

critical heat flux in boiling heat transfer. Besides, it requires higher pumping power to leads to higher initial and operational cost.

On the other hand, single-phase flow heat transfer could remove equivalent amount of high heat flux with some minor modification. While additional pumping power associated with such modification is minimal, there numerous advantages identified with this method such as no vibration, no noise due to the boiling bubbles and no corrosion of the heat transfer surface. Generally, the heat transfer surface area is extended to enhance single-phase heat transfer. Aside of that, high heat transfer rate could be achieved by maintaining thermal boundary layer at non-fully developed condition. Furthermore, by enhancing the fluid mixing between the finned heat sinks, each takes advantage of this thermal inertia effect.

Several methods were suggested to remove a heat flux beyond 100 W/cm^2 (Steinke & Kandlikar, 2004). While active enhancement methods such as introducing pulsating flow and magnetic flow seem to be promising, they require highly engineered setups to implement these techniques that subsequently increase the initial as well as the operational cost. The passive method appears to be more practical for heat transfer enhancement in the MCHS where it only requires some additional machining(Abouali & Baghernezhad, 2010; D. Ansari, Husain, & Kwang-Yong, 2010; M. A. Ansari & Kim, 2007; Chai, Xia, Zhou, & Li, 2011; Herman & Kang, 2002; Kuppusamy, Mohammed, & Lim, 2013, 2014; P.-S. Lee & Teo, 2008; Xia, Chai, Wang, Zhou, & Cui, 2011; Xia, Chai, Zhou, & Wang, 2011; Xia, Zhai, & Cui, 2013; Zhai, Xia, Liu, & Li, 2014). Some of the passive enhancement methods that can be considered are the secondary channel, re-entrant cavity, venturi effect, constrictions and micromixer. Heat enhancement significantly surpasses the pressure drop drawn by the passive enhancement.

1.2 Problem Statement

As highlighted previously, that heat flux from integrated circuit such as Central Processing unit (CPU) is increasing drastically. A comprehensive solution is needed to manage such enormous heat dissipation without compressing to non-uniform heat on the surface. Considering simple MCHS heat sink is reaching to its limitation, an alternative solution must be established.

While two phase heat transfer solution has some potential, a lot of issue is associated with this solution aside of additional pumping power. On the other side, single phase heat transfer can be enhanced by two methods; active and passive method. However, active enhancement involves a lot of complication in the engineering design that could also lead to additional cost.

Considering this fact, the present work focuses on the passive enhancement in micro channel heat sink. This research primarily focuses on the effect of passive enhancement in the MCHS and its effect on the thermal and flow performance. An extensive numerical study is performed to investigate the effects of geometrical parameters of passive enhancement together with various flow configurations.

1.3 Objective of Study

It is expected at the end of this project to provide optimization conditions of the cooling performance of the MCHS in practical applications. The objectives of this study are:

- To study the behavior of fluid flow and heat transfer rate in the MCHS with passive enhancement.
- To study the effect of the geometrical parameters of the passive enhancement in MCHS on its thermal enhancement and pressure drop.

- To study the effect of the flow condition in the MCHS with passive enhancement on the heat transfer and fluid flow mechanism.

- To understand the fluid flow behavior near the passive enhancement section in the MCHS, as well as its correlation with convective heat transfer.

1.4 Methodology

The research started with an extensive study on prior literature reviews to attain a deep understanding on the enhancement methods available, especially for the MCHS. A large number of publications, including journals and conference papers are studied. A few results from these past literatures were used to validate the preliminary results of the present research. The numerical model is developed based on the prior literature and validated with the existing results and correlations. The model is then analyzed according to the objectives of the study. The data obtained from the investigation is gathered, analyzed and presented in the form of graph and tables. Finally, the entire process of this research (literature reviews, methodology, results and discussion, and conclusion) was documented in the form of a thesis. Besides that, a few journals on the topic of this research are also published. This is to ensure that all efforts that have been put in can be continued in the future by other researchers to a greater height.

1.5 Outline of the Thesis

This thesis contains five chapters all together. The arrangement of these five chapters are shown below:

In chapter 1, the background of the research, problem statement, scope of the study and the objective methodology are discussed.

In Chapter 2, the previous work done by other researchers are reviewed to fulfill the knowledge gap in the present work.

Chapter 3 focuses on the methodology that has been taken for this research. The grid independent test, code validation, governing equation and its solving method in Computational Fluid Dynamics (CFD), together with the geometrical design of the passive enhancement are discussed.

Chapter 4 presents the results of the analysis from the passive enhancement and its geometrical parameters together with a comprehensive discussion.

Chapter 5 concludes the thesis with the conclusion that is obtained from the research.

CHAPTER 2: LITERATURE REVIEW

Researchers have given a great deal of interest to investigate the fluid flow and heat transfer in a microchannel heat sink (MCHS) after its pioneering work from (Tuckerman & Pease, 1981). The first MCHS was fabricated using silicon and it was able to dissipate a heat flux of 7.9×10^6 W/m^2 with maximum temperature difference of 71°C between the substrate and inlet water. Numerous numerical and experimental works were done after this research in order to improve the performance of the MCHS, considering the miniaturization of the electronic device and increase in the power density (Adams et al., 1998; K. Balasubramanian et al., 2011; P. Balasubramanian & Kandlikar, 2005; Chu, Teng, & Greif, 2010; Li, Feng, He, & Tao, 2006; J.-T. Liu, Peng, & Yan, 2007; Ma, Li, & Tao, 2007; Morini, 2004; Owhaib & Palm, 2004; Qu & Mudawar, 2002b; Rahman & Gui, 1993; Wu & Cheng, 2003; Xi, Yu, Xie, & Gao, 2010; B. Xu et al., 2000; Yang & Lin, 2007). The analyses were primarily focused on optimizing the geometry of the micro channel such as the height, width and aspect ratios (Gamrat, Favre-Marinet, & Asendrych, 2005; Peng & Peterson, 1996; Rahman & Gui, 1993). Besides that, the MCHSs were also designed in various shapes, such as circular and trapezoidal channel (Barba, Musi, & Spiga, 2006; Chen, Zhang, Shi, & Wu, 2009; McHale & Garimella, 2010; Muzychka, 2007; Owhaib & Palm, 2004; Sohel et al., 2013; Yong, Yong Jiun, & Xiaowu, 2013). For instance, a numerical investigation was done on the MCHS with a different cross-sectional shape to study their flow behavior and wall heat flux (Nonino, Savino, Del Giudice, & Mansutti, 2009). In another research, a multi-objective optimization algorithm was implemented on an inverse trapezoidal MCHS to achieve the best performance (Khan, Kim, & Kim, 2015). Some of the researchers proposed analytical models to predict the convective heat transfer in microchannel heat sinks (D. Liu & Garimella, 2005). Furthermore, optimization techniques were also employed on double-layered microchannel heat sinks to maximize

the heat dissipation in MCHS (Leng, Wang, Wang, & Yan, 2015a, 2015b). The existing literatures showed that the single–phase liquid flow in microchannels obeys the classical theory of Stokes and Poiseuille flow (Steinke & Kandlikar, 2006). Another review of heat transfer in the MCHS suggested that a standard theory and correlations are sufficient to describe heat transfer in the MCHS. However, the scaling effect has to be considered critically (Rosa, Karayiannis, & Collins, 2009).

Nevertheless, optimization of the basic geometry of the microchannel heat sink and the variation of flow configuration are insufficient to sustain the further demand of electronic cooling where the heat dissipation may reach up to 10^6 W/m^2. There are a few downsides associated with simple MCHS, such as trivial flow mixing and thickened boundary layer with flow length that result in weak heat dissipation. It has to be noted that the usage of thermally enhanced fluid such as nanofluids lead to a higher energy consumption due to bigger pumps where it also results in sedimentation on the channel wall (J. Lee & Mudawar, 2007). On the other side, there are a lot of issues involved in a boiling heat transfer such as nucleate formation, bubble growth and critical heat flux that must be managed carefully (Sui et al., 2010).

A few researchers reviewed the experimental results of a single phase heat transfer in the MCHS as well as a few methods that were suggested to enhance the performance of the MCHS. These methods include the shortening of the thermal boundary layer; the increase of flow interruptions and the increase of the velocity gradient near the heated surface for the single-phase heat transfer enhancement (Morini, 2004; Tao, He, Wang, Qu, & Song, 2002). Another article suggested a few techniques to enhance the thermal performance such as the use of the secondary passage, groove/cavities and ribs/protrusion (Steinke & Kandlikar, 2004). These enhancement methods have been adopted by many researchers to improve the thermal performance of the MCHS

(Abouali & Baghernezhad, 2010; Agarwal, Bandhauer, & Garimella, 2010; Alam & Kim, 2012; D. Ansari et al., 2010; Chai, Xia, Wang, Zhou, & Cui, 2013; Chai et al., 2011; Chai, Xia, Zhou, Li, & Qi, 2013; Chen et al., 2009; Steinke & Kandlikar, 2004; Xia, Chai, Wang, et al., 2011; Xia, Chai, Zhou, et al., 2011; Zhai et al., 2014).

A group of researchers introduced re-entrant cavities in the MCHS to enhance the convective heat transfer (Chai et al., 2011; Xia, Chai, Wang, et al., 2011; Xia, Chai, Zhou, et al., 2011). These re-entrant cavities are also formed in different shapes, such as triangular and circular (fan-shaped) and are then arranged in the different orientations. Several numerical studies were performed to predict the effect of these cavities on the thermal performance of the MCHS. The results showed that the MCHS with cavities had a good improvement compared to the simple MCHS. The authors highlighted that the re-entrant cavities in the MCHS enhanced the thermal performance significantly due to the jet and throttling effect, the vortices generation and the boundary layer redevelopment. Combination of the internal ribs and re-entrant cavities in the MCHS further enhanced the thermal performance with the expense of a larger pressure drop (Xia et al., 2013).

Introduction of constrictions in the main flow stream can also enhance the thermal performance of the MCHS significantly. The experimental and numerical study on the effect of expansion and constriction cross sections in the MCHS showed a good improvement in the heat transfer performance (Chai, Xia, Wang, et al., 2013). Analysis of interrupted MCHS with rectangular ribs in the transverse micro chambers exhibited a momentous augmentation in heat transfer. However, it was greatly dependent on its geometrical parameter and the Reynolds number (Chai, Xia, Zhou, et al., 2013). Advanced analysis was performed on this model by varying the shapes of the ribs. The result was then presented based on the 1st and 2nd law of thermodynamics (Zhai et al.,

2014). It was found that heat transfer improved and the irreversibility was reduced when ribs are added in between the cavities in the MCHS. For certain Reynolds numbers, the Nusselt number enhanced up to 3 times while the friction factor increased up to 6.3 times.

In a numerical study on the MCHS with grooves, geometrical parameters and the pitch of the grooves were optimized using a multi-objective evolutionary algorithm to reduce the thermal resistance and to increase the Nusselt number while maintaining the associate pumping power penalty (D. Ansari et al., 2010). It was found that the grooved MCHS had a lower thermal resistance and a higher Nusselt number compared to the straight channel with a higher pressure drop penalty. Throughout the optimization of the design variables, the ratio of the groove pitch to the height of MCHS was found most Pareto-sensitive, whereas the ratio of the width of the MCHS to the height was found least Pareto-sensitive. It was concluded that the grooved MCHS is better when compared to the simple channel in availability of a higher pumping power.

Another numerical investigation was performed on a single-phase water cooling enhancement by creating grooves on the rectangular MCHS channel wall surfaces (Abouali & Baghernezhad, 2010). There were two shapes of the grooves; rectangular and arc shapes, which were created on the side and bottom walls of the MCHS and analyzed in a laminar flow (Re=900). Besides this, the geometry and the pitch of the groove were also optimized and the results were compared to the simple MCHS. The heat removal rate of the grooved micro channel was generally much higher compared to the simple MCHS. The heat removal was also found to vary significantly with different groove shapes and configurations. It was highlighted that a grooved microchannel with a thicker wall and lower mass flow rate of cooling water results in a higher heat dissipation and coefficient of performance compared to a simple microchannel with

thinner walls. It was also found that while the arc groove had a higher overall heat removal rate, the rectangular had a higher COP when the grooves were created on both, the side and bottom walls.

A 2D and 3D numerical analysis was performed to simulate the heat transfer and fluid flow in intermittently grooved channels at Reynolds numbers ranged from $600 \leq \mathrm{Re} \leq 1800$ (Greiner, 1991; Greiner, Faulkner, Van, Tufo, & Fischer, 2000). Seven sets of adjoining grooves were placed opposite symmetrically, and these models were compared with the straight wall in the computational domain periodic inflow and outflow boundary conditions. The grooved section had a continuous developing flow, whereas the flow gradually reached to a fully developed condition in the flat surface. Therefore, the grooved channel has a higher heat transfer than the simple channel.

An experimental study was performed on the heat transfer enhancement of transverse ribs in circular tubes (San & Huang, 2006). The mean heat transfer and friction data were measured for air flow starting from the entrance. The entrance effect on the Nusselt number was found to be insignificant, whilst geometrical parameters had a drastic effect on the thermal performance. Several correlations for the average Nusselt number and friction factor were proposed based on the geometrical parameters. An optimal strip-fin size was found to minimize the pressure drop in a study of laminar forced convection of water in an offset strip-fin MCHS for microelectronic cooling (Hong & Cheng, 2009).

One research showed that grooves can apparently reduce the friction factor. In that particular numerical study, the effect of the grooves on the flow rate in a microchannel was investigated (Hwang & Simon Song, 2008). The grooves were formed on the sidewalls of the channel to reduce the frictional drag, where the grooves and channel were assumed to contain air and water respectively. The results revealed that the

numbers of the grooves affected the flow rate notably as the pressure drop increases. The flow rate increased by 13% in a microchannel with 64 grooves, 37% for a groove with 100μm width and 180 % for a triangular groove, compared to the smooth wall channel at a pressure drop of 10 Pa. The triangular groove had the highest flow rate compared to the semicircular and square grooves. It was concluded that the number, size, and shape of the grooves significantly affected the flow rate of the fluid. This outcome contradicts with other researchers where it is generally known that grooves on the wall increase the pressure drop.

A numerical study of flow and heat transfer in a stacked two–layer micro channels with easy-processing passive microstructures showed that a stacked microchannel has a better thermal performance compared to a simple MCHS (Cheng, 2007). It is also found that longitudinal internal fins can enhance the heat transfer in a microchannel (Foong, Ramesh, & Chandratilleke, 2009). Numerous studies were conducted to understand the effect of ribs on the heat transfer and pressure drop. A V-shaped rib increased both, heat transfer and friction factor in a rectangular duct (Kumar, Saini, & Saini, 2012). Roughness elements in structured sinusoidal elements in a microchannel provided flow modifications and extended areas that enhances the heat transfer (Dharaiya & Kandlikar, 2013).

Thermal developing flow can also be obtained by separating the flow length into several independent zones (J. Xu, Song, Zhang, Zhang, & Gan, 2008; J. L. Xu, Gan, Zhang, & Li, 2005). A 3D numerical simulation was conducted to examine the conjugate heat transfer in straight and interrupted MCHS which contains separate sets of short parallel channels joined by transverse micro chambers (J. Xu et al., 2008). The flow characteristics in all the channels were found to be almost similar. The fluid flow remained in a developing condition throughout the channel due to the shortened

constant cross-sectional length. This has resulted in a large thermal enhancement in the MCHS. The pressure drop that the fluid experiences when it moves from a micro chamber to a channel was compensated by the pressure gain while the fluid is in the micro chamber. Thus, the pressure loss of the interrupted channel was almost similar to the straight channel.

The effect of the variable shear stress at the liquid and vapor interface was investigated in a microchannel with sinusoidal and trapezoidal grooves at both, parallel and counter flows (Suh, Greif, & Grigoropoulos, 2001). The existing correlation predicted for liquid friction was modified for trapezoidal and sinusoidal groove based on the velocity contour. The results obtained from the modified correlation are found acceptable. Another researcher attempted to enhance the heat transfer by generating a travelling wave using the vortex shedding from the constriction and expansion in a horizontal channel (Korichi & Oufer, 2007). A grooved channel with curved vanes was also found to be able to dissipate heat effectively due to the velocity gain in the groove region. However, such improvement will be accompanied by a considerable pressure drop (Herman & Kang, 2002). A computational model was proposed to explain the effect of vortices on heat transfer (McGarry, Campo, & Hitt, 2004). The effect of turbulent flow and heat transfer in a square channel with internal cavity was studied and it was deduced that the flow structure and the Reynolds number are the main reasons of improvement of the local Nusselt number (Mesalhy, Abdel Aziz, & El-Sayed, 2010).

The performance of rectangular wavy micro channels examined at laminar conditions and with an enormous thermal enhancement was found due to the secondary flow (Dean Vortices) (Sui et al., 2010). It was revealed that Dean Vortices were generated when the liquid coolant flows through the wavy microchannel. This phenomenon significantly enhances the heat transfer with an acceptable pressure drop.

A numerical investigation performed on the fluid mixing in a curved microchannel with rectangular grooves revealed that the fluid mixing was enhanced with the variation of groove width for a given Reynolds number (Alam & Kim, 2012). However, the fluid mixing was insensitive to the variation of depth of the groove. An experimental study on the mixed convection heat transfer from longitudinal fins in a horizontal channel with a uniform heat flux showed that there is an optimum pin height to achieve the best performance (Dogan & Sivrioglu, 2009). This optimum fin is dependent on the fin height and modified Rayleigh number for heat transfer enhancement. CFD (computational fluid dynamics) and LB (lattice Boltzmann) approaches were used to study the forced convection heat transfer occurring in the MCHS (Y. Liu, Cui, Jiang, & Li, 2011). The results exhibited that the shield shaped groove microchannel possessed the high heat exchange performance with the increment of the Nusselt number at approximately 1.3 times than that of the plain surface structure.

A numerical analysis on the thermal and flow performance of the MCHS with different shapes of grooves on the sidewall of the MCHS using nanofluids showed that thermal performance enhanced significantly, compared to the simple MCHS using water with negligible pressure loss (Kuppusamy et al., 2013, 2014) . A group of researchers created smaller branching channels that cuts through obliquely along the fins. These small channels could induce the secondary flow that which will allow the working fluid to move from one channel to another channel and decreasing the thickness of thermal boundary layer at the same time (P.-S. Lee & Teo, 2008; Y.-J. Lee, Lee, & Chou, 2009; Y. J. Lee, Lee, & Chou, 2012). The heat transfer performance improved significantly with a negligible pressure drop. The primary reason of such thermal performance was due to the boundary layer rupture in the adjoining region and the redevelopment in the main stream area.

A similar method was used to enhance the thermal performance of a cylindrical oblique fin mini channel heat sink (Fan, Lee, Jin, & Chua, 2011). The results showed that the average Nusselt number increased up to 73.5%, while the total thermal resistance decreased up to 61.7% compared to the conventional straight fin mini channel heat sink. In another article, the same authors mentioned that the Nusselt number increased by 75.6%, but the thermal resistance only decreased to 59.1% due to the combined effect of the thermal boundary layer re-development and flow mixing (Fan, Lee, Jin, & Chua, 2013, 2014). The edge effect is studied by forming a blockage in a few channels and it was found that this blockaded section resulted in weaker flow mixing in the draining and filling region (Fan, Lee, & Chua, 2014). The local temperature distribution curves were in a unique concave shape due to the edge effects. However a lower and uniform temperature distribution was found on the surface of a regular cylindrical oblique. The improved flow mixing was due to the absence of the edge effects.

In a study on a channel with alternated opposed ribs, the results showed that the pressure drop increased consistently with the increase of Reynolds number (Desrues, Marty, & Fourmigué, 2012). Comparison of various offsets in fin geometries from experimental results showed that the staggered fins with a pitch of 100 μm and 75 μm width gives an excellent heat transfer performance (Colgan et al., 2005). An experimental study on turbulent air flow in a channel fitted with different shaped ribs showed that the ribs in the channel enhance the heat transfer significantly with a higher friction loss compared to a channel with a smooth wall (Promvonge & Thianpong, 2008). In another work, baffles were placed on an isothermal wall square channel at a 45° angle to generate a pair of mainstream wise vortex over the channel (Promvonge, Sripattanapipat, & Kwankaomeng, 2010). This vortex has induced impinging flows near the sidewall and wall of the baffle cavity that resulted in drastic intensification in heat

transfer rate. Measurement of mass flow rate and pressure distribution along the micro channel showed that constricted sharp corners can result in flow separation (Wing Yin, Man, & Zohar, 2002).

2.1 Summary

From the literature review, it can be concluded that passive enhancement has a great potential for heat transfer enhancement in the microchannel heat sink. This fact prompts the present study to perform an investigation on various passive enhancements and its geometrical parameters on the thermal enhancement in the MCHS, while at the same time maintaining the pressure drop at a desired level.

CHAPTER 3: METHODOLOGY

3.1 Outline

This chapter explains the methodology that is used in this study to investigate heat transfer and fluid flow characteristics of the MCHS with passive enhancement. The numerical analysis was performed using the commercial Computational Fluid Dynamics (CFD) software ANSYS Fluent 14.5. A brief description on the numerical model and computational domain, together with its computational grid is given. Besides this, the mathematical foundation to describe the thermal and flow characteristic is also explained. Using this mathematical foundation, the preliminary results of the study is validated with the existing correlation. The methodology of analysis, geometry configuration and boundary condition associated with all the passive enhancement methods investigated in the present study is discussed thoroughly in this chapter.

3.2 Physical Model of MCHS

The MCHS has a series of straight rectangular channels that are arranged in parallel at an equal distance as shown in Figure 3.1.

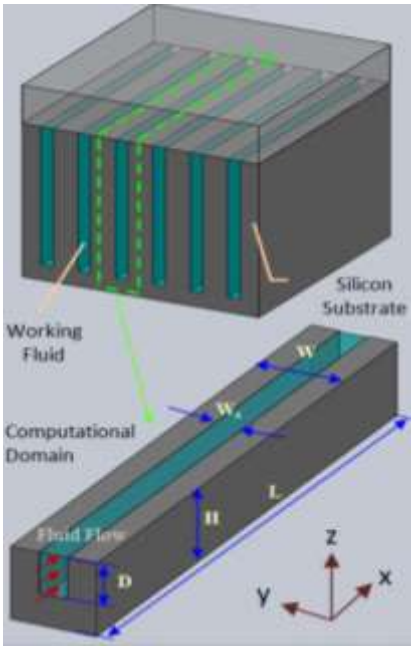

Figure 3.1: Schematic view of micro channel heat sink

Since each channel has a periodic boundary condition, a single channel is selected as the computational domain from the physical model to reduce the computational time. The top cover of the channel is assumed adiabatic and does not affect the thermal or hydrodynamic condition in the MCHS.

Therefore, it was not considered in the computational domain. The dimensions of the MCHS computational domain are shown in Table 3.1.

Table 3.1: Dimension of the Straight MCHS

Parameter	L (mm)	W (µm)	H (µm)	W_c (µm)	D_c (µm)
Values	10	300	350	100	200

3.3 Computational Grid for Solution Domain of the MCHS

The computational domains and the grids are created using the meshing tool in ANSYS 14.5. The mesh was generated using the Hex dominant scheme where most of the computational domains were built in a structured mesh. The pictorial view of the computational grids is shown in Figure 3.2 (a) and (b).

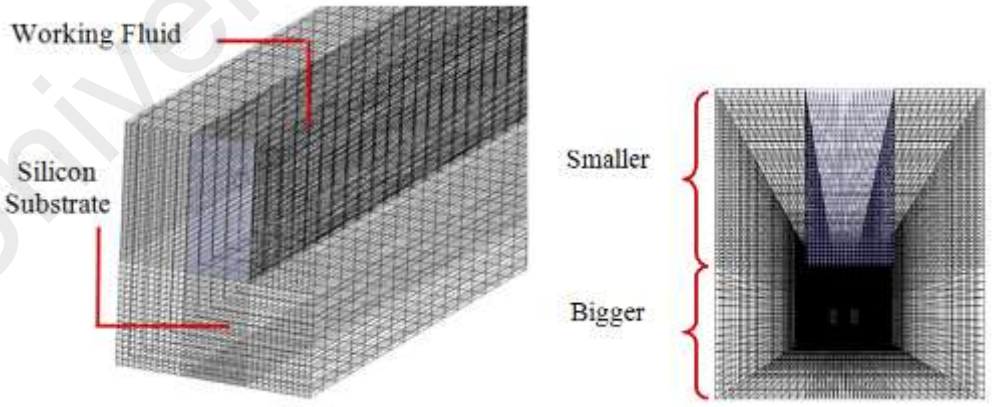

(a) (b)

Figure 3.2: Structured mesh of the straight MCHS (a) isometric view (b) front view.

3.4 Governing Equation

The following assumptions were considered in this numerical analysis:

1. The fluid flow is in a steady state, incompressible and laminar condition.
2. Properties of the fluid are not dependent on temperature, except for viscosity.
3. Neglected radiation heat transfer and gravitational force.
4. No viscous dissipation in fluid.

The governing equations were developed based on the aforementioned assumptions:

3.4.1 Fluid

Continuity equation:

$$\frac{\partial}{\partial x}(\rho u) = 0 \tag{3.1}$$

Momentum equation:

$$\frac{\partial}{\partial x}\left(\rho_f uv\right) = \frac{\partial p}{\partial y} + \frac{\partial}{\partial x}\left[\mu_f\left(\frac{\partial v}{\partial x} + \frac{\partial u}{\partial y}\right)\right] \tag{3.2}$$

Energy equation:

$$\frac{\partial}{\partial x}\left(\rho_f u c_p T\right) = \frac{\partial}{\partial x}\left(k_f \frac{\partial T}{\partial x}\right) \tag{3.3}$$

3.4.2 Solid

$$\frac{\partial}{\partial x}\left(k_s \frac{\partial T}{\partial x}\right) = 0 \qquad \text{(Solid)} \tag{3.4}$$

3.5 Boundary Conditions

3.5.1 Thermal Boundary Conditions

$T_f = T_{in} = 293\text{K}$ at $x = 0$ (Direction 1, *D1*) and $x = L$ (Direction 2, *D2*),

$$-k_f \frac{\partial T_f}{\partial x} = 0$$ at $x = L$ (Direction 1, *D1*) and $x = 0$ (Direction 2, *D2*),

No axial heat transfer in solid region.

$$-k_s \frac{\partial T_s}{\partial x} = 0$$ at $x = 0$ and $x = L$

$$\frac{\partial}{\partial y} = 0$$ at $y = 0$, $y = W$,

$$-k_s \frac{\partial T_s}{\partial z} = q$$ at $z = 0$

$$-k_s \frac{\partial T_s}{\partial z} = 0$$ at $z = H$

The conjugate heat transfer between solid and fluid was defined by Fourier's Law:

$$-k_f \left(\frac{\partial T_f}{\partial n} \right) = -k_s \left(\frac{\partial T_s}{\partial n} \right) \quad (3.5)$$

where n is the local coordinate normal to the wall

3.5.2 Hydrodynamic Boundary Conditions

$u = v = w = 0$ at the fluid-solid wall

$u_f = u_{in}$ at $x = 0$ (Direction 1 '*D1*', Case A) and $x = L$ (Direction 2 '*D2*', Case B),

$P_f = P_{out}$ = 1 atm at $x = L$ (Direction 1) and $x = 0$ (Direction 2),

The properties of the fluid flow at the solid/fluid interface were utilized to calculate the shear stress at the wall. The shear stress was obtained using the velocity gradient at the MCHS wall for laminar flow:

$$\tau_f = \mu\left(\frac{\partial u}{\partial n}\right) \tag{3.6}$$

Figure 3.3 shows the fluid entrance region in the wall with a non-slip condition. As the fluid hits the wall at the inlet, a boundary layer is created that grows along the channel and creates an inviscid core. The flow is considered fully developed when the boundary layers meet.

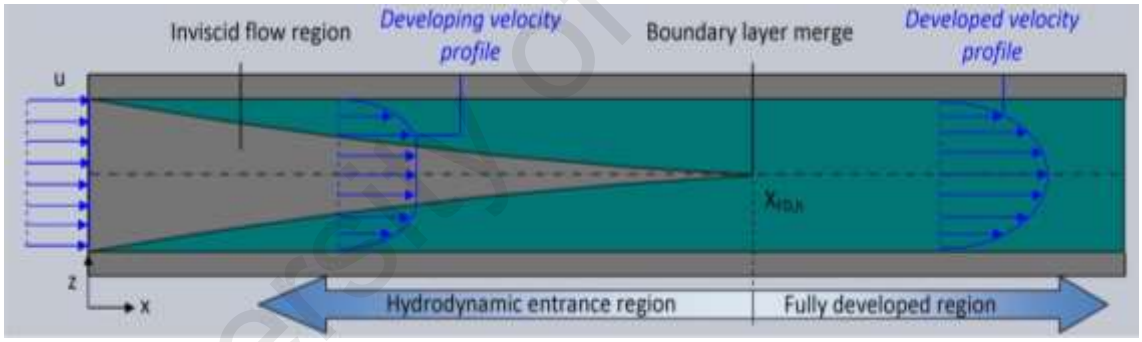

(a)

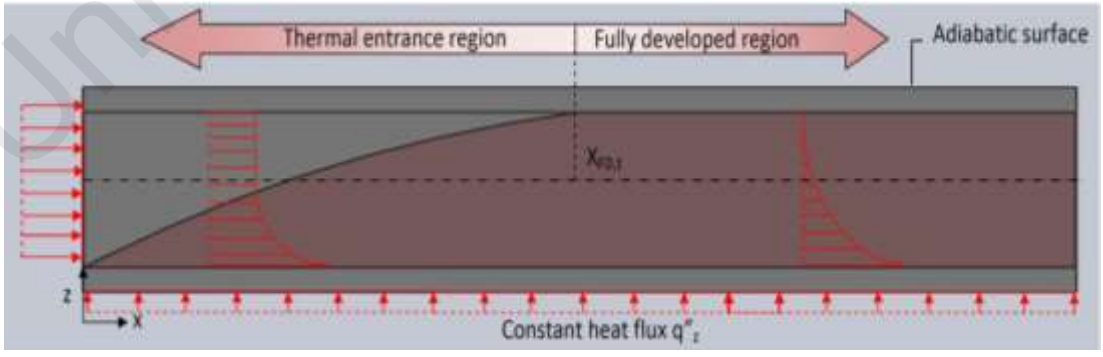

(b)

Figure 3.3: Entrance region of the flow in MCHS (a) laminar hydrodynamic boundary layer development in MCHS in constant inlet fluid velocity. (b) thermal boundary layer in MCHS with constant heat flux.

3.6 Solution Method

The governing equations were solved using the finite volume based Computational Fluid Dynamics (CFD) solver, ANSYS FLUENT 14.5. The momentum and energy convective term were discretized by the second order upwind differencing scheme. As for the pressure-velocity decoupling, it was done with the SIMPLE algorithm. The solutions are considered converged when the normalized residual values reach to 10^{-7} for all variables except for the energy equation that is less than 10^{-8}. Standard discretization and the second order upwind discretization schemes were selected respectively for the pressure equation and both, momentum and energy equations.

3.7 Mathematical Formulation

3.7.1 Thermal Characteristic

The thermal performance of the microchannel heat sink was determined by its Nusselt number that is calculated using Eq. (5).

$$Nu = \frac{\bar{h} D_h}{k_f} \qquad (3.7)$$

where $\bar{h}$, $D_h = \frac{2W_c H_c}{(W_c + H_c)}$ and k_f are the average heat convection coefficient, hydraulic diameter of the channel, and thermal conductivity of the fluid.

The average convective heat coefficient $\bar{h}$ determined from:

$$\bar{h} = \frac{1}{L}\int_L h(x) \cdot dx \qquad (3.8)$$

where L is the length of the channel.

The local convective heat transfer coefficient, $h(x)$, is evaluated using the following equation:

$$h(x) = \frac{1}{\sum_{x,y} dA(x,y,z)} \left[\frac{\sum_{x,y} q''(x,y,z) dA(x,y,z)}{\sum_{xy} \left[T_w(x,y,z) - T_m(z) \right] dA(x,y,z)} \right] \tag{3.9}$$

$T_w(x,y,z)$ is the local wall temperature, and $T_m(x)$ is the local fluid bulk-mean temperature given by:

$$T_m(x) = T_{in} + \frac{1}{\dot{m} c_p} \sum_{x,y,z} q''(x,y,z) dA(x,y,z) \tag{3.10}$$

The local Nusselt number is calculated as follows:

$$Nu(x) = \frac{h(x) D_h}{k_f} \tag{3.11}$$

Thermal resistance is calculated as follows:

$$R = \frac{\Delta T_{\max}}{q} \tag{3.12}$$

where ΔT_{max} and q is the maximum temperature difference and heat flux.

The maximum difference is determined as follows:

$$\Delta T_{\max} = T_{out} - T_{in} \tag{3.13}$$

3.7.2 Fluid Characteristic

The friction factor of the fluid is calculated from the following formula:

$$f = \frac{\Delta P D_h}{2 u_m^2 \rho L} \tag{3.14}$$

where ΔP, u_m, ρ and L are the pressure drop, mean velocity, fluid density and length of the micro channel.

The pressure drop is defined as:

$$\Delta P = P_{in} - P_{out} \tag{3.15}$$

where P_{in} and P_{out} are the inlet and outlet pressure respectively.

The Reynolds number is calculated as follows:

$$\mathrm{Re} = \frac{\rho u_m D_h}{\mu} \tag{3.16}$$

where μ, is the fluid viscosity.

The Poissulle Number calculated using following equation:

$$f\,\mathrm{Re} = 24\left(1 - 1.3553\,\alpha_c + 1.9467\,\alpha_c^2 - 1.7012\,\alpha_c^3 + 0.9564\,\alpha_c^4 - 0.2537\,\alpha_c^5\right) \tag{3.17}$$

3.7.3 Performance Enhancement Factor

The heat transfer augmentation in the MCHS with passive enhancement compared with simple MCHS is calculated based on the ratio of the Nusselt number '$\frac{Nu}{Nu_0}$'. Thermal resistance ratio of MCHS with passive enhancement to simple MCHS is calculated to compare the overall heat transfer enhancement '$\frac{R}{R_0}$'.

Whereas the changes in the flow performance is determined based on the ratio of the friction factor '$\frac{f}{f_0}$'. Nu, Nu_0, R, R_0, f and f_0 represents Nusselt number of the MCHS with passive enhancement, Nusselt number of simple MCHS, thermal resistance of the MCHS with passive enhancement, thermal resistance of simple MCHS, friction factor of MCHS with passive enhancement and friction factor of simple MCHS respectively.

The performance enhancement factor is determined by:

$$\eta = \frac{Nu/Nu_0}{(f/f_0)^{1/3}} \tag{3.18}$$

Eq. 3.16 can be also simplified for analysis without comparison:

$$\varepsilon = \frac{Nu}{f^{1/3}} \tag{3.19}$$

3.8 Grid Sensitivity Study

The computational grid of the numerical model of the simple MCHS is tested at different concentrations to reduce the computational time, while at the same time maintaining the accuracy of the results. The coarse, fine and very fine mesh had 523,466, 745,256 and 1, 541, 256 nodes respectively. Since the percentage error of the fine mesh achieved is less than 1%, this mesh is selected for further analysis.

3.9 Model Validation

The computational model of the simple MCHS is validated with the available analytical equation and numerical results (Phillips, 1990; Steinke & Kandlikar, 2005; Xia, Chai, Wang, et al., 2011). An identical geometry and boundary condition are used where the inlet flow rate is u_m= 4m/s and heat flux is q=10^6 W/m^2.

The results show that the present study has a good agreement with both, the analytical and numerical result for both, thermal and flow field as shown in Figure 3.4 (a) and (b).

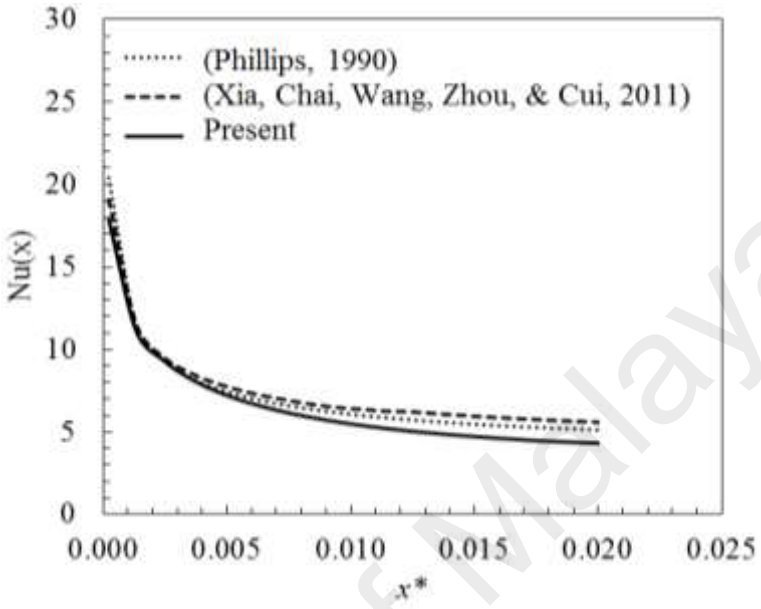

(a)

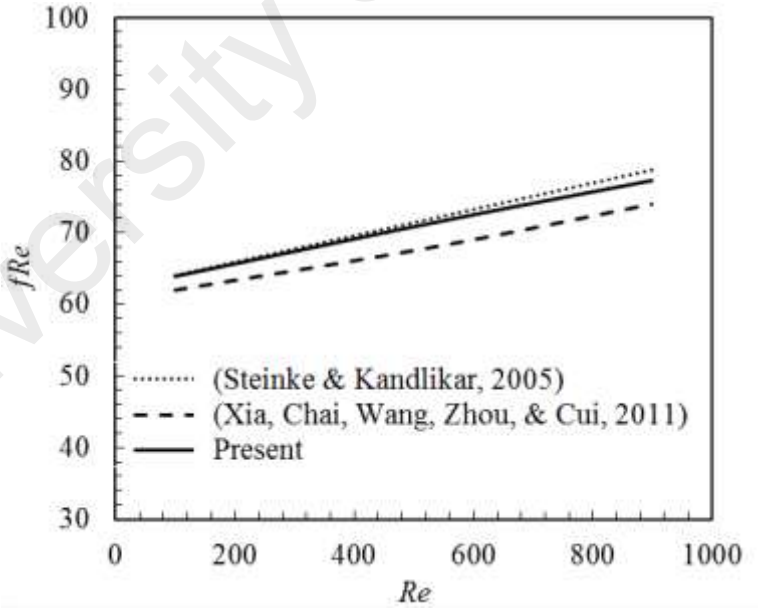

(b)

Figure 3.4: Model validation with prior analytical (Phillips, 1988; Steinke & Kandlikar, 2005) and numerical results (Xia et al., 2011a) (a) local Nusselt number (b) Poiseuille number.

Generally, a single channel with a wall on both sides was selected for the numerical analysis. However, in this study, another computational domain with a single wall and channels at both sides were designed instead of the usual design. The new computational domain was designed for the analysis of the secondary flow and micromixer through the channel wall. Figure 3.5 shows the configuration of both of these computational domains.

A simulation with an identical boundary condition (u_{in}=4m/s, q''=10^6W/m^2) and solution method was performed to compare the performance of these channels. The result for the local Nusselt number shows that both of these computational domains are comparable as shown in Figure 3.6.

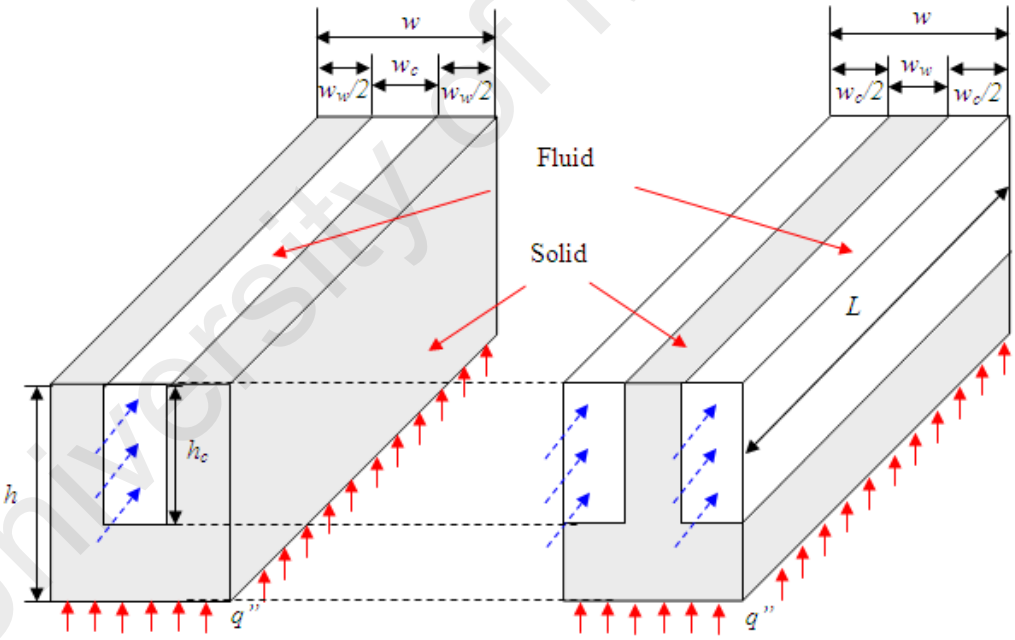

(a) (b)

Figure 3.5: Computational domain of MCHS with single (a) channel (CD 1) (b) wall (CD 2).

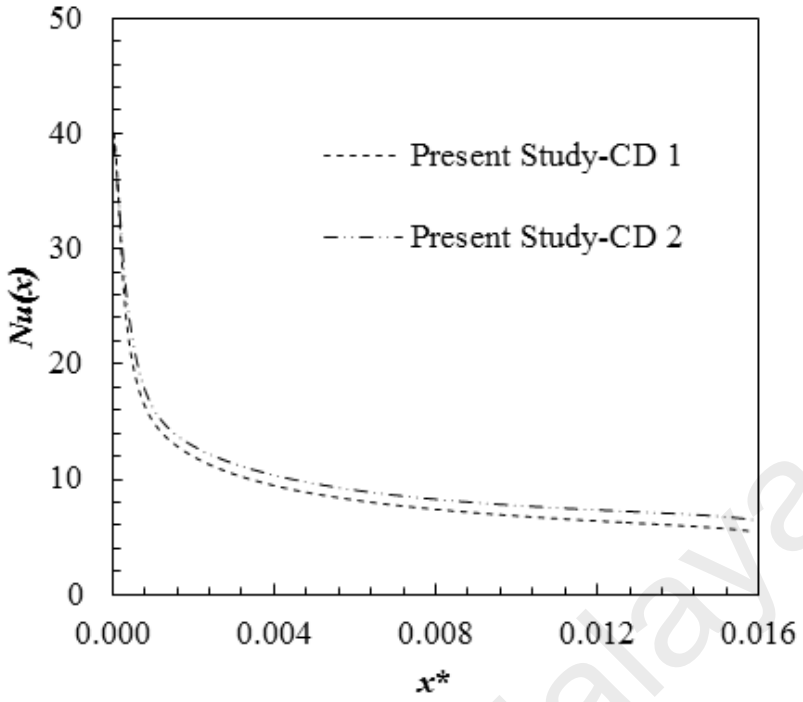

Figure 3.6: Comparison of computational domains for *Nu(x)*.

3.10 Passive Enhancement in MCHS

The present study focuses on five different types of passive enhancements, which are the introductory secondary channel, micromixer between the channels, periodic constrictions, re-entrant obstruction and cavities.

3.10.1 Thermal Enhancement Using Secondary Channel

This study also highlights the potential of using the secondary passage in the MCHS in alternating directions that could enhance the thermal enhancement without pressure loss or with a minimal pressure drop at most. Figure 3.7 shows the MCHS with the alternating slanted secondary passage, together with a detailed view of the computational domain where the fluid flows in the main channel and diverts into the secondary channel.

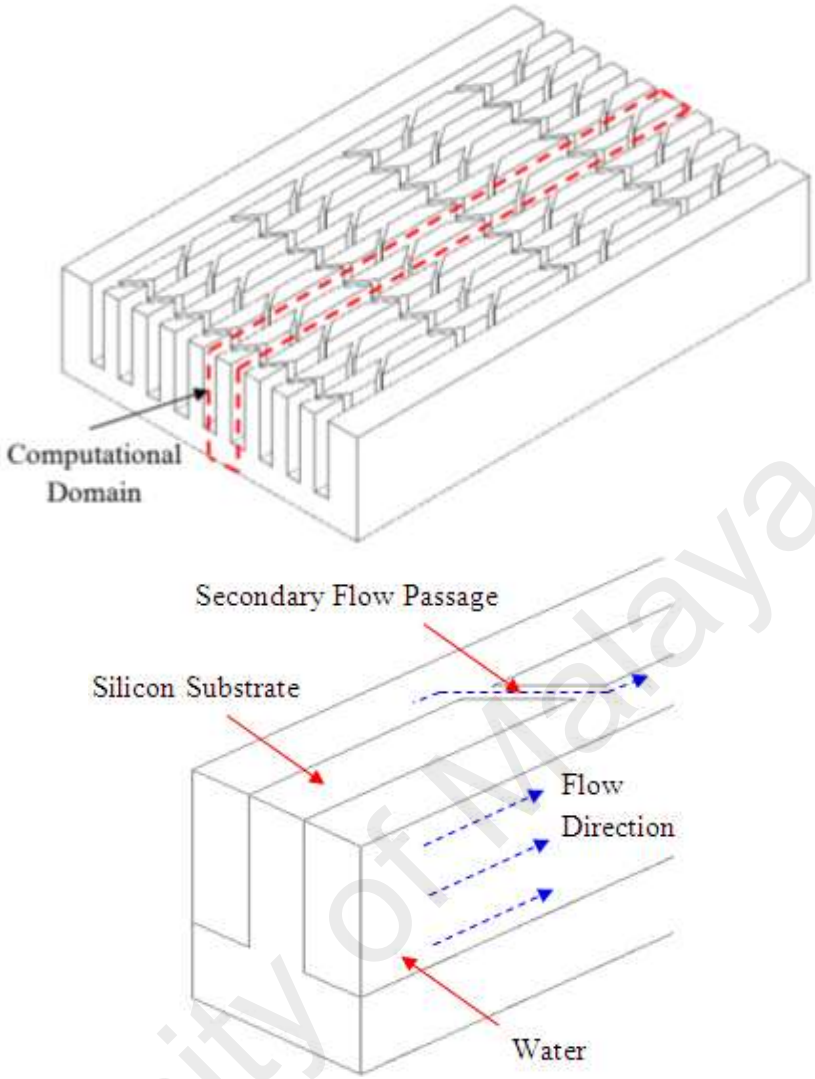

Figure 3.7: Schematic diagram and detailed view of the computational domain of MASP.

All three parameters of the secondary flow passage were analyzed in the present study as illustrated in Figure 3.8. These parameters were the width of the secondary flow passage (α), the length of the longer edge of the channel (β) and the angle of the secondary channel (θ).

The parameters mentioned above were analyzed as follows; $a = \alpha/2w$, $b = \beta/2w$ and θ are the ratios of the secondary passage's width to the channel width, ratio of longer side of the wall to the shorter side and angle of the slanted passage where *w* is

fixed at 100μm. The boundary condition was set as follows; q"=10^6 W/m^2 and $\dot{m}$ = 10^{-3} kg/s.

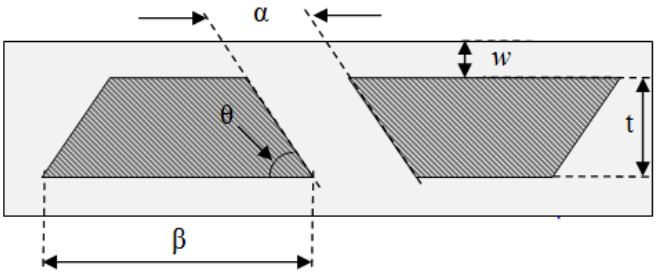

Figure 3.8: Detailed view of wall of the channel with its design variable.

When *a* varies at a fixed value of *b* and θ, the width of the secondary channel varies without any changes in the number of the secondary channel and its angle as shown in Figure 3.9.

Figure 3.9: Geometrical view of variation in *a*.

As the value of *b* change at a fixed value of *a* and θ, the length of the constant cross sectional area changes. It has to be noted that change length of the constant cross sectional area will also change the number of the secondary channel. In another word, variation of b reflects the variation in number of secondary channel. Figure 3.10 shows the geometrical view with variation of *b*.

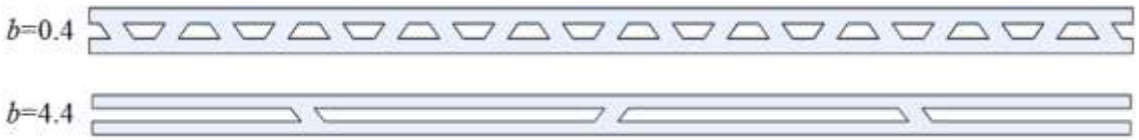

Figure 3.10: Geometrical view of variation in *b*.

Finally, the variation of θ will change the angle of the secondary channel without any other changes as shown in Figure 3.11.

Figure 3.11: Geometrical view of variation in θ.

3.10.2 Thermal Enhancement Using Triangular Micromixer (MTM)

This work focused on introducing micromixers in the MCHS. Figure 3.9 shows the computational domain of the MTM together with its geometrical parameters. The parameters of the MTM; θ, τ and d represents the inner and outer angle and the depth of meeting point of the two edges of the micromixer (depth of micromixer).

The geometrical parameters of the micromixers are not dependent on each other. The distance of the two adjacent micromixers depends on its quantity, where the total distance of the channel is divided equally with the numbers of the micromixers. The integer value considered as the pitch between the micromixers and the floats are also divided equally at the entrance and the exit of the channel.

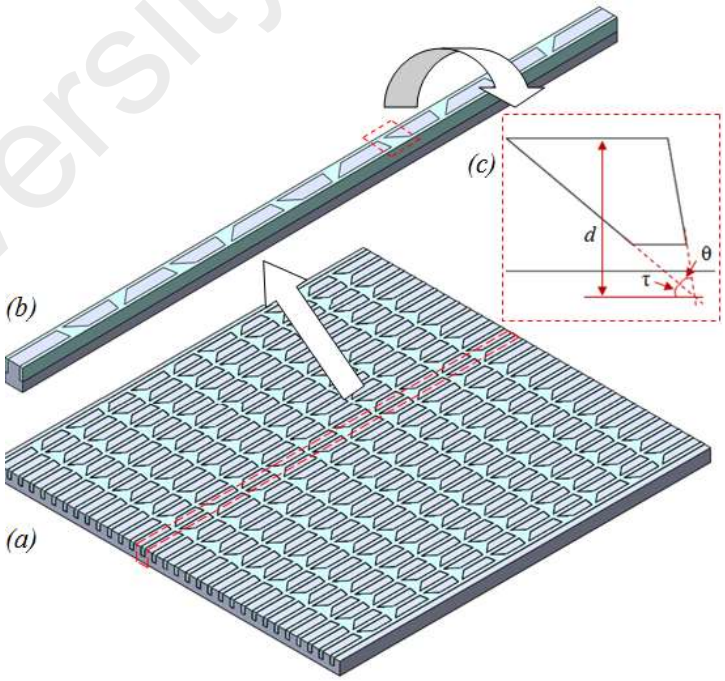

Figure 3.12: (a) schematic diagram of MCHS with secondary channel (b) computational domain and (c) the geometrical parameters of the secondary channel.

The micro mixers are arranged in two different orientation; alternating and parallel as described in Figure 3.13.

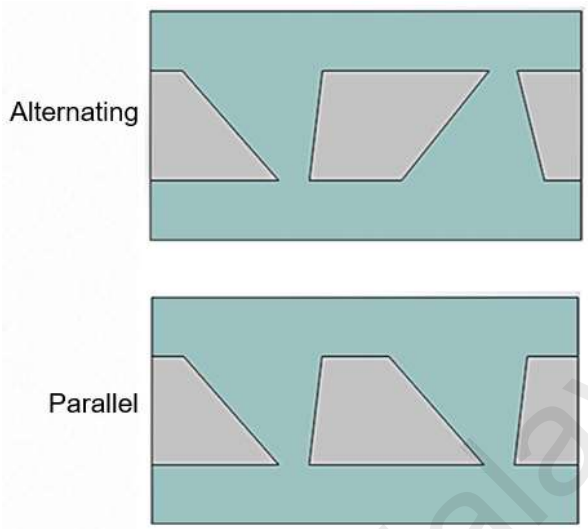

Figure 3.13: Arrangement of micro mixer in MTM.

Simultaneously, the effect of the flow orientation is analyzed based to different flow direction; Direction 1, '*D1*' and Direction 2, '*D2*'. At '*D1*', the micro mixer constrict with flow direction and at '*D2*', the micro mixer expand with flow direction as shown Figure 3.14. The boundary condition associated with these two flow directions are described in

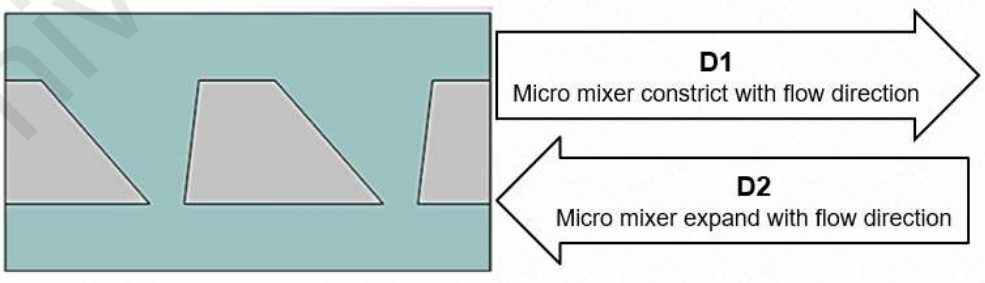

Figure 3.14: Flow Orientation in MTM.

3.10.3 Thermal Enhancement Using Shield-shaped Re-entrant Obstruction

Re-entrant obstructions were introduced on the side walls of the channel in an aligned position. The geometrical configuration and the computational grid of the MCHS with re-entrant obstruction are presented in Figure 3.15. The height, frontal

length and bottom length of the re-entrant obstruction are presented as *a*, *b* and *c* respectively. The dimension of these parameters as set as follows:

$$a = b = c = 20 \ \mu m \tag{3.17}$$

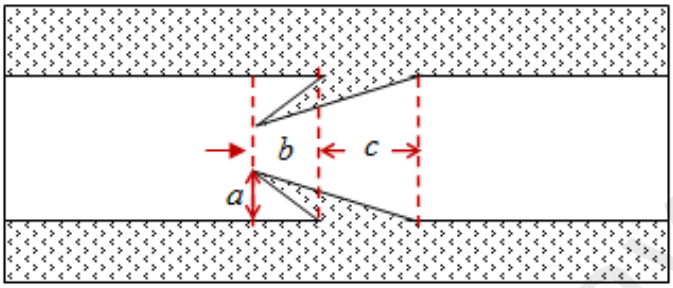

(a)

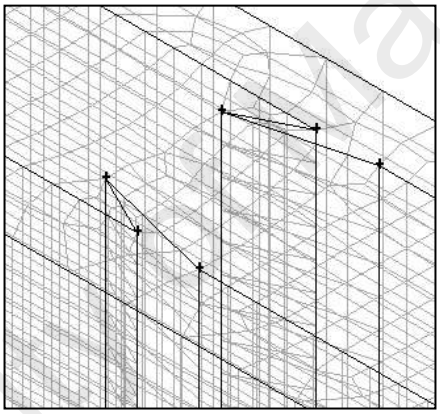

(b)

Figure 3.15: (a) Geometrical configuration of the re-entrant obstruction and (b) its computational domain.

The numerical study was conducted using water as the working fluid at various inlet flow velocities with an inlet temperature of 300 K. The flow was also tested in opposite directions i.e. Direction 1 and Direction 2.

As shown in Figure 3.16, the fluid experiences a sudden constriction and gradual expansion in a stream wise direction when it flows in Direction 1 and oppositely in Direction 2.

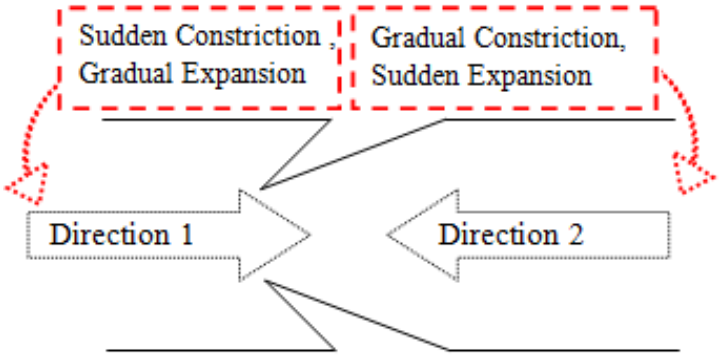

Figure 3.16: (a) Description of flow direction.

3.10.4 Thermal Enhancement Using Elliptical Shaped Periodic Constriction

This study involves the investigation of the effect of the periodic constrictions on the thermal and flow characteristics of the MCHS. Figure 3.17 shows the computational model of the micro channel, together with a closer view of constriction, as well as a detailed frontal view.

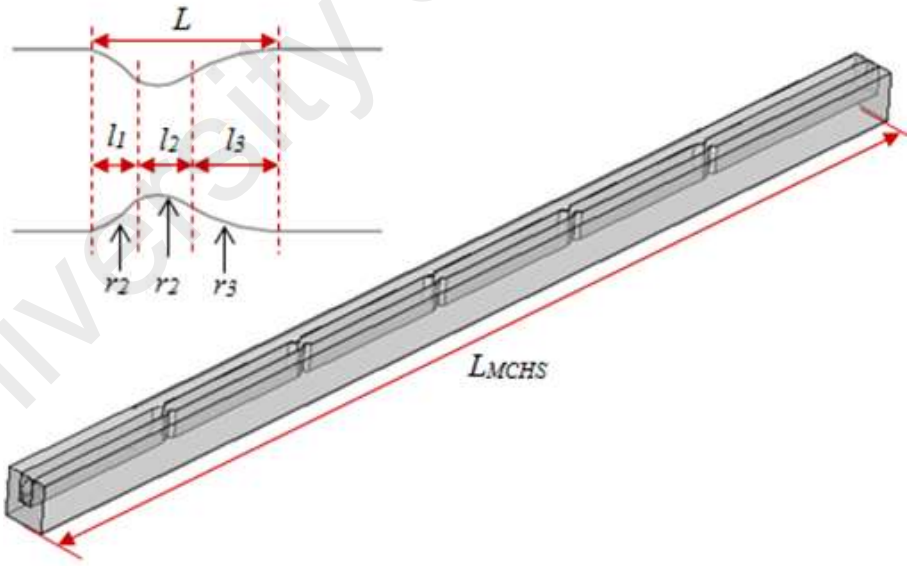

Figure 3.17: (a) Computational model of MCHS with constrictions to detailed view of the constriction and frontal view of the MCHS.

Constrictions in the microchannel heat sink were designed using a curvature profile with three sections; entry, intermediate and exit. In other words, the introduction of the constriction into the fluid stream will change the local stream wise flow area gradually

and repetitively. The geometrical parameters of the constrictions with different numbers of constrictions were assigned into different cases and analyzed at various Reynolds numbers.

The constriction curves were designed in 12 different geometrical configurations based on its length and radius, as well as assigned into different cases. The geometrical configurations of constrictions that were studied are:

a) number of constrictions (n)
b) total length of a constriction (L)
c) entry length of a constriction (l_1)
d) intermediate length of a constriction (l_2)
e) exit length of constriction (l_3)

The detailed descriptions of the geometrical configurations of constrictions for each case are presented in Table 3.2.

A constriction was placed in the middle of the microchannel heat sink and was projected towards the inlet and outlet of the channel at the pitch of 130 μm and 160 μm for n=5 and n=7 respectively.

Table 3.2: Geometrical Parameters of Constriction.

Configuration	n	L (mm)	l_1	l_2	l_3	r_1	r_2	r_3
C1	5	0.1	*L/4*	*L/4*	*L/2*	$2l_1$	l_2	*L*
C2			*3L/8*	*L/4*	*3L/8*	*L*	l_2	*L*
C3			*L/2*	*L/4*	*L/4*	*L*	l_2	$2l_1$
C4		0.2	*L/4*	*L/4*	*L/2*	$2l_1$	l_2	*1.5L*
C5			*3L/8*	*L/4*	*3L/8*	*L*	l_2	*L*
C6			*L/2*	*L/4*	*L/4*	*1.5L*	l_2	$2l_1$
C7	7	0.1	*L/4*	*L/4*	*L/2*	$2l_1$	l_2	*L*
C8			*3L/8*	*L/4*	*3L/8*	*L*	l_2	*L*
C9			*L/2*	*L/4*	*L/4*	*L*	*L*	$2l_1$
C10		0.2	*L/4*	*L/4*	*L/2*	$2l_1$	l_2	*1.5L*
C11			*3L/8*	*L/4*	*3L/8*	*L*	l_2	*L*
C12			*L/2*	*L/4*	*L/4*	*1.5L*	l_2	$2l_1$

A constriction was placed in the middle of the microchannel heat sink and was projected towards the inlet and outlet of the channel at the pitch of 130 μm and 160 μm for n=5 and n=7 respectively.

3.10.5 Thermal Enhancement Using Re-entrant Cavities

The heat transfer enhancement in a microchannel with elliptical shaped cavities on the sidewall is studied. The elliptical cavities could possibly enhance the heat transfer by increasing the fluid mixing, disruption of boundary layer, as well as increase the solid-fluid interface area. The thermal and flow characteristics in the cavity region and the effect of its geometrical parameters are evaluated. The elliptical shaped cavities were created on the side wall of the MCHS and were arranged symmetrically on the opposite walls. The detailed view of the configuration of the cavity in the microchannel heat sink with elliptical cavities on the side walls (MECS) is shown in Figure 3.18. The cavity was constructed with three curvatures that were dependent on the length of each section; expansion (*c*), middle (*d*) and constriction (*e*). The total length and depth of the cavity is defined as '*a*' and '*b*' respectively.

CHAPTER 4: RESULTS AND DISCUSSION

4.1 Outline

The improvement of the thermal performance due to the passive enhancement in the microchannel heat sink and its effect on the fluid flow performance at different flow conditions are presented and discussed in this chapter. The flow characteristic of working fluid at the passive enhancement area and its influence on the heat transfer mechanism is discussed thoroughly.

4.2 Thermal Enhancement Using Secondary Flow

Thermal and hydraulic performance of the microchannel heat sink with an alternating secondary passage (MASP) together with its overall enhancement is presented. The result for the variation of its geometrical parameters is presented in terms of Nu, ΔP, R and η.

4.2.1 Analysis of Design Variable *a*

Firstly, the thermal and hydraulic performance of the MASP with variation of a is studied. Figure 4.1 shows the trend of Nu and ΔP with the comparison of the simple MCHS. It is found that Nu increased noticeably from a=0.4 to 1.6, with a fluctuation at a=0.6. For ΔP, a gradual reduction was observed from a=0.4 to 1.0. It is also found that ΔP was comparable with the simple MCHS at a=1.08 and reduced drastically from a=1.08 to 1.6.It is generally known that thermal enhancement is accompanied with additional pressure loss. However for this analysis, the increase of pressure drop comes together with the reduction in ΔP.

Figure 4.2 demonstrates the tendency of η and R with the increase of a. A tremendous increase was observed in ε considering the fact that the slanted passage gain benefits of both enormous increment of Nu and the decline of ΔP.

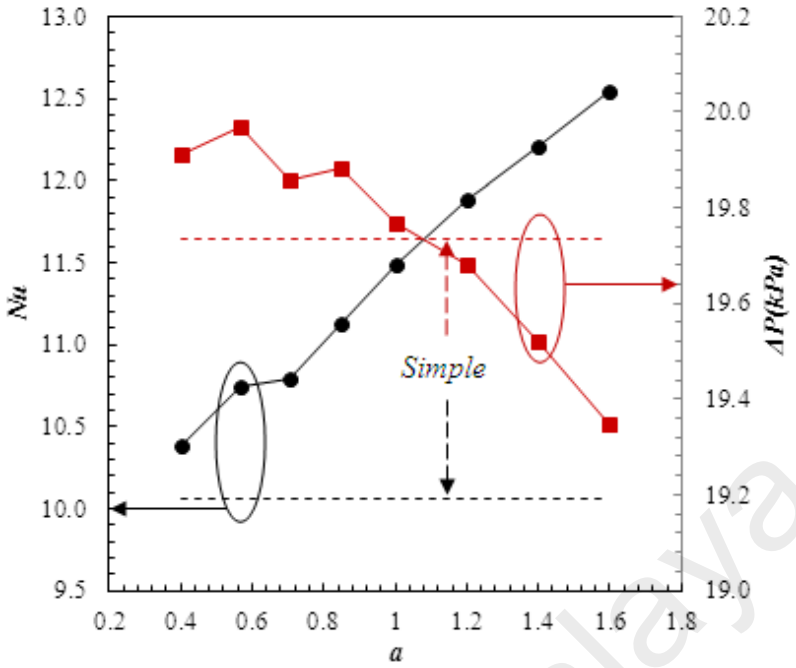

Figure 4.1: Variation of *Nu* and *ΔP* with *a*.

A tremendous increase was observed in ε considering the fact that the slanted passage gain benefits of both enormous increment of *Nu* and the decline of *ΔP*. Besides this, *R* decreased greatly with the increase of *a*, especially from *a*=1.4 to 1.6.

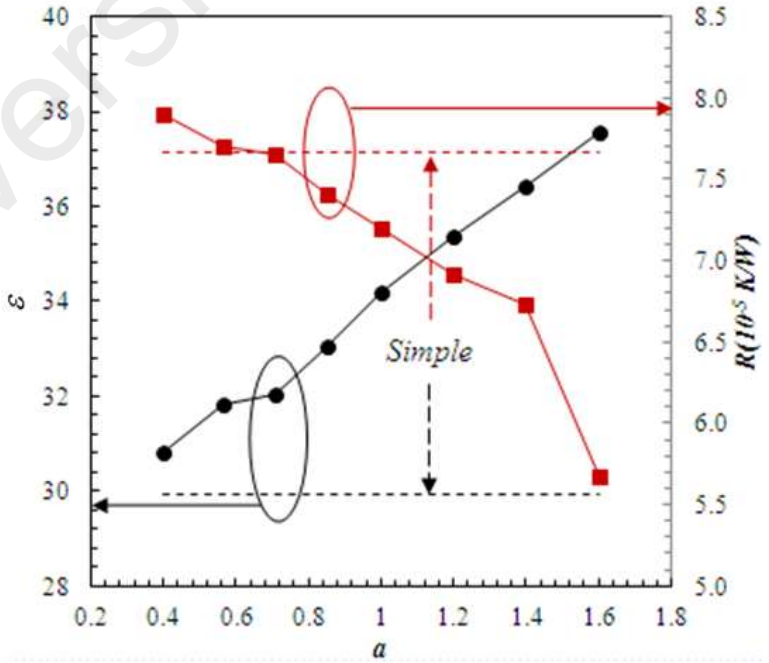

Figure 4.2: Variation of ε and *R* with *a*.

The normalized enhancement for the thermal and flow performance is plotted in Figure 4.3. It can be seen that Nu/Nu_o and η increased, and f/f_o and R/R_o reduced η drastically. It has to also be highlighted that even though Nu/Nu_o and η were experiencing a similar trend, η is higher than Nu/Nu_o from a=1.4 to 1.6, since f/f_o reduced with the increase of Nu/Nu_o. The total improvement of Nu/Nu_o and η was 1.25 and 1.26 respectively. The total reduction of f/f_o and R/R_o for this analysis was 0.98 and 0.74 respectively. Based on variation of this parameter, it can be inferred that the thermal performance enhances with the enlargement of width of the secondary passage. This is because more fluid diverts from the mainstream channel into the secondary channel and eventually improves the convection heat transfer.

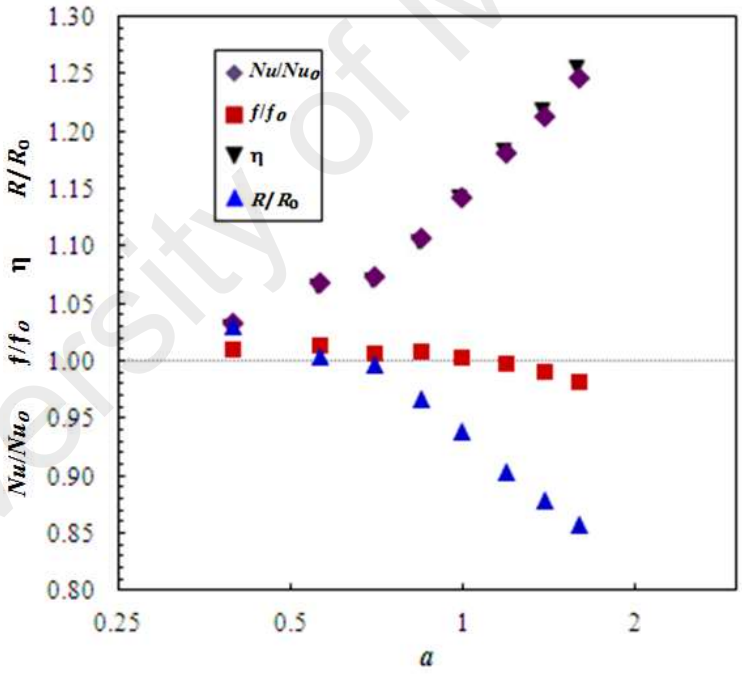

Figure 4.3: Variation of Nu/Nu_o, f/f_o, η, R/R_o with a.

4.2.2 Analysis of Design Variable *b*

The analysis of the dimensionless parameter b was conducted with a=1.6 that was obtained from the previous analysis, and θ was constrained at 45°. Figure 4.4 portrays the trend of Nu and ΔP with the variation of b. This variation can be divided into two

sections; Section 1: 2.8>*b*>1.2 and Section 2: 0.4<*b*<1.2. In Section 1, it can be seen that *Nu* increases gradually with the reduction of *b*.

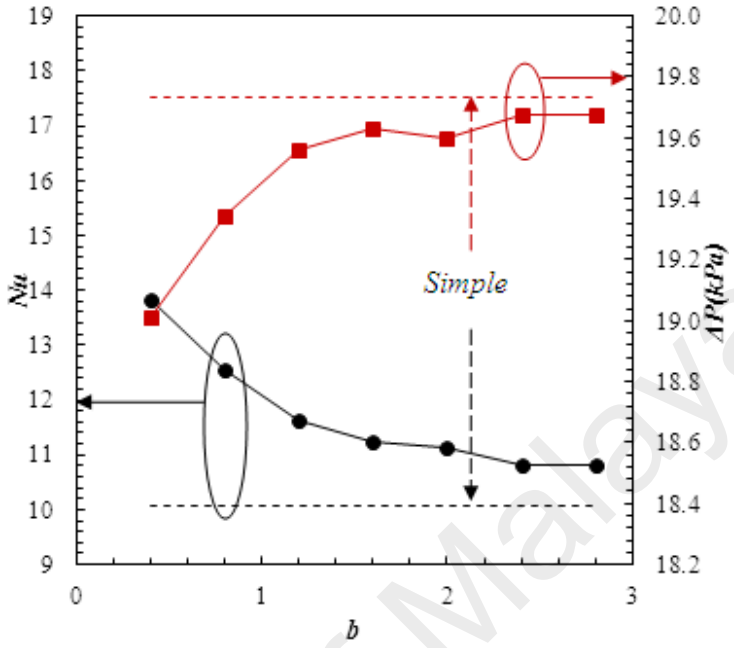

Figure 4.4: Variation of *Nu* and *ΔP* with *b*.

It is also observed that *ΔP* lessens and *Nu* intensifies as *b* reduces. A similar trend is observed in the previous analysis. Besides this, *R* was also found to be reduced with the reduction of *b* as shown in Figure 4.5.

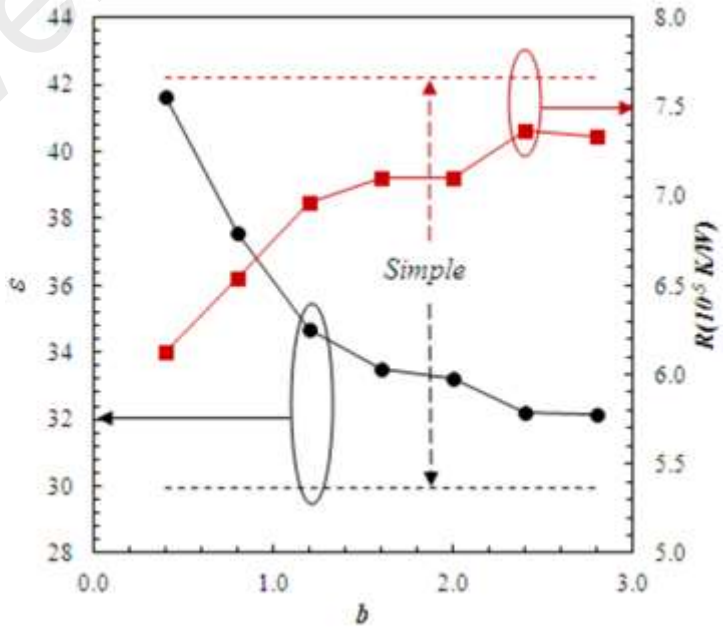

Figure 4.5: Variation of ε and *R* with *b*.

Considering the tremendous enhancement of *Nu* and the reduction of ΔP, it was found that ε increased enormously with the reduction of *b*.Since f/f_o <1, η is higher compared to Nu/Nu_o for all values of *b*. The improvement of η compared to Nu/Nu_o is much higher from *b*=1.2 to 0.4. As observed in Figure 4.6, η=1.39 compared to Nu/Nu_o *b*=1.37 at *b*=0.4. Aside of that, the R/R_o also lessen drastically with reduction of *b* with a minor fluctuation at *b*=2.0.As mentioned earlier, the reduction of *b* reflects the reduction of length of the cross sectional area in the MCHS. It has to also be noted that the numbers of the secondary passage increase as *b* reduces. These two factors result in an increase in the redevelopment of the boundary layer, the diversion of fluid from the main stream channel, the vortices and the interface area of the fluid, and the solid substrate that ultimately enhances the heat transfer.

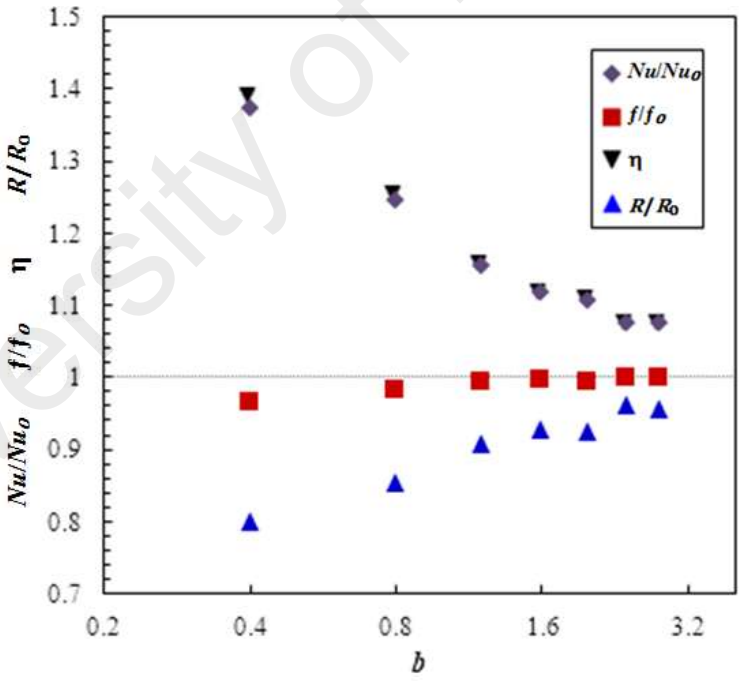

Figure 4.6: Variation of Nu/Nu_o, f/f_o, η, R/R_o with *b*.

4.2.3 Analysis of Design Variable θ

Figure 4.7 portrays the trend of *Nu* and ΔP with a variation of θ, while *a* and *b* are constrained at 0.16 and 0.4 respectively (the best geometry obtained from the previous

analysis). *Nu* increased slightly with the increase of θ. Similar to the previous analyses, the intensification of *Nu* comes together with the lessening in *ΔP*.

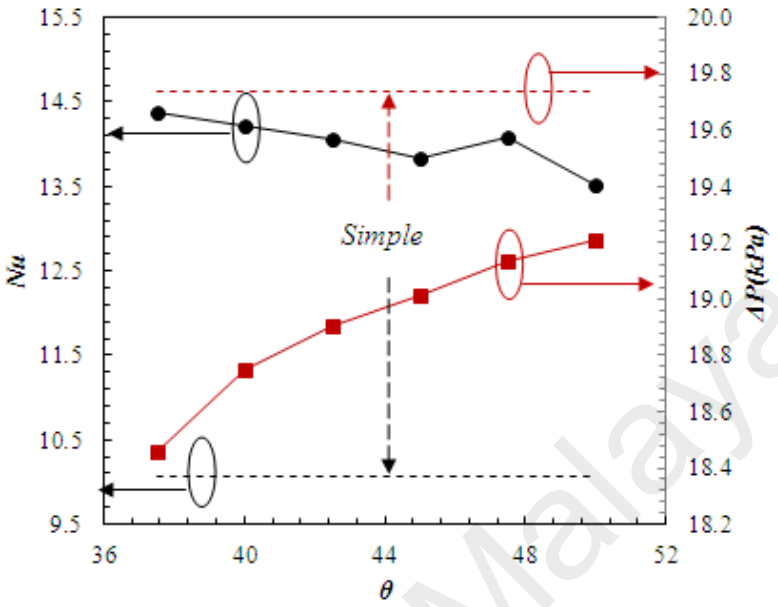

Figure 4.7: Variation of *Nu* and *ΔP* with θ.

In addition, it is also found that *R* reduced dimly with the reduction of θ. A similar trend was observed for *Nu*, *R* and ε with a small fluctuation at θ=48°.Again, η was observed to be consistently higher compared to Nu/Nu_0.

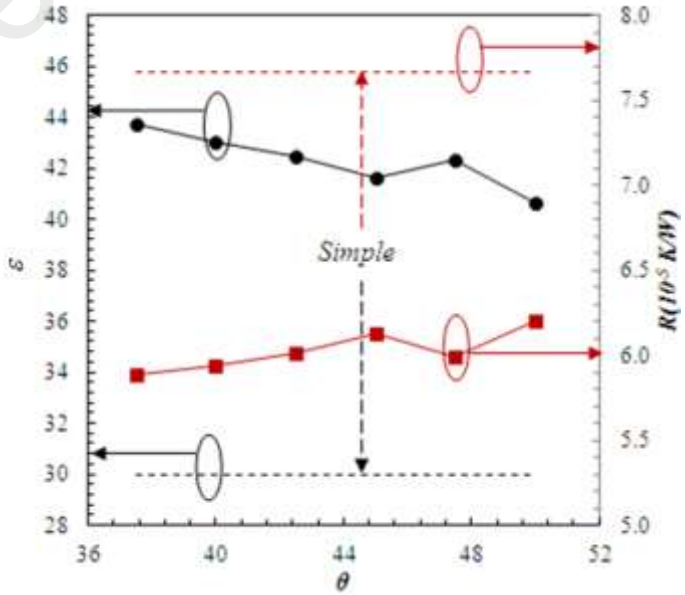

Figure 4.8: Variation of ε and *R* with θ.

Augmentation in the thermal performance due to the reduction of θ can be explained as follows; reduction of θ provides a larger diagonal/entry length at the diversion area of the fluid from the mainstream channel. Furthermore, the fluid tends to divert with a smaller angle and thus, reduction of θ encourages a larger volume of fluid to enter into the secondary channel from the mainstream channel. Ultimately, Nu/Nu_0 and η reached the value of 1.43 =1.46 as the final result. Besides that, f/f_0 and R/R_0 was also observed to reduce faintly with the reduction of θ.

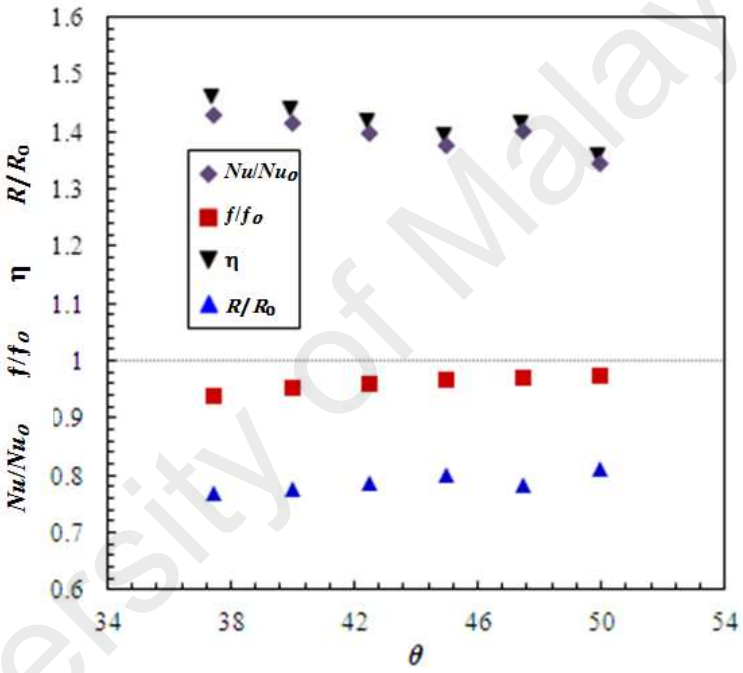

Figure 4.9: Variation of Nu/Nu_0, f/f_0, η, R/R_0 with θ.

4.2.4 Detailed Analysis of Thermal and Hydraulic Characteristic in MASP.

The thermal and hydraulic characteristic of MASP were analyzed in detail and presented in terms of pressure, contour plot, and streamlines to understand the fluid flow mechanism that contributed to the thermal enhancement, together with the reduced pressure drop. The streamline in the secondary passage is shown in Figure 4.10(a). Principally, a fluid vortex is generated when the fluid goes through an interruption. In this case, fluid is diverted from one mainstream channel to the secondary channel, and re-enters to another mainstream channel. Vortices are formed in the secondary channel

since the fluid diverts and mixes from different directions. It can be seen that two vortices are induced in the secondary passage as (highlighted as *A*). The upper vortices that are largely generated due to the fluid diversion from the upper main stream channel and lower one due is due to the vortices generated from the fluid exiting from the upper vortices, bounded by the fluid flow in the bottom mainstream channel.

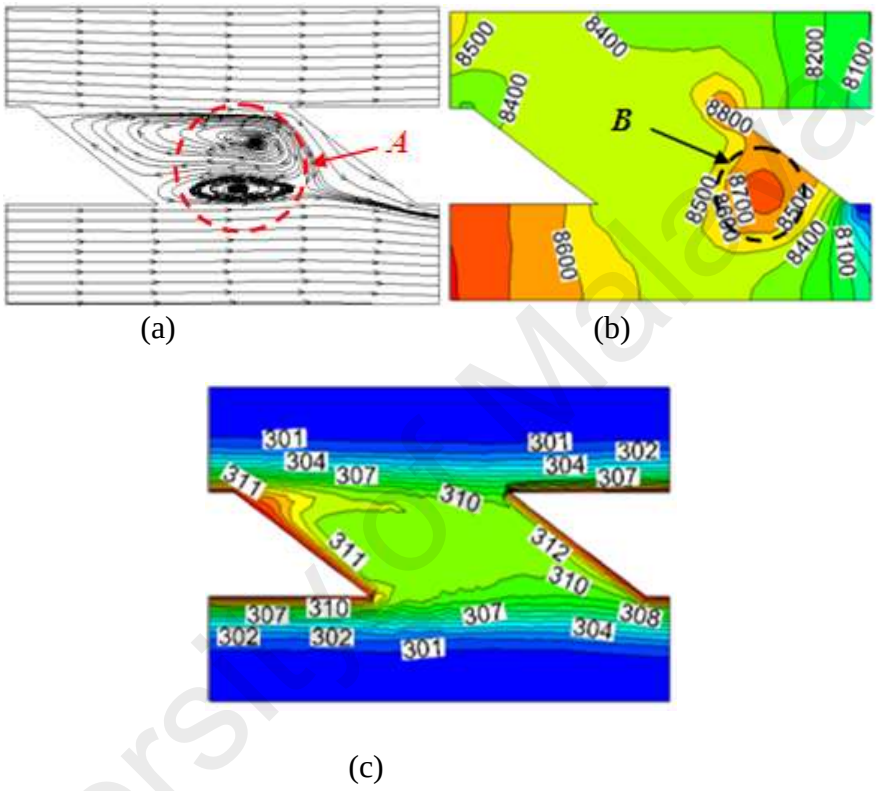

Figure 4.10: (a) Pressure contour plot (Pa), (b) isotherms (K) and (c) streamlines of MASP (*a*=0.16, *b*=0.40 and θ=37.5°) at *x*=0.48-0.52mm and *y*=0.3mm.

The stagnation point in the secondary passage (highlighted as *B* in the pressure contour plot in Figure 4.10(b)) is formed due to the merge of fluids from various directions. The fluid travels in three different directions at this point. The first direction is the fluid diverting from the upper vortices to the lower vortices (-*x* direction). The second direction is the remaining fluid from the upper vortices together with some fluids from the upper mainstream travelling to the lower mainstream channel (+*y* direction). The third direction is where the fluid leaves from the lower vortices to the lower mainstream channel (+*x* direction).

It is also observed from isotherms in Figure 4.10(c) that the fluid temperature in the secondary passage, especially in area of the vortices, is in the medium range, when compared to the mainstream fluid and wall temperature. On the other hand, a large temperature gradient was observed in the peripheral area of the vortices. This suggests that the vortices created great fluid mixing and heat absorption from the wall.

4.3 Thermal Enhancement Using Triangular Shaped Micromixer

Thermal enhancement of the microchannel heat sinks with triangular shaped transverse micromixer (MTM) is numerically investigated. The effect of the geometrical parameters of the micromixers in the MCHS on the thermal and flow performance is analyzed. These performances are shown in the form of the friction factor and the average Nusselt number. The tradeoff between the thermal enhancement and pressure loss is measured using an overall enhancement coefficient.

4.3.1 Effect of Micromixer Orientation, Cooling Fluid Volume Flow Rate and its Flow Direction

Micromixers are designed in two orientations; parallel and alternating. This is in order to investigate the effect of the flow pattern in the MTM. The volume flow rate of the cooling fluid was studied from $G = 4\times 10^{-7}$ to 10×10^{-7} m^3/s with different inlet directions; *D1* and *D2*. The boundary conditions associated with the different flow directions are explained in Section 3.5. The arrangement of the micromixer is defined as *A1* and *A2* for alternating and parallel arrangement respectively. To be specific, *A1* provides an alternating flow between one to another channel, whereas the flow diverts consistently into the only channel in *A2*. As for the flow arrangement, the micromixer converges with the flow direction in *D1* and diverges in *D2*. Heat flux of 1.2×10^6 W/m^2 was supplied at the bottom surface of the silicon substrate. Both the inner (θ) and outer

angle (τ) were constrained at 30°. The numbers of the micromixers between channels were fixed at 6.

4.3.1.1 Heat Transfer Characteristic

The evaluation of the thermal characteristic was performed based on the Nusselt number since the advection heat transfer is dominant. The propensity of *Nu* and Nu/Nu_0 with the increase of *G* at different flow directions and micromixer arrangements is shown in Figure 4.11. *Nu* of the MTM is higher compared to the simple MCHS for all given values of *G*, and *Nu* increases with *G* for both, the MTM and simple MCHS. However, *Nu* increases at higher rate in the MTM compared to the simple MCHS. For instance, at $G=4\times10^{-7}$ m^3/s, MTM (*A1, D2*) bettered the simple MCHS by 17.6%, whereas at $G=9\times10^{-7}$ m^3/s, it improved by 25.2% compared to simple MCHS.

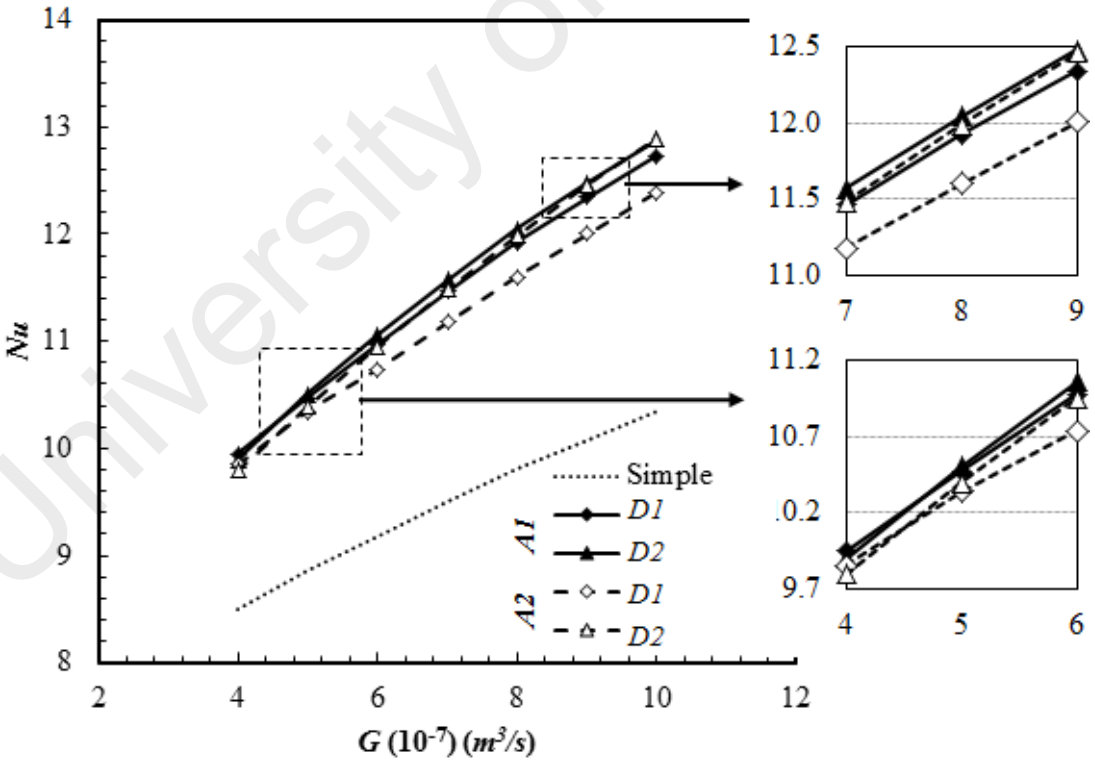

Figure 4.11: Variation of *Nu* with Variation of *G*, Flow Orientation and Micromixer Arrangement.

A very trivial difference was found between *D1* and *D2* at $G=4\times10^{-7}$ m^3/s for both arrangements. It was also found that at the lower flow rate, the flow direction did not seem to affect the thermal performance of the MTM for both arrangements. This trend prolonged for *A1* until $G= 5 \times 10^{-7}\ m^3/s$, where *Nu* in both directions lie at the same point and gradually dispersed after that. In Direction 2, *Nu* began to rise with a larger accretion compared to Direction 1 in both arrangements, as *G* passes $5 \times 10^{-7} m^3/s$. Arrangement *A1* exhibited a higher *Nu* for both flow directions until $G<6\times10^{-7}$ m^3/s. However, the ascent of *A2* became more precipitous and outperformed others at $G=10\times10^{-7}$ m^3/s

The trend of Nu/Nu_0 is presented in Figure 4.12 in order to provide a clearer perception of the variation in Nu/Nu_0 at different flow rates, flow directions and micromixer arrangements. Generally, a gradual increment was observed in Nu/Nu_0 for all configurations, and *D2*, *A1* reached to the peak value at $G=10\times10^{-7}$ m^3/s.

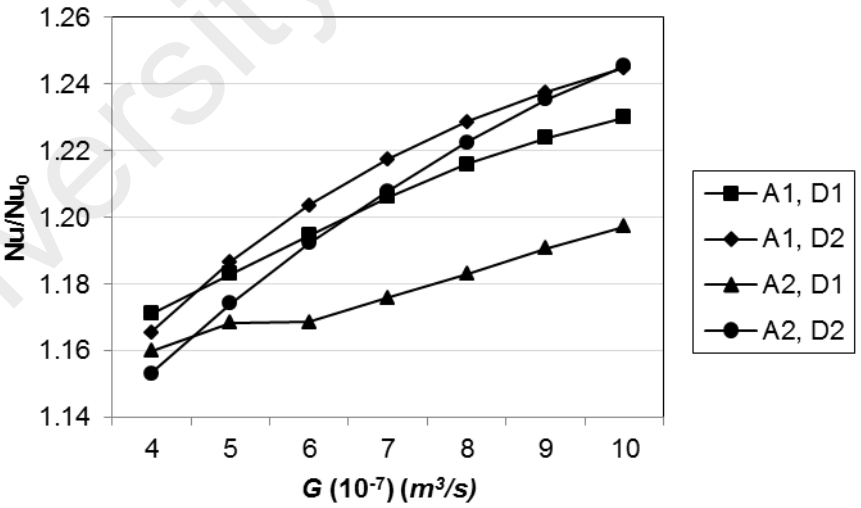

Figure 4.12: Variation of Nu/Nu_0 with variation of *G*, flow orientation and micromixer arrangement.

A higher heat transfer was achieved in a diverging micromixer. This is due to the reverse pressure gradient micromixer encouraging the fluid to enter the micromixer and

spool up into vortices before exiting. This will then ultimately improve the convection heat transfer. The alternating flow orientation also enhanced the flow oscillations that signified the heat transfer.

4.3.1.2 Friction Factor Characteristic

It is known according to the Moody chart, that f through a straight channel reduces with an increase in flow rate in laminar flow before it reaches the transition zone. On the other hand, f of the MCHS with passive enhancement will typically increase, compared to the simple MCHS with the increase of flow rate (Chai, Xia, Wang, et al., 2013; Chai et al., 2011; Kuppusamy et al., 2013, 2014; Xia, Chai, Wang, et al., 2011; Xia, Chai, Zhou, et al., 2011; Xia et al., 2013).

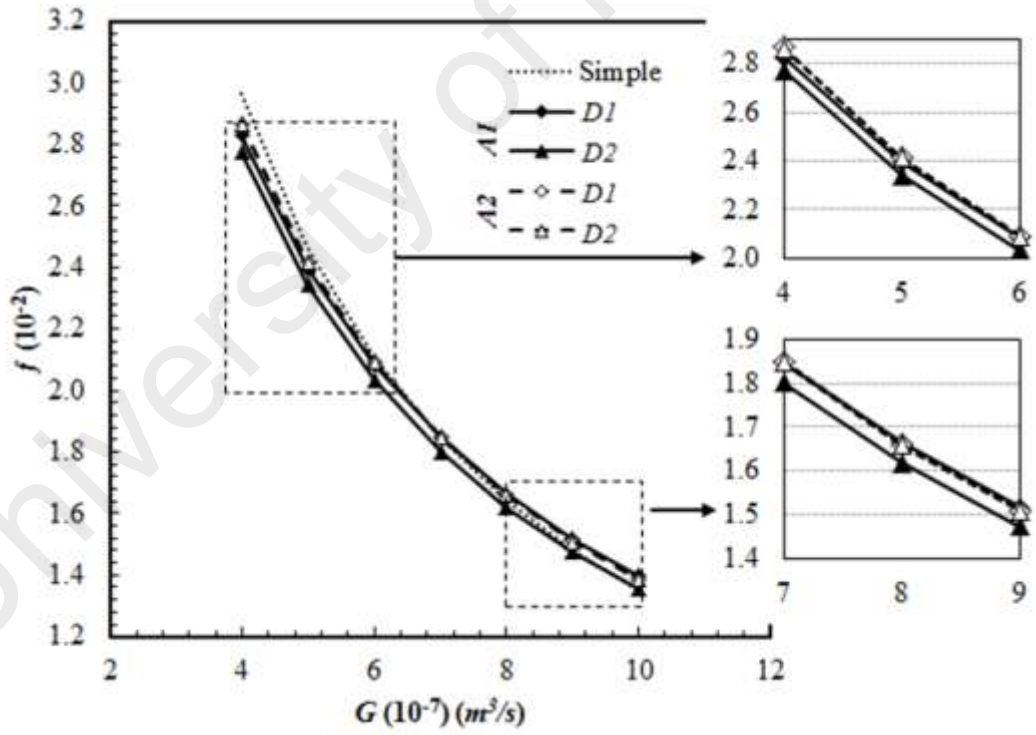

Figure 4.13: Variation of f with variation of G, flow orientation and micromixer arrangement.

As expected, in Figure 4.13, f reduces gradually for both, the MTM and simple MCHS as G increases from 4 to 10×10^{-7} m^3/s. Ironically, f of the simple MCHS is higher compared to all MTM at $4\times10^{-7}<G<5\times10^{-7}$ m^3/s. However, since its degree of

descent for the simple microchannel is greater compared to the MTM, it overlapped all MTM at G=7×10^{-7} m^3/s except '*D2, A2*' where it overlapped at G=9×10^{-7} m^3/s. It was found that the flow direction had a negligible effect on f for *A2* where f reached to the lowest value at G=9×10^{-7}.

In Figure 4.14, the plot shows that f/f_0 increases gradually with *G*. f/f_0 of '*A2, D2*' is found to be expressively smaller compared to others and it meets its lowest point at G=4 × 10^{-7}. f/f_0 reached its apical point at '*A2, D1*' at G=10 × 10^{-7}. The fluid flow in the micromixer with an alternating direction had a better performance compared to the parallel direction. This is because in a parallel direction, the cooling fluid is repeatedly forced into one channel, while the other channel discharges the cooling fluid from the mainstream continuously. This phenomenon results in pressure being built up in one of the channels. On the other side, the convergent micromixers with flow direction have a smaller outlet than the inlet that impedes the flow and deteriorates the pressure drop. Diverging micromixers with flow direction at alternating positions demonstrated the least pressure loss and overlap the simple MCHS at G=9 × 10^{-7}.

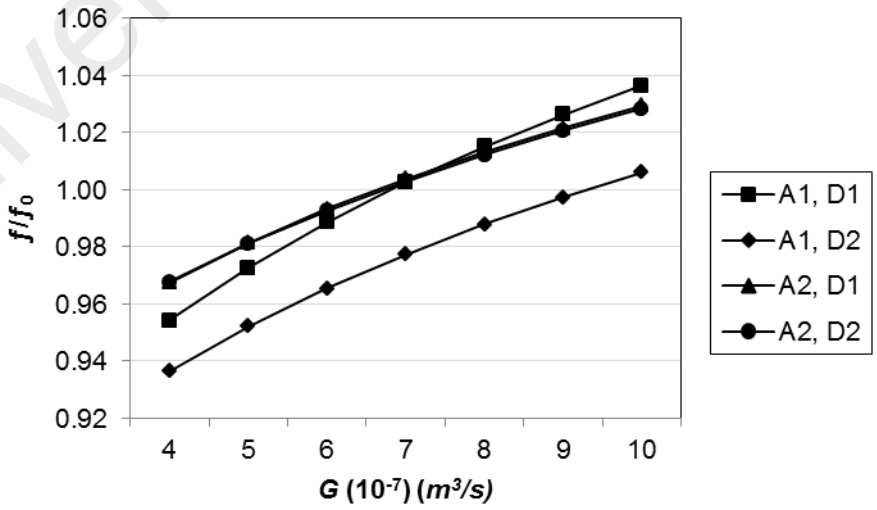

Figure 4.14: Variation of f/f_0 with variation of *G*, flow orientation and micromixer arrangement.

Water from the main stream channel that slips over the micromixer ensued less friction factor compared to the simple channel at a lower flow rate, especially in Direction 2. Nevertheless, this effect fades as the flow rate increases. This is because as the flow rate increase, the secondary flow regime from the micromixer interrupts the main stream flow that increases the pressure loss of MTM.

4.3.1.3 Overall Enhancement

It is a general fact that the increment of *Nu* is always accompanied by an additional pressure drop. The compensation of Nu/Nu_o with f/f_0 is assessed based on the overall enhancement of η. The plot shows that Nu/Nu_o intensifies progressively with the increment of *G* as shown in Figure 4.15. As the *G* increases, the improvement of η for the respective micromixer arrangement and flow direction starts to increase at a different acclivity.

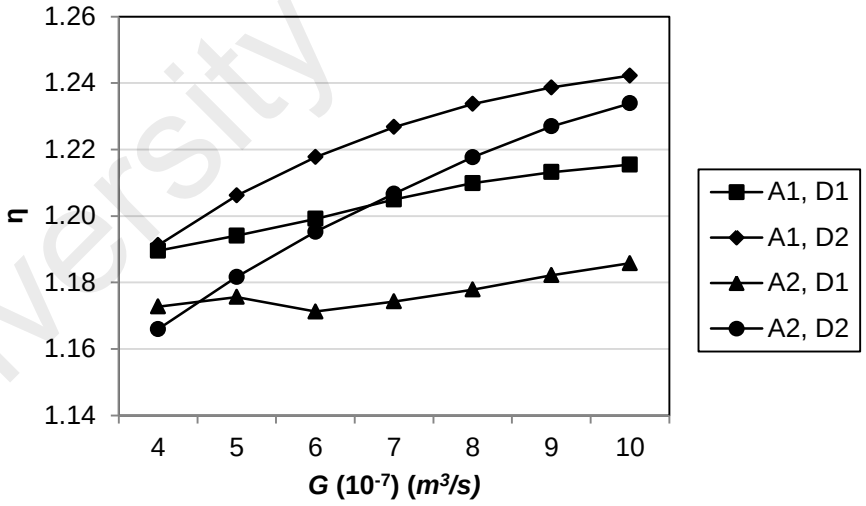

Figure 4.15: Variation of η with variation of *G*, flow orientation and micromixer arrangement.

The most significant improvement observed among the MTM is for *A2, D1* where η increases from the lowest among the MTM to the highest. In terms of sensitivity of flow direction on the micro mixer arrangement, *A2* was more responsive to the flow direction, where a larger difference was observed between the flow directions at a

higher *G*. Besides, a drastic improvement can be observed in η at *A1, D2* from $G = 4\times10^{-7}$ m^3/s to 10×10^{-7} m^3/s. This was followed by *A2, D2* where it was with a slightly lower η for a given *G*. It should be noted that the variation of Nu/Nu_0 for both, *A1, D2* and *A2, D2* with *G* were almost the same, but f/f_0 of *A1, D2* was significantly lower compared to *A2, D2*. This fact leads to a significant improvement of η at *A1, D2*.

It is a common fact that with the increase of flow rate, the magnitude of vortex enhances and the thermal boundary layer in the constant cross-sectional area shrinks. Inclusion of micromixers in a MCHS signifies this effect as vortices are formed in it. The cooling fluid temperature in the center of vortex region is higher compared to the surrounding vicinity. Figure 4.16 portrays the pressure contour plots and isotherms of the micromixer at *A1, D2* at $G = 9 \times 10^{-7}$ m^3/s and *A2, D1* from $G = 4 \times 10^{-7}$ m^3/s. While the former has a large fluid vortex, the latter has two vortices that are comparatively smaller where each of them swirls at the opposing direction. These inimical whirlpools are formed owing to the repetitive diversion of the mainstream fluid into the same channel (upper channel) that makes it very repulsive.

It can be observed in Figure 4.16(b) that the pressure at end of the latter mainstream, the pressure at the upper channel is much lower compared to the lower channel, unlike in the former channel where the exit pressure of both mainstreams are almost same. Thus, the fluid in the micromixer is deterred from entering the channel and it circulates at a different stationary focal point in an opposing direction continuously. Unfortunately, such adverse fluid circulation impeded the heat transfer and increased the pressure significantly. A very high temperature was observed in this proximity and this can seriously deteriorate the heat transfer.

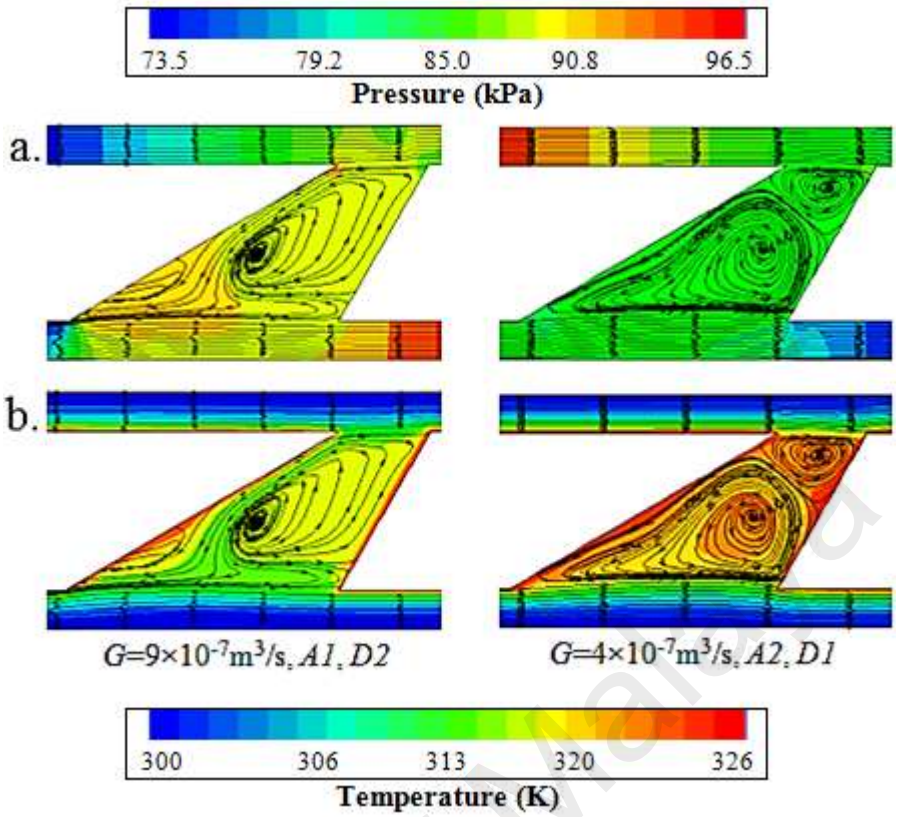

Figure 4.16: (a) Pressure contour plot and (b) isotherms in the secondary channel with different flow rate (*G*), micromixer arrangement (*A*) and flow direction (*D*).

4.3.2 Effect of Inner Angle 'θ' and Outer Angle 'τ' of the Micromixer

Effect of the variation in the inner angle 'θ' and outer angle 'τ' on the thermal and flow characteristic is studied. These two parameters determine the shape of the micromixer. Even though the highest performance was obtained from '*A1, D1*' from the previous analysis, it had a higher friction factor compared to the simple MCHS at $G = 9 \times 10^{-7}$ m^3/s. Since the objective of the study is to attain the thermal enhancement without additional pressure loss, configuration '*D2, A2*' was selected at $G = 9 \times 10^{-7}$, for this analysis. The '*d*' is fixed at 10μm whereas '*n*' is constrained at 6.

4.3.2.1 Heat Transfer Characteristic

Nu increased greatly with the increment of θ for all τ as shown in Figure 4.17. While having the baseline value of the simple MCHS at *Nu*=10.08, a noticeable changes can

be observed in Nu of MTM with va f and τ. For a given θ, *Nu* accretes with τ. Indeed, the accession progress of f with θ also improves at τ=30°.

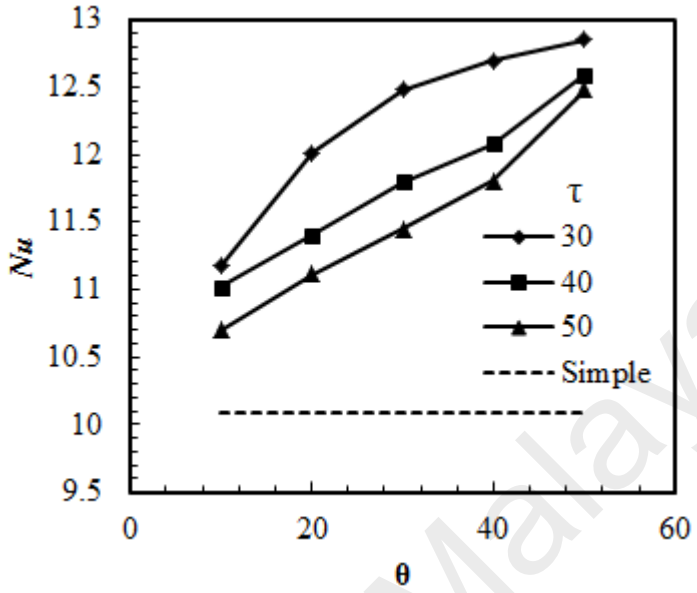

Figure 4.17: Variation of *Nu* with variation of θ at different τ.

The micromixer θ=50°, τ=30° exhibited a very poor heat transfer due to its sharp diversion angle and confined area. Thus, only a small amount of fluid from the main stream channel was redirected into the micromixer.

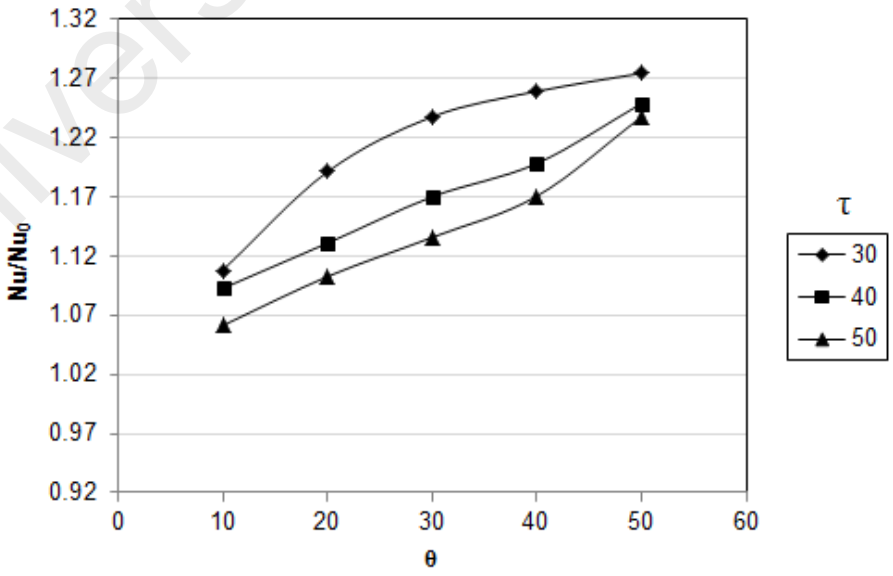

Figure 4.18: Variation of Nu/Nu_0 with variation of θ at different τ.

Aside from that, there was no fluid circulation observed in the micromixer and the cooling fluid directly flowed towards the lower main stream channel. It was also observed that the micromixer was environed with a very high fluid temperature. This suggests poor fluid mixing in that region, consequently lowering the thermal enhancement. As $\theta \rightarrow 50°$ and $\tau \rightarrow 30°$, the convective heat transfer progressively improved as illustrated in Figure 4.18. Besides the changes in the shape, the size of the micromixer was also enlarged. This encouraged more fluid to imp into the micromixer and engender more vortices that will consequently improve the fluid mixing and shorten the thermal boundary layer.

Laminar stagnation was built up at the adjoining section between the mainstream region and the micromixer. This is due to the collision of fluid from these two regions that lead sudden reduction in the fluid velocity. This laminar stagnation zone has slightly hampered the heat transfer. In spite of this impediment, the overall heat transfer improved due to several factors; (1) multiple fluid recirculation; (2) redevelopments of the boundary layer; and (3) enlargement in the heat transfer area at the solid- fluid interface. The enormous heat transfer intensification due to these factors has compensated the minor heat transfer deterioration that happened at the pressure stagnation.

4.3.2.2 Friction Factor Characteristic

A tremendous reduction in f is observed with a decline of θ, especially for $\tau=30°$ as portrayed in Figure 4.19. The escalate amplitude of f varies depending on τ, where; as τ reduces, the reduction of f becomes more vigorous with the increment of θ. For instance, for $\tau=30°$, f crosses the simple MCHS with only a small increment of θ ($<30°$), since the descent scope is very large. This is followed by $\tau=40°$ at $40° < \theta < 50°$. Whereas for $\tau=50°$, f remains the same compared to that of the simple MCHS for all

values of θ. From the trend of f, it can be inferred that the increment in the inner angle and reduction in the outer angle reduces f greatly.

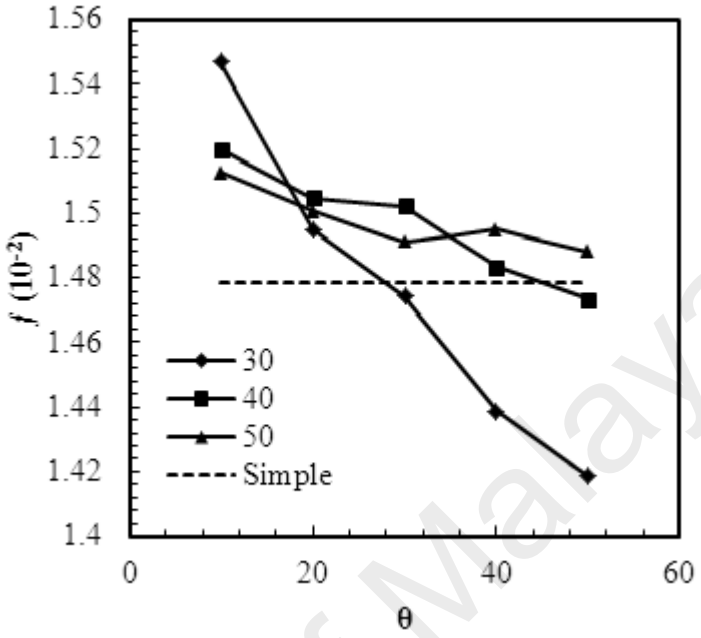

Figure 4.19: Variation of f with variation of θ and τ.

Reduction of τ provides a smaller diversion angle and eases the cooling fluid to impinge from the mainstream channel to the mixer section.

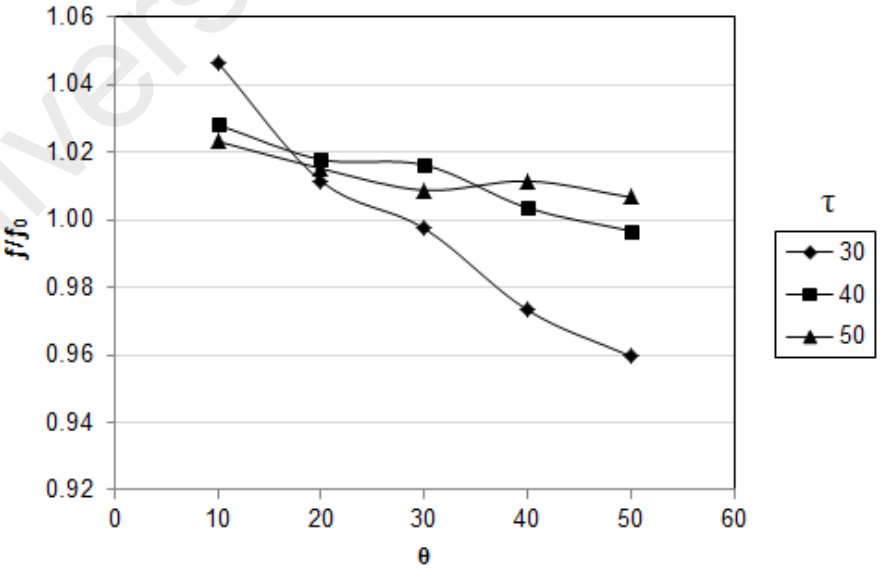

Figure 4.20: Variation of f/f_0 with variation of θ and τ.

Likewise, increment of the θ results in an inverse pressure also invades the fluid into the micromixer section. Moreover, the micromixer area enlarged and the fluid in the

mainstream channel slipped over this area. The velocity of the fluid decreased and it redirected at the periphery of the exit of the micromixer and the mainstream channel because of the wall stagnation and the viscosity of fluid. This resulted in a bigger area of laminar stagnation area in this section that also helped the fluid to slip over this region. These are the two major reasons of significant reduction in a friction factor in this analysis.

4.3.2.3 Overall Enhancement

For the comparison of tendency of f/f_0 and Nu/Nu_o, the variation of η with θ was plotted at different τ. On one hand, the variation of f receded drastically with θ. Conversely, *Nu* improved considerably where a noticeable improvement was noticed in η. As shown in Figure 4.21, the proclivity is very much similar to Nu/Nu_o, but at a greater ratio proportion due to the reason mentioned above.

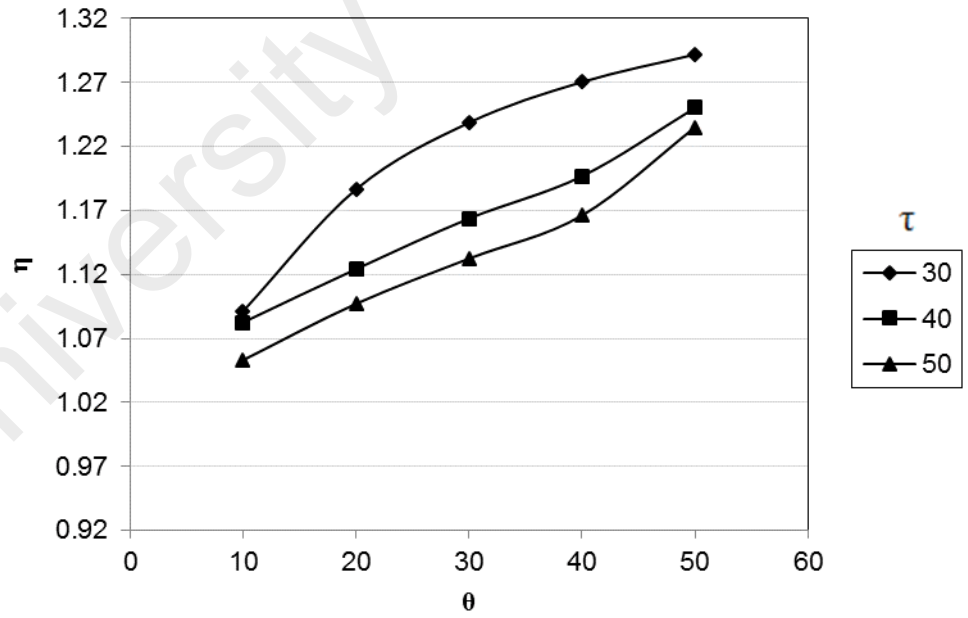

Figure 4.21: Variation of η with variation of θ and τ.

Figure 4.22 shows that the angle of the micromixer is very steep and its size is very slender. Therefore, only a partial amount of fluid enters this region and directly flows towards the lower main stream channel. No fluid recirculation was observed due to the

limited space. As θ→50° and τ→30°, the micromixer becomes sharper in its shape and therefore, the pressure gradient becomes much larger. Moreover, the size of the micromixer size is also enlarged and consequently increases the solid-fluid interface area. This allows the convection heat transfer in the micromixer to increase immensely. As more fluid enters the micromixer, multiple vortices are generated with high intensity due to the reverse pressure difference across it.

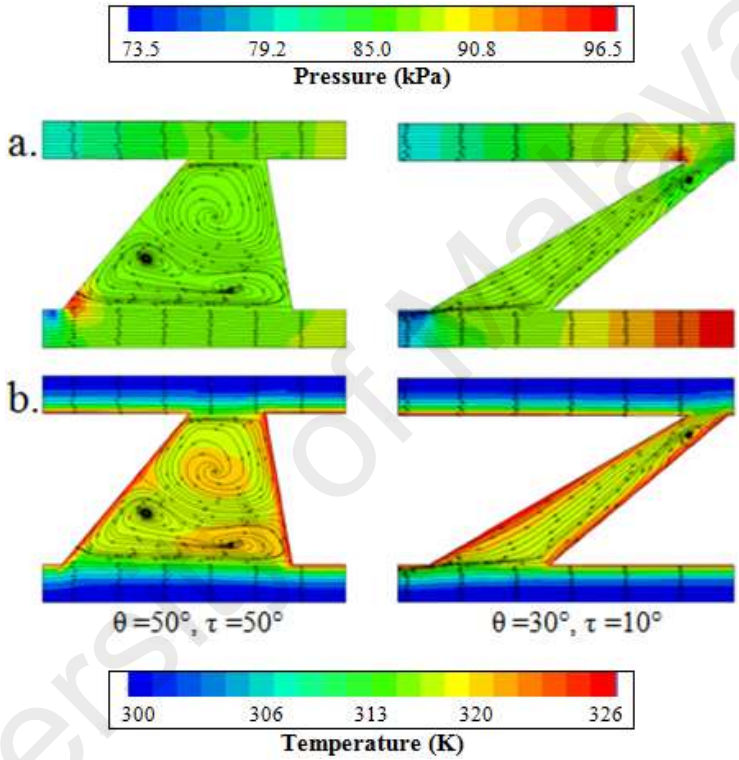

Figure 4.22: (a) Pressure contour plot and (b) isotherms in the secondary channel with different θ and τ.

Isotherms in Figure 4.22 shows that higher cooling fluid temperature in the core of the vortices in θ=50°, τ=50° implies that a greater heat transfer happens in this micromixer. The fluid pressure is in the same locality, nevertheless, it is lower compared to the neighboring region. The pressure plot in the micromixer θ=50°, τ=50° shows that the pressure stagnation is formed at the adjoining point of the micromixer and lower main stream channel. A low pressure area is typically formed at the area flow split from the mainstream region and the high pressure area (pressure stagnation) that is normally built when the fluid merges from different directions.

4.3.3 Effect of Depth '*d*' and Number '*n*' of the Micromixer.

Variation in the thermal and flow performance with an increment in depth (*d*) and numbers (*n*) of the micromixer in the microchannel heat sink is analyzed. The analysis was performed by maintaining θ and τ at 50° and 30° respectively in a micromixer '*A1,D2'* at $G = 9 \times 10^{-7}$ m^3/s. The range analysis performed is from 0.1 to 0.2μm and 6 to 10 for *d* and *n* respectively. It has to be underlined that the varying of d directly affects the size of the micromixer and a combination of *d* and *n* will determine the sectional length of the constant segment of MTM.

4.3.3.1 Heat Transfer Characteristic

Figure 4.23 shows that *Nu* increased progressively with the increment of *d*. Besides that, a visible increment was observed in the variation of *n*. However, a smaller increment was observed at $6<n<8$ compared to $8<n<10$. This trend suggests that the increment of the numbers of the micromixer has reached to its maximum potential to enhance the thermal performance. Two possible reasons can be proposed for the reduction in the ascent scope: (1) the thermal boundary layer has shrunken sufficiently; (2) the breadth of the vortex has begun to increase in size rather than its quantity. Further increment *d* and *n* would probably not improve the heat transfer or deteriorate the thermal performance in a worst case scenario. Nu/Nu_0 reached to its peak at $d=0.2$ and $n=10$ as a corollary from the increment and reduction of *d* and *n* as portrayed in Figure 4.23. This trend makes sense as the increment of the size of the micromixer would provide a larger area in the micromixer that will consequently enhance the fluid diversion from the main stream flow region and its mixing in the micromixer. Similarly, increment of the numbers of the micromixer also results in more fluid quivering and mixing. Moreover, a repetitive boundary layer development in the constant cross sectional area also improves the thermal enhancement.

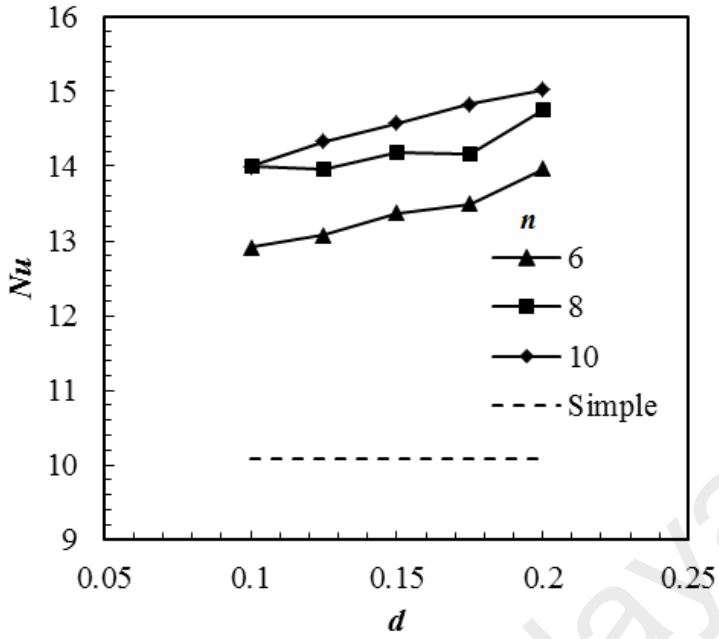

Figure 4.23: Variation of *Nu* with variation of *d* at different *n*.

As discussed earlier, the significance of the forced convection is dependent of the fluid recirculation and directly affects the size and the intensity of the vortices.

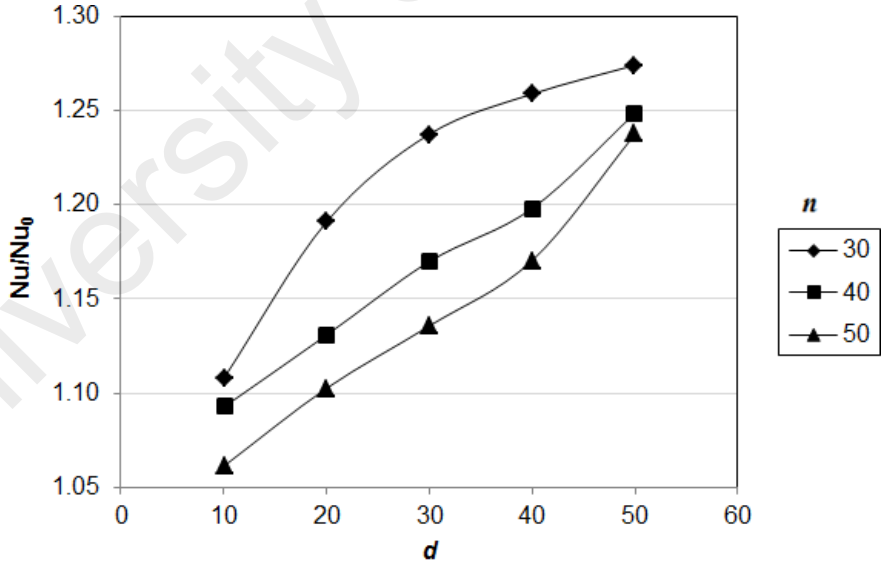

Figure 4.24: Variation of Nu/Nu_0 with variation of *d* at different *n*.

Enlargement of the micromixer augments the peripheral area of the vortex that increases the size of the vortex and eventually improves the fluid mixing in the bulk flow. As *d* and *n* increase, the numbers of vortex are amplified and the thermal boundary development is shortened which will impede the heat transfer rate. The fluid

oscillation, concurrently outweighing the heat transfer rate drawback over the shorter length of the total constant cross-sectional area.

4.3.3.2 Friction Factor Characteristic

An opposing trend is seen in *f* compared to the *Nu* in Figure 4.25 where a drastic reduction is observed with the increment of *d*. Increase of *n* also reduced the friction factor of the MTM, even though the tendency of the reduction was found to be inconsistent. Based on this phenomenon, it was found in Figure 4.26 that the combined effect of *d* and *n* that is weighted based on the simple MCHS had a peak value at *d*=0.1 and *n*=6, where the lowest point at *d*=0.2μm and *n*=10. It can be inferred that the larger area between the micromixer and the mainstream flow could reduce the flow friction. The reason for this occurrence was possibly due to the slip fluid flow over the micromixer area.

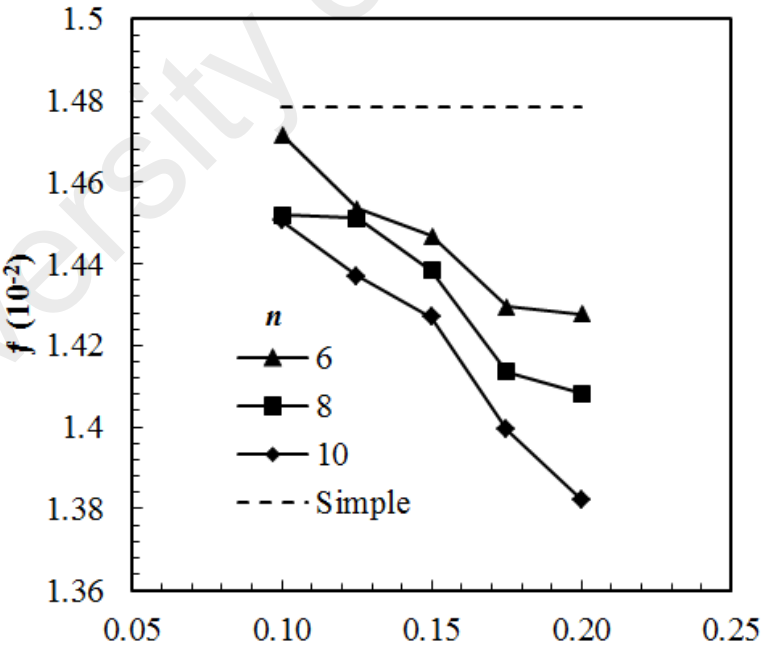

Figure 4.25: Variation of *f* with variation of *d* at different *n*.

Furthermore, the velocity of the cooling fluid abated and the redirected due to the wall stagnation, fluid viscosity and fluid association from the mainstream region and

micromixers. Consequently, a large stagnation area was formed in this section which enabled the fluid to slip over it and diminish the friction factor.

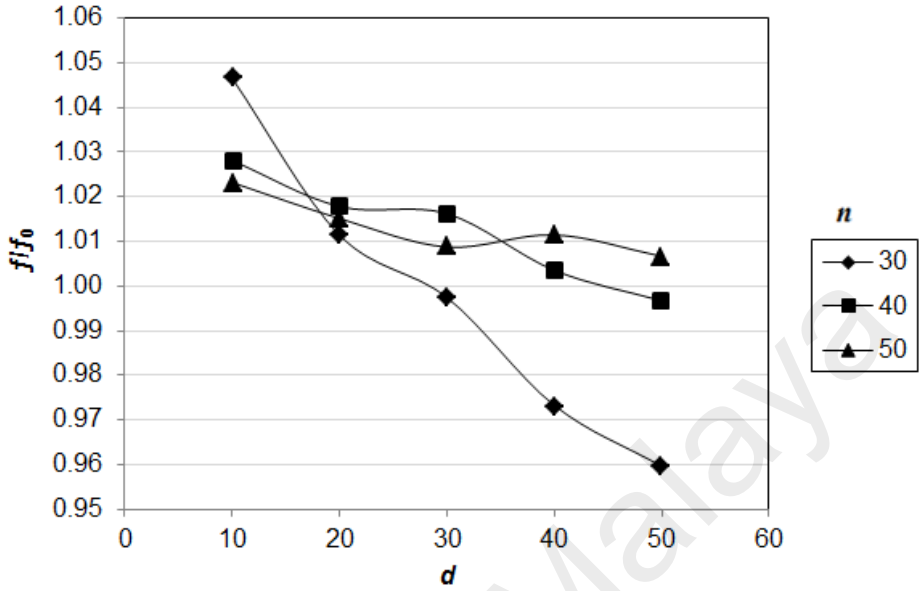

Figure 4.26: Variation of f/f_o with variation of d and n.

4.3.3.3 Overall Enhancement

It is observed that the increase of d and n has multiplied the benefits of the MTM by increasing the Nu, as well as reducing f. This has resulted in a tremendous improvement in η. As $d \rightarrow 0.2$ μm and $n \rightarrow 10$, η increased up to 1.53, as shown in Figure 4.27.

A detailed study of the flow and thermal field shows that multiple vortices are developed in both micromixers, as displayed in Figure 4.27. In virtue of the large impinging area, the fluid flows into the micromixer and then whirls up creating a recirculation due to the converse pressure difference across the micromixer. It has to also be noted that the laminar pressure stagnation on the verge of the main stream and the micromixer outlet becomes larger with the increment of d and n. The streamlines, temperature and pressure plot for both micromixers (d=0.2μm, n=10 and d=0.1μm, n=10) were observed to be similar (except for numbers and sizes of vortices).

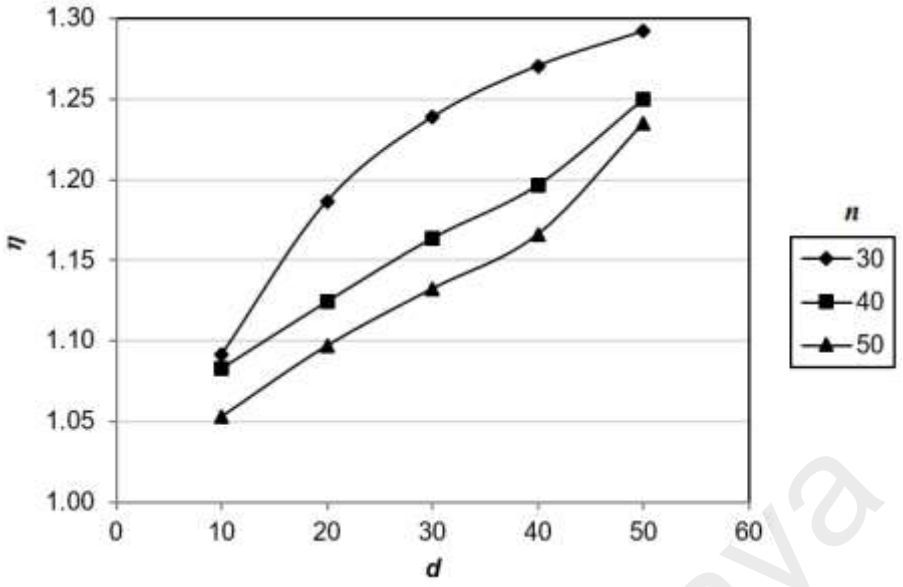

Figure 4.27: Variation of η with variation of *d* at different *n*.

The isotherms show that the temperature cooling fluid is much higher at d=0.2μm and n=10. This suggests that it has a higher heat transfer, compared to d=0.1μm and n=6. More vortices were formed in the former at larger sizes in three different positions; one at the entry section and two at the exit section.

Higher temperature was also observed in the focal vicinity of the vortices as in the previous analysis. The cooling fluid pressure in the same locale on the other hand, was lower when compared to the neighboring region. Thus, it can be deduced that greater heat absorption was induced in the micromixer if it has more vortices generated.

As mentioned earlier, an increase of d broadens the width micromixers. The significance of the heat absorption is dependent on the fluid recirculation where the size and intensity of the vortices significantly influence the heat transfer enhancement. Enlargement of the micromixer augments the peripheral area of the vortex which increases the quantity and size of the vortices.

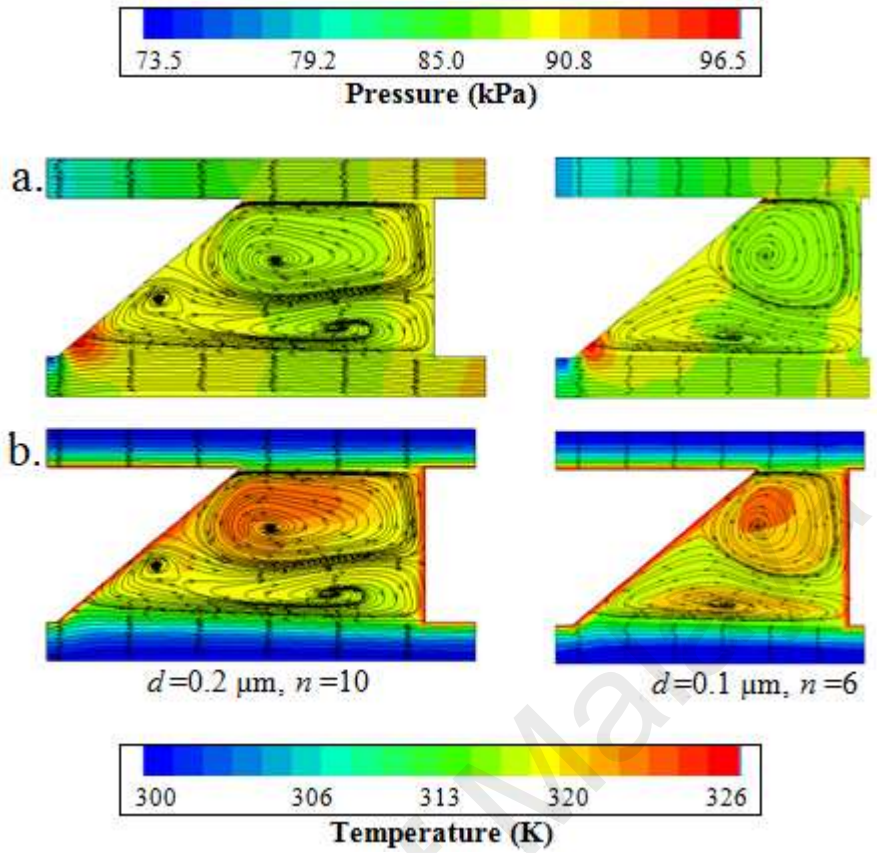

Figure 4.28: (a) Pressure contour plot and (b) isotherms in the secondary channel with different *d* and *n*.

Increase of *n* also increases the number of the vortices and this will eventually improve the fluid mixing in the bulk flow tremendously. Aside of the size and numbers of the vortices, the solid-fluid interface area and the repetitive development of the boundary layer also increase as *d* and *n* increase. On the other hand, excessive proliferation of *d* and *n* might shorten the thermal boundary development and reduce the intensity of the vortices that could impede the heat transfer rate. Thus, it can be inferred that a moderate increase of *d* and *n* can improve the heat transfer.

4.4 Thermal Enhancement Using Shield-Shaped Re-Entrant Obstruction

The thermal and flow characteristic of the MCHS with re-entrant obstruction at various flow velocities (u) are presented in Nusselt number (Nu) and friction factor (f). The MCHS was made of different types of materials where the materials aluminium and silicon were analyzed at different flow direction and velocity. A detailed analysis was

performed on the fluid flow mechanism and the convection heat transfer near the obstruction area and the results were presented as streamline and isotherms.

4.4.1 Effect of Flow Velocity and Direction in Different Materials

4.4.1.1 Aluminium

It can be observed in Figure 4.29 that the f/f_0 in the MCHS with aluminium substrate proliferates gradually with the increase of *u.* The proportion of this escalation becomes higher as *u* increases. A substantial increase was observed in f/f_0 at Direction 1 after *u*=4.12 m/s.

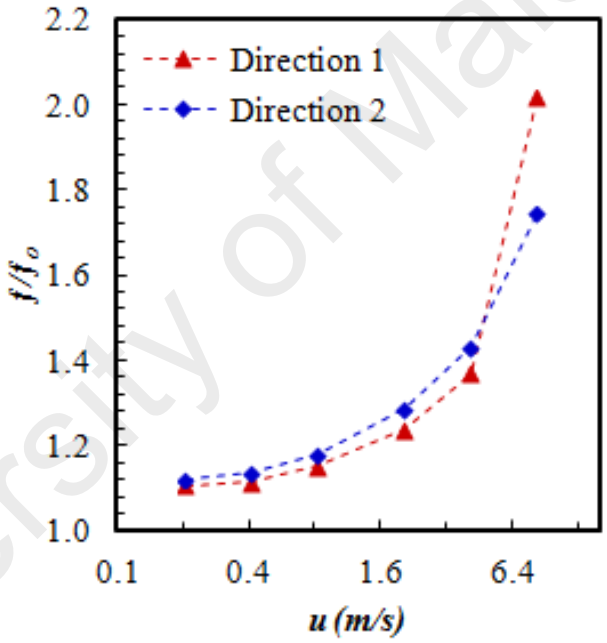

Figure 4.29: Variation of f/f_0 in aluminium MCHS with flow velocity.

Similarly, the growth of Nu/Nu_0 improved with the increase of *u* for both flow directions as shown in Figure 4.30. As the fluid passes through the obstruction with greater flow velocity, the fluid mixing becomes more intense. Besides that, other effects such as a thinner boundary layer and an extended solid-fluid interface area also improved the thermal performance. The escalation rate of f/f_0 and Nu/Nu_0 in flow

Direction 2 is higher compared to Direction 1. Similarly, Nu/Nu_0 is much higher compared to f/f_0 for any given u at Direction 2.

The repetitive growth of the boundary layer is due to the obstruction results in a higher heat transfer but consequently worsens the pressure drop significantly. It can be inferred that the gradual constriction and sudden expansion induces a greater convection heat transfer. For the same reason, it results in an excessive pressure build up in the fluid.

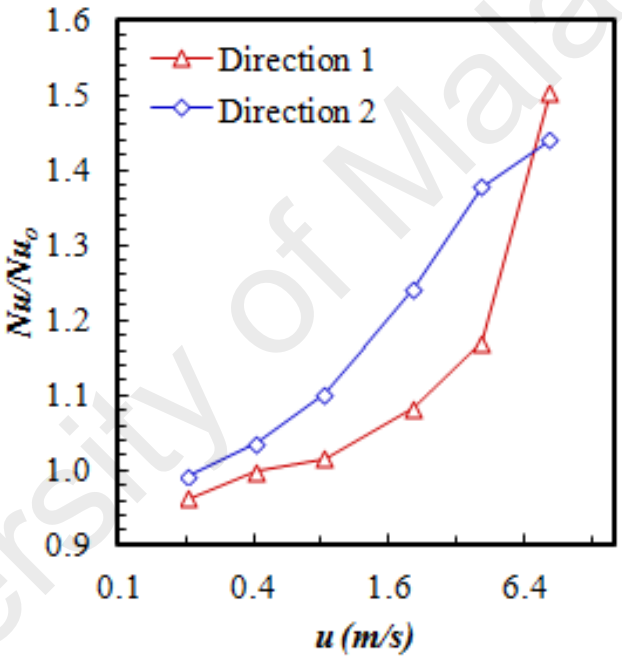

Figure 4.30: Variation of Nu/Nu_0 in aluminium MCHS with Flow Velocity.

Figure 4.31 shows η increasing in a greater acclivity in Direction 2 compared to Direction 1. However, after it reached to its peak at u=4.12 m/s, where η bettered up to 1.25, it is followed by a sudden drop in performance. This trend is possibly due to the combined effect of f/f_0 and Nu/Nu_0 where the thermal enhancement comes with a hefty pressure drop. Figure 4.32 shows that Nu/Nu_0, f/f_0 and η of the MCHS with silicon substrate varies with u in a similar trend with the MCHS with silicon substrate.

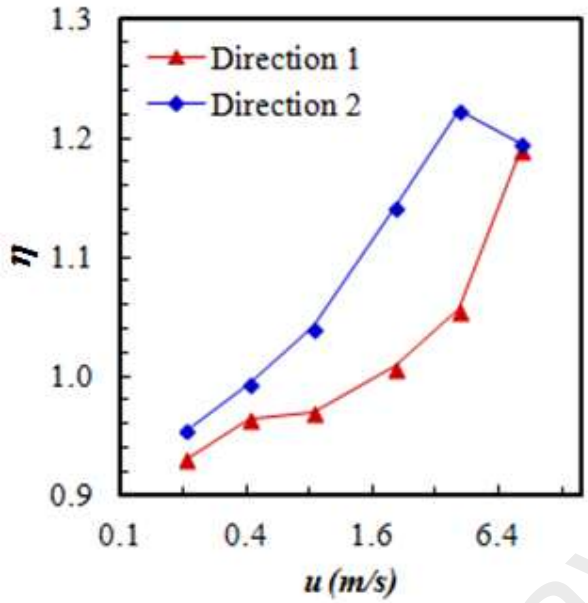

Figure 4.31: Variation of η/η_o in aluminium MCHS with flow velocity.

4.4.1.2 Silicon

It can be observed from Figure 4.33 that the significance and propagation tendency of f/f_0 for silicon are indistinguishable with aluminum.

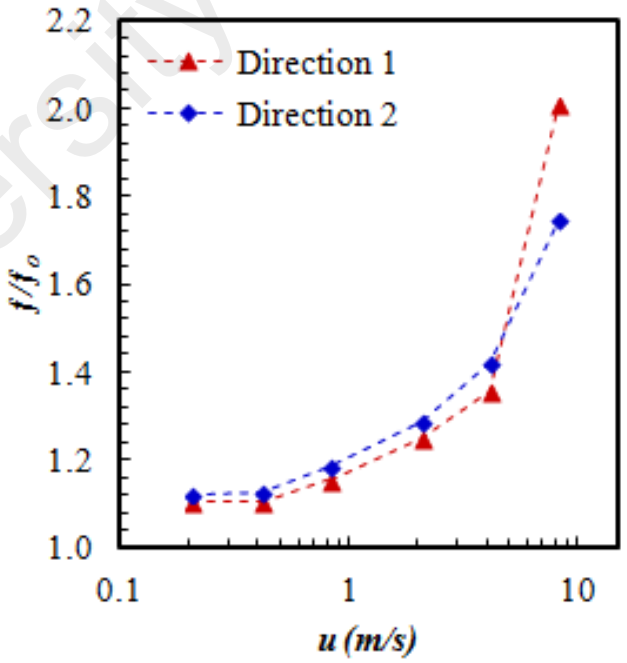

Figure 4.32: Variation of f/f_o in silicon MCHS with flow velocity.

Such result implies that the flow regime and pressure drop is only affected by the geometry of the obstruction. As for the thermal enhancement, for the simple MCHS, the

improvement in silicon MCHS is lower than aluminium. It has to also be noted that for simple MCHS, the aluminium MCHS outperformed the silicon MCHS. This is because, in simple MCHS, conduction heat transfer more dominant compared to the convection heat transfer where heat absorption from the bottom surface of MCHS to solid-fluid interface is comparatively significant. Thus, aluminium outperformed silicon due to its superior thermal conductivity.

However, when the re-entrant obstruction was introduced in the MCHS, the convection heat transfer improved significantly and therefore, silicon surpasses aluminium when it is compared with the simple MCHS. It is observed in Figure 4.34 that Nu/Nu_0 improves up to 2.7 and 2.6 in Direction 1 and Direction 2 respectively.

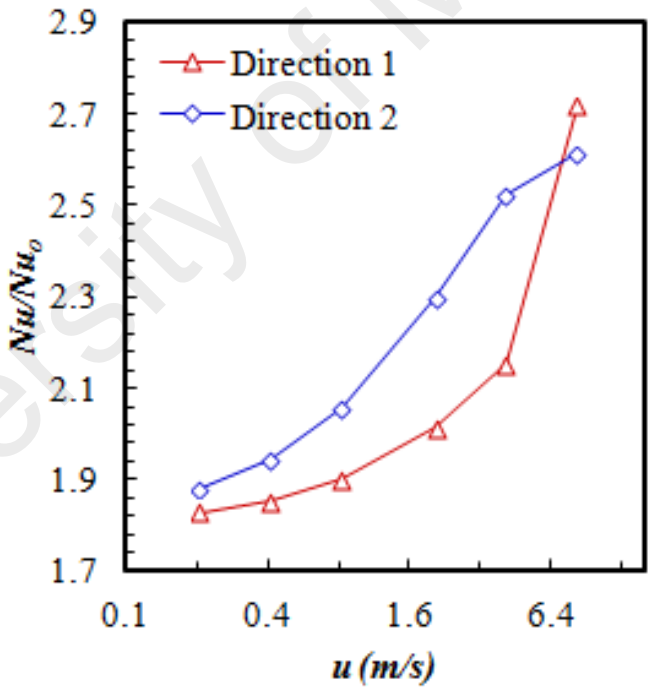

Figure 4.33: Variation of Nu/Nu_0 in silicon MCHS with flow velocity.

Based on the changes in Nu/Nu_0 and f/f_0, the deviation of η with increasing u is plotted in Figure 4.35. It is perceived that η in Direction 2 is better than Direction 2 for all given u and it reached its highest point at 4.12 m/s. The efficiency enhanced up to 124 %. Based on these findings, it can be deduced that material choice is significant

when employing a passive enhancement in MCHS. For simple MCHS, aluminium is a better choice due to the dominance of the conduction heat transfer. Whereas silicon would be the better choice for interrupted MCHS as the convection heat transfer dominates.

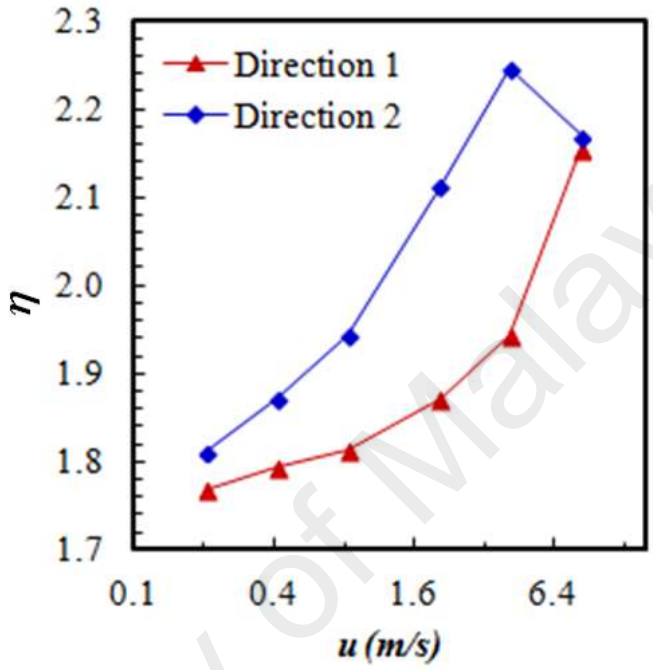

Figure 4.34: Variation of η/η_o in silicon MCHS with flow velocity.

4.4.2 Detailed Analysis of Flow and Thermal Characteristic in MCHS for Different Substrate Materials

Figure 4.35 shows the variation in the local pressure (P_x) and bulk fluid temperature (T_{bf}) in the simple MCHS with a different substrate material. Since the range of Reynolds number analyzed is wide (40<Re<800), P_x is plotted in a logarithm scale for better illustration. It is observed that P_x reduces consistently with the flow length in the simple MCHS, obeying the Moody loss. Similar to prior literatures (Garimella & Singhal, 2004; Satish G. Kandlikar, 2006; Kuppusamy et al., 2013; Xia, Chai, Wang, et al., 2011), the pressure drop in the simple channel increases with the increase of Reynolds number.

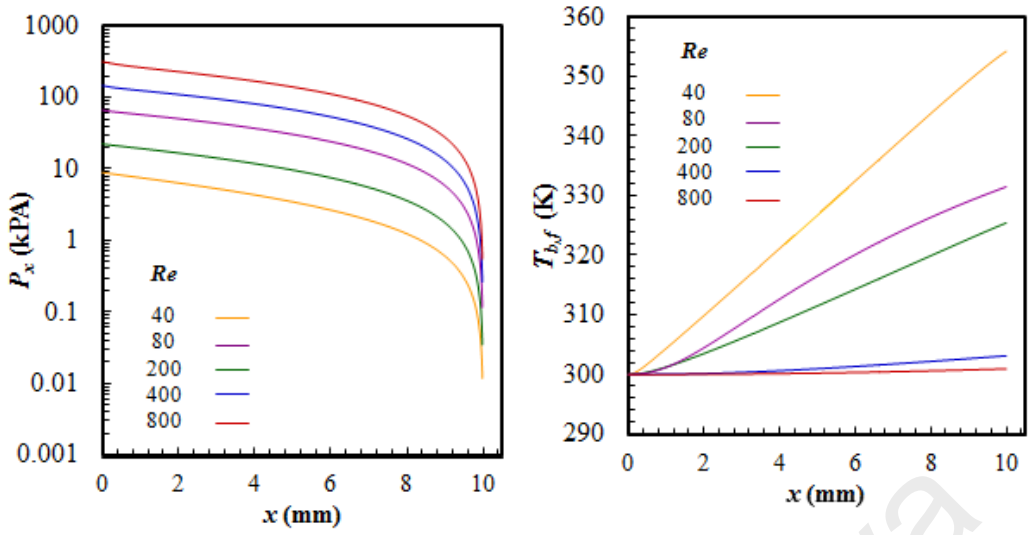

Figure 4.35: Variation of the simple MCHS made of silicon for the increase of flow velocity.

T_{bf} raises throughout the flow length. For the increasing Reynolds number, it can be divided into three sets; low, moderate and high. At a high Reynolds number (Re=400 and 800), T_{bf} is very low due to the great convection heat transfer that is induced by the high fluid velocity. This effect significantly reduces when the flow velocity lessens. No visible difference was observed in P_x between the aluminium and silicon MCHS, but T_{bf} of the aluminium MCHS is larger since aluminum have a greater heat transfer compared to silicon.

A similar trend was observed for P_x and T_{bf} in MCHS with re-entrant obstruction for both, aluminum and silicon, as shown in Figure 4.36 and Figure 4.37 respectively. It has to be noted that P_x and T_{bf} fluctuate throughout the flow length due to the re-entrant obstruction. These fluctuations occur due to the redevelopment of the boundary layer and fluid mixing at the re-entrant obstruction. Moreover, the jet and throttling effect that occurs due to the constriction and expansion also could be the possible reason for the fluctuation in P_x and T_{bf}. It can be seen that P_x dropped significantly and was raised again before gradually reducing. However, there was some unrecoverable heat loss that occurred when this process took place.

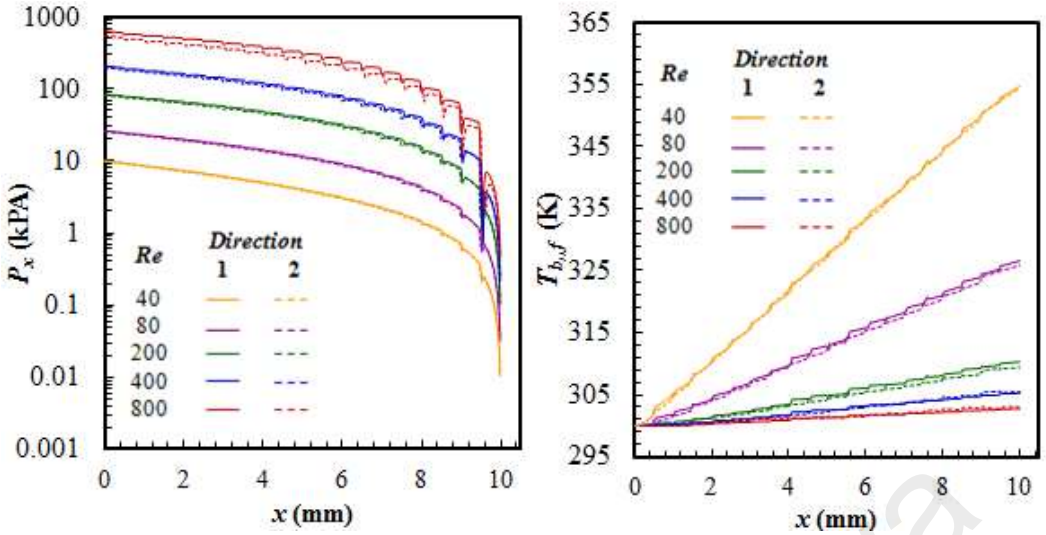

Figure 4.36: Variation of MCHS re-entrant obstruction made of aluminum for increase of flow velocity

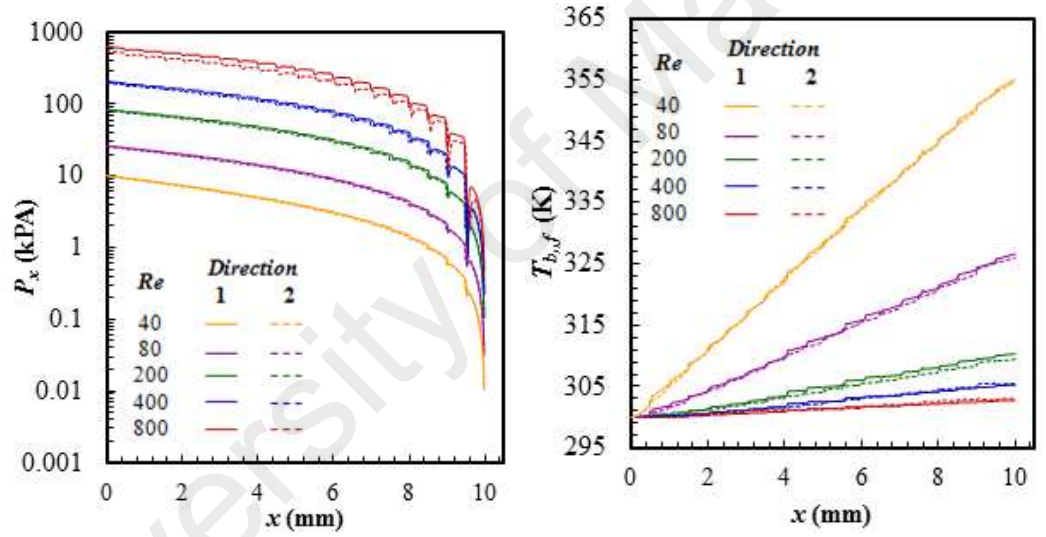

Figure 4.37: Variation of MCHS re-entrant obstruction made of silicon for increase of flow velocity.

4.4.3 Jet and Throttling Effect and Dead Water Region

So far, the results have shown that the introduction of the re-entrant can enhance the heat transfer performance, even though the pressure drop is high. However, the detailed study of fluid and heat transfer near the obstruction area showed that there is another downside of having re-entrant obstructions in the MCHS from where the fluid flows between the channel wall where the obstruction becomes static and inactive.

For this study, sectional areas from the middle re-entrant obstruction were projected in the *x* and *y* direction. For the *x*-*z* plane, a single plot was taken from the middle constriction. For the *y*-*z* plane, 5 sectional plots were projected from the middle obstruction at an equivalent distance of 0.01 mm, as shown in Figure 4.38. The pressure contour plot and isotherms were plotted together with flow streamlines in these cross sectional areas.

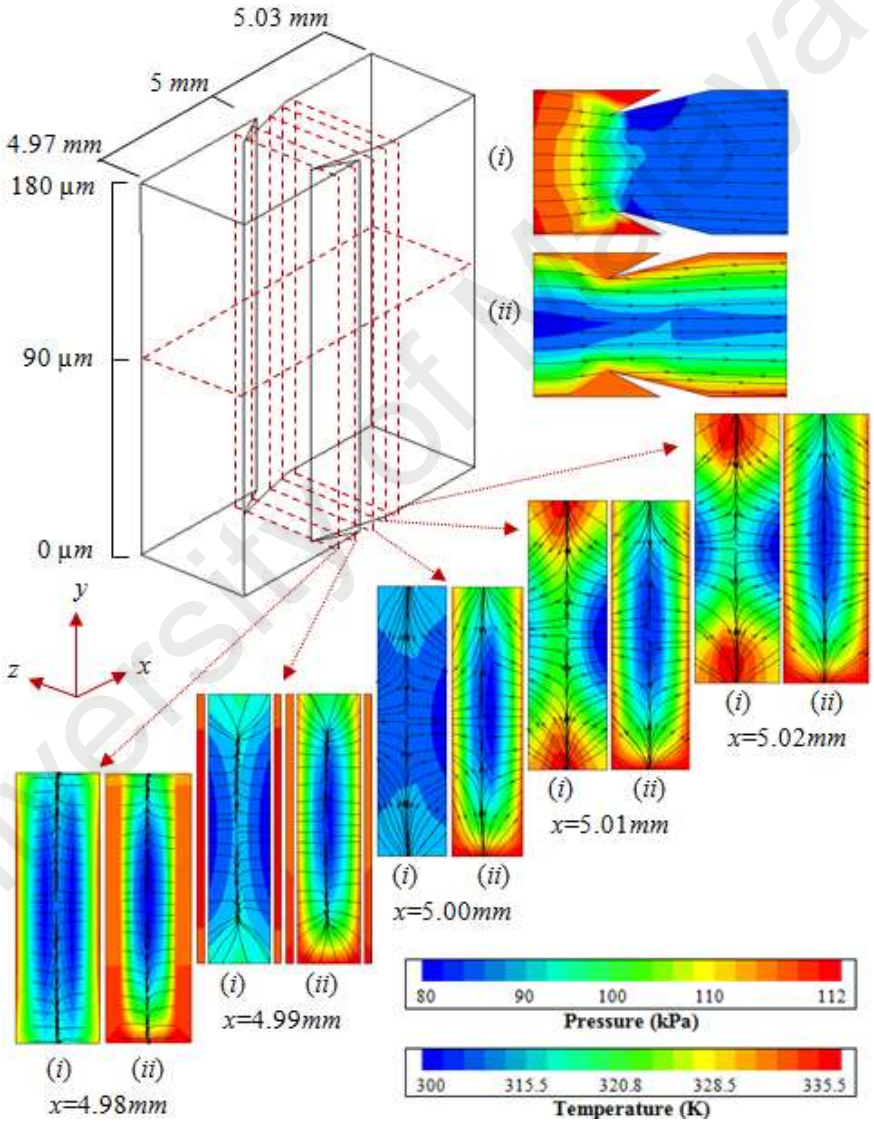

Figure 4.38: (i) Pressure plot and (ii) isotherms of fluid at re-entrant obstruction area.

The pressure contour showed that the fluid experienced a large pressure build-up at the leading edge of the obstruction. This phenomenon is known as the jet and throttling

effect where the heat transfer is enhanced greatly due to this effect. Pressure stagnation is formed underneath the re-entrant obstruction. Since there was no fluid motion in this area, it is called a 'dead-water region'. Pressure stagnation in this area provides a smooth surface that lets the fluid slip over the re-entrant region smoothly. This could somewhat reduce the pressure drop in the fluid flow to a certain degree. However, heat transfer between the fluid and solid region was impeded significantly and the fluid temperature became significantly high.

4.4.4 Possible Issue in Two Phase Flow in Re-Entrant Obstruction

While this study focuses on the single phase laminar flow, a few critical issues associated with the re-entrant obstruction has been found such as the upsurge of fluid temperature and dead water region. This could lead into further complications when incorporating this enhancement in a two phase heat transfer. Therefore, it is critical to manage this issue carefully before advancing the MCHS with the re-entrant obstruction into the two phase flow.

Firstly, usage of this MCHS in boiling flow regime (liquid-gas) could result in the trapping of bubbles in this region since there is no fluid motion. Secondly, the usage of fluid with solid particles e.g. nanofluid (liquid-solid) could result in sedimentation in this vicinity.

Consequently, heat transfer enhancement due to the flow wake and Brownian motion that resulted from the flow boiling and particle mixture respectively would deteriorate. These matters have raised the authors' concern on the implementation of this technology in a two phase flow. A comprehensive experimental study is required to investigate and validate these possibilities.

4.5 Thermal Enhancement Using Periodic Constriction

Influence of periodic constriction and its geometrical parameters is studied. For this study, water was used as the working fluid and tested at the Reynolds numbers ranging from 149.5057 to 373.74642 that correspond to inlet velocity of 1 m/s, 1.5 m/s, 2 m/s and 3 m/s. A heat flux of 1.25×10^6 W/m^2 was supplied at the bottom surface of the MCHS. The improvement of the Nusselt number, increase of friction factor and the overall enhancement that was compared with the corresponding simple MCHS geometry is presented. Special attention is given to the flow behavior near the constriction area and its relation with the heat transfer augmentation.

Figure 4.41 presents the variation of the Nusselt number for different cases. It can be perceived that Nu/Nu_0 contrasts tremendously in different cases. From *C1* to *C3*, the slight increase of Nu/Nu_0 suggests that a gradual increase and sudden expansion could advance the heat transfer significantly. A similar trend was observed from *C4* to *C6* and *C10* to *C12* at different magnitudes. These trends are identical based on the variation of peak positions of the constriction at different sizes and quantity of constrictions.

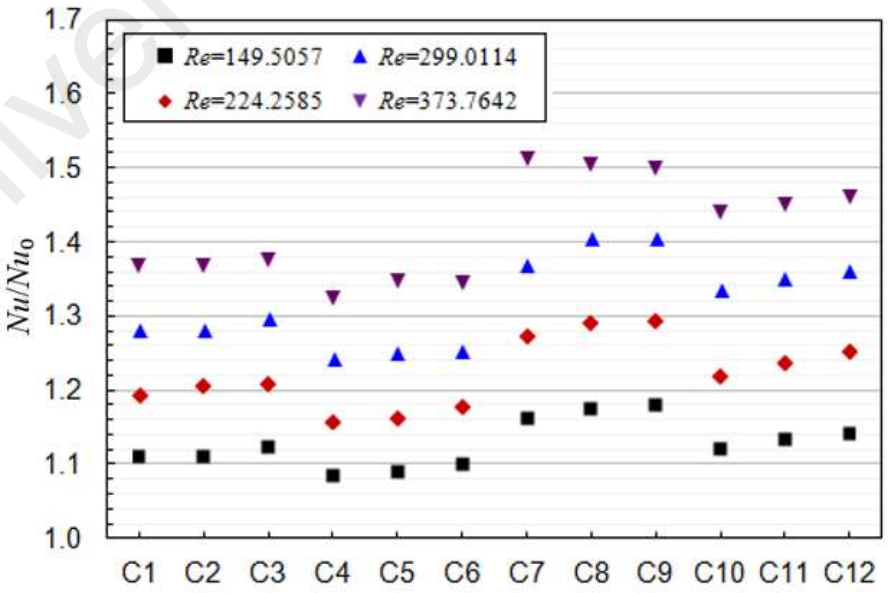

Figure 4.39: Variation of Nu/Nu_0 for different cases.

Based on this identical trend, the cases were divided into four sets ; Set 1: *C1* to *C3* Set 2: *C4* to *C6*, Set 3: *C7* to *C9* and Set 4: *C10* to *C12*. It can be seen that *Set 2* has a lower value than *Set 1*.This means that for *n*=5, the enhancement of Nu/Nu_o is higher for a shorter constriction compared to the larger constriction for the identical arrangement for a given Reynolds number. A similar pattern was observed for Set 3 and 4 (*n*=7) where a larger incremented Nu/Nu_o was observed at a higher Reynolds number except for *C7* where it was highest among all the cases. Based on this trend, it can be inferred that the reduction in constrictions size and increase in numbers of constrictions can enhance the thermal performance.

4.5.1 Flow Characteristic

Study of the flow characteristic fluid indicates that the disposition of f/f_0 is very much similar with Nu/Nu_o for all the cases as shown in Figure 4.40.

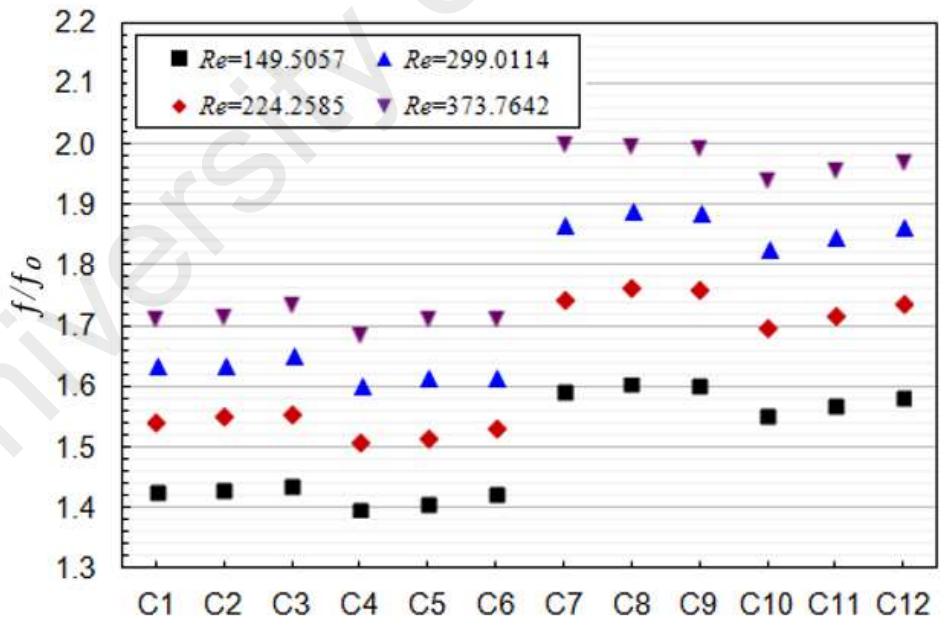

Figure 4.40: Variation of f/f_0 for different cases.

However, the significance of f/f_0 is higher compared to Nu/Nu_0 for all cases. Thus, it is deduced that the enhancement in thermal performance is overshadowed by the serious increase in the pressure drop. The flow impediment in the constriction area and

the subsequent reverse flow is the primary cause of rise in f/f_0. Similar issues have been highlighted in previous works of interruption in the MCHS (Chai, Xia, Zhou, et al., 2013; Zhai et al., 2014).

4.5.2 Performance Enhancement Factor

A novel parameter called the performance enhancement factor (η) is used to determine the tradeoff between the augmentation of Nu/Nu_0 and the increase of f/f_0. The propensity of η is found to be analogous with Nu/Nu_0 and f/f_0 as shown in Figure 4.41.

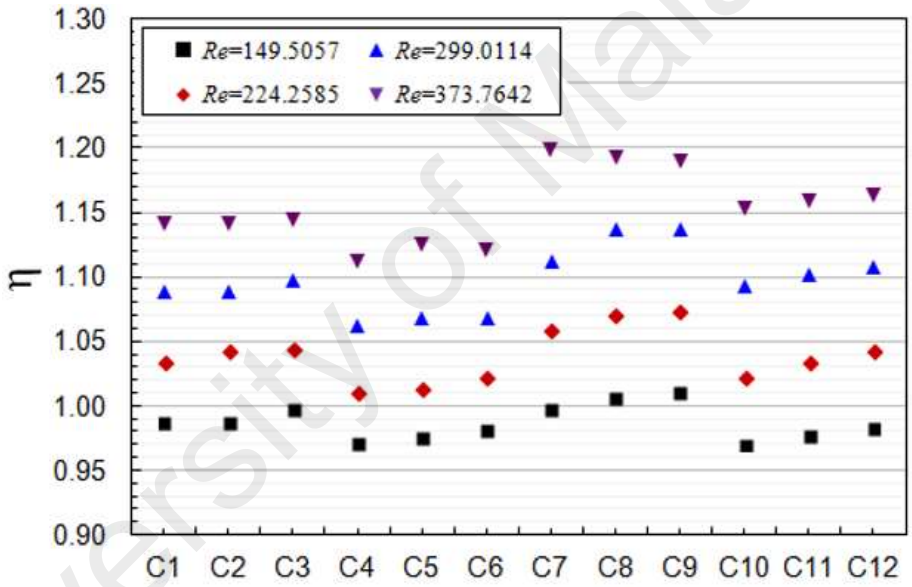

Figure 4.41: Variation of η for different cases.

For Re=224.2585, the overall enhancements for all the cases are lower than the unity except for C8 and C9. The highest η obtained was 1.2 at C7 and Re=373.7642. The thermal performance enhanced due to the jet and throttling effect and fluid circulation. However, this enhancement was overshadowed by a large pressure drop. Therefore, constriction in the MCHS couldn't provide a significant enhancement compared to the simple MCHS.

4.5.3 Orifice Effect in Constriction

It is found that as fluid flows through the constrictions in the MCHS, it experiences an orifice effect. Due to this effect, the fluid gains speed, but such fluid acceleration comes with a large pressure drop. On the other hand, this effect could possibly enhance the fluid mixing and the heat transfer. Considering this fact, a detailed study was performed on the flow behavior near the constriction region by plotting the local pressure 'P_x'.

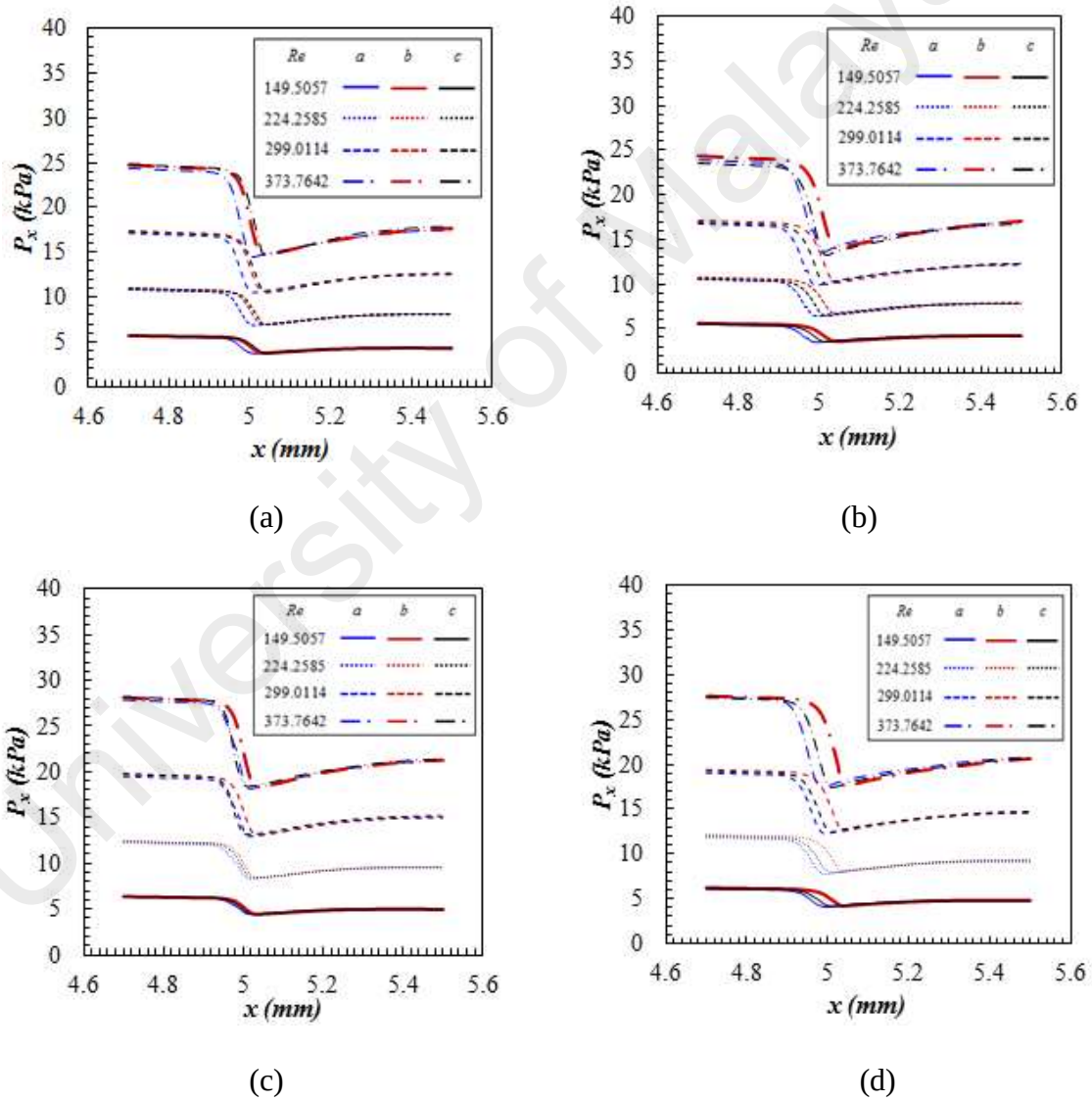

Figure 4.42: Variation of α with different constriction configurations and flow of Reynolds number (a) *n*=5, *L*=0.1 mm (b) *n*=5, *L*=0.2 mm (c) *n*=7, *L*=0.1 mm and (d) *n*=7, *L*=0.2 mm.

For comparison purpose, the MCHS was categorized into three configurations; *a*, *b* and *c* which were based on their arrangements. The trend of local pressure is generated from the middle constriction of the MCHS. Figure 4.42 shows the variation of the local pressure of fluid for the different number of constrictions and its length.

Pressure reduces drastically at the constrictions and the pressure loss grows larger at higher Reynolds numbers. Thus, it can be perceived that the effect of constriction is highly sensitive with the Reynolds number. It intensifies the flow acceleration as well as the jet and throttling effect momentously with the rising Reynolds number. The location of sudden pressure loss shifts with the peak of the constriction. The pressure drop of the arrangement '*a'* is larger than '*b'* and '*c',* but the succeeding pressure recovery compensates the loss after the constriction. Therefore the pressure drop for a single constriction for a given length is the same, regardless the pattern of the constriction. It has to also be highlighted that the non-coverable pressure loss after the constriction is another main reason for the high pressure loss in the MCHS with constriction.

4.5.4 Dimensionless Flow Coefficient (*a*)

The dimensionless flow coefficient (α) was calculated from the middle constriction of the MCHS for each configuration using the following equation:

$$\alpha = u_m \sqrt{\frac{2\Delta P_{local}}{\rho}} \tag{4.1}$$

where ΔP_{local} is the pressure drop across the constriction.

The value of α at different geometrical configurations is shown in Figure 4.43 and Figure 4.44 for 5 and 7 constrictions respectively. It is observed that α increase tremendously with the growing Reynolds number and the inclination becomes more intense at a larger Reynolds number. Besides that, the width of the constriction (*L*) also

has a trivial influence on the value of α where the larger (wider) constriction has a higher α.

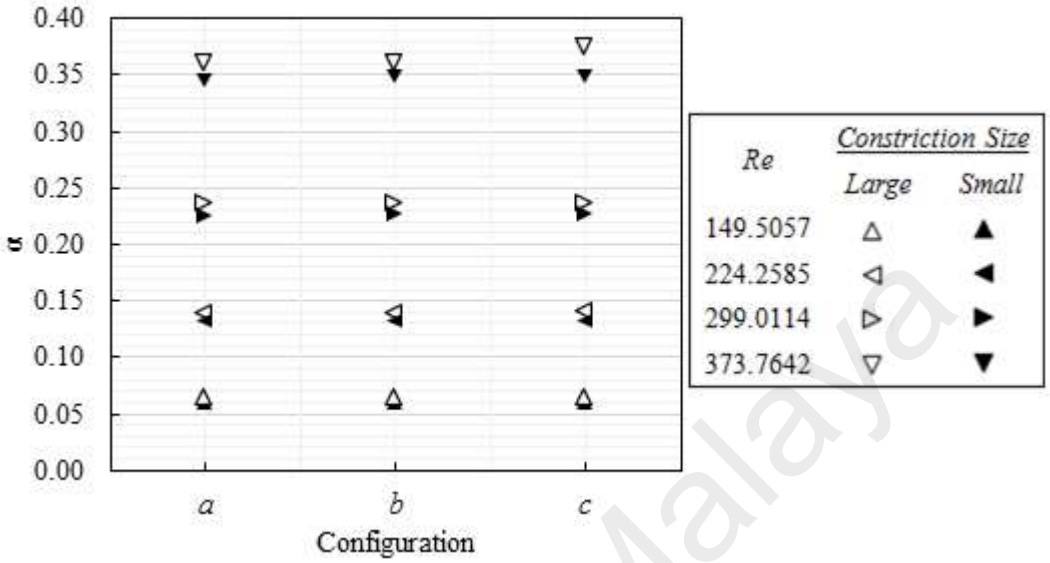

Figure 4.43: Variation of α in MCHS with 5 constrictions at various configurations and flows of Reynolds number.

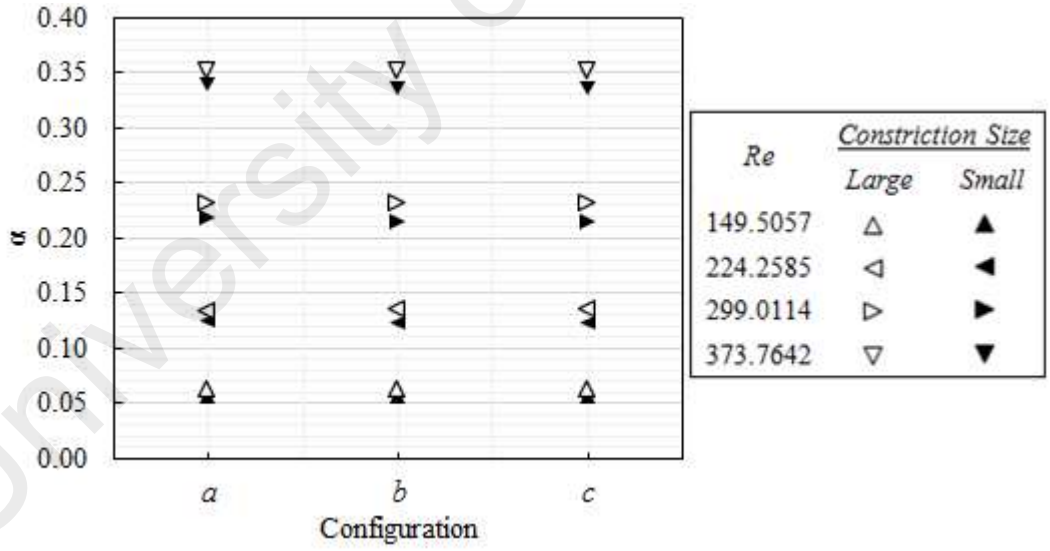

Figure 4.44: Variation of α in MCHS with 7 constrictions at various configurations and flows of Reynolds number.

There is no visible difference observed in α for configuration *a*, *b* and *c*. Thus, it can be inferred that the shift in the position of the constriction peak does not affect the value of α and it only depends on the size of the constriction.

4.5.5 Eddy Effect

The Eddy effect is the fluid circulation opposed to the mainstream flow direction when the fluid passes through an obstruction e.g. constriction. This phenomenon could possibly enhance the convective heat transfer due to enhanced fluid mixing. Since the fluid experiences an orifice effect in this present study, the flow characteristic after the constriction is studied in detail to observe the occurrence of the Eddy effect as well as its influence on thermal enhancement.

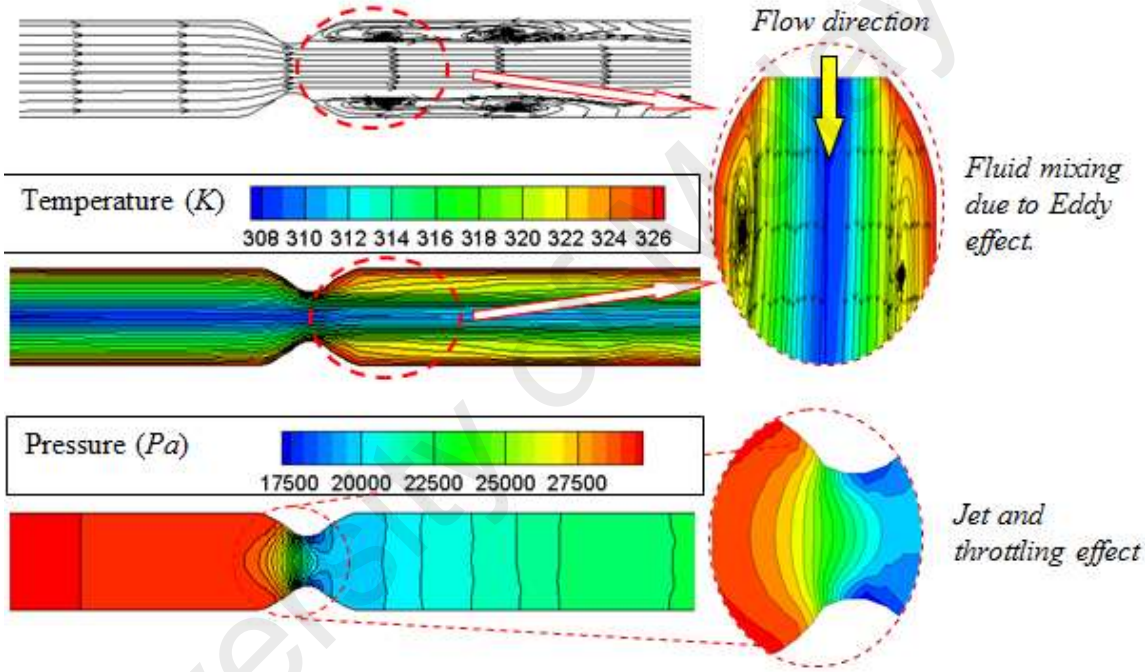

Figure 4.45: Streamlines, pressure plot and isotherms in the constriction area (*x*-*z* plane).

Figure 4.45 shows that the fluid flow from the mainstream channel is confined when it reaches the constriction section and the Eddy effect occurs, following the heights of the constriction. After the constriction, it is observed that there is a reverse flow and multiple fluid circulations were formed. The mainstream flow became much more narrow, conforming to the width of the constriction section. In the pressure contour plot, a drastic pressure build up was observed in the constriction area. The jet and throttling effect was observed at the entry section of the constriction. Isotherms showed that the

heat transfer also improved due to the Eddy effect since the fluid mixing has enriched. Therefore, the isotherms were distributed more evenly compared to the prior constriction. Velocity profile of the fluid flow is studied in order to analyze the influence of ribs on the flow characteristic. It can be seen in Figure 4.46 that fluids experience a great acceleration when passed through the rib.

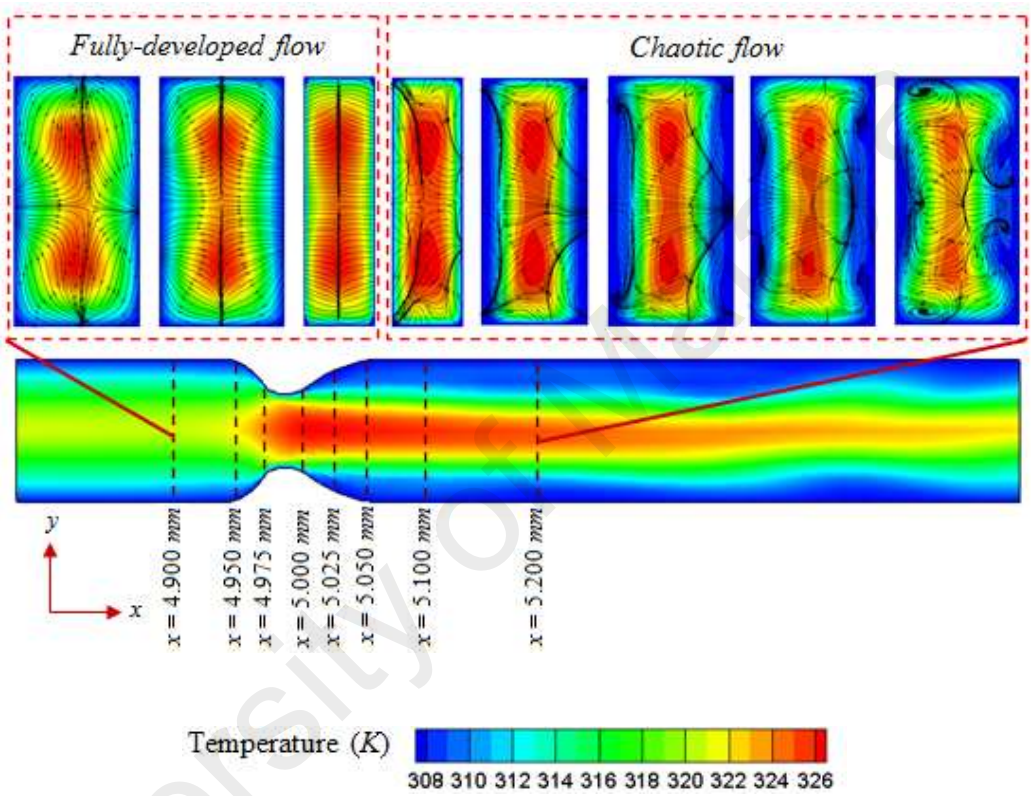

Figure 4.46: Velocity profile at various sections of constriction (*C7*, *Re*=373.7642).

This flow hastening resulted in a large pressure drop such as what was discussed earlier. The fluid acceleration reduced gradually as the fluid moved further from the rib and faded off completely after a certain distance (approx. 0.5 mm from rib). Thus, it can be inferred that the growth of boundary layer was complete and the fluid has reached the fully-developed condition. A similar phenomenon was also reported in past literatures (Xia et al., 2013). The projection of a sectional view in the *y*-*z* plane at a different *x* location near the ribs shows that the flow characteristic near the ribs can be categorized into two sections; before the full disruption developed flow and after the

disruption-disrupted flow/chaotic flow. The streamlines show that the flow is in a fully-developed condition and is 'systematic'. The streamlines are well-aligned and symmetrical from the side walls flow towards the middle section of the channel. Once the fluid passes through the constriction, the flow immediately becomes chaotic due to the disruption by the constriction. The rupture in the flow boundary layer is also visible where the highest velocity occupies a larger portion of the channel. However, this effect slowly diminishes as the fluid flows away from the constriction, suggesting that the boundary layer has grown to its maximum thickness.

4.6 Thermal Enhancement using Re-entrant Cavities

The intensification of the thermal performance in the microchannel with elliptical cavity in the sidewalls (MCES) with respect to the simple MCHS was studied at u_{in}=4m/s and q''=10^6 W/m^2. The effect of variation in the number of the cavities, flow direction, size and the geometrical parameters of the cavity on the heat transfer, friction factor and overall performance is discussed.

4.6.1 Comparison of the Performance of Simple MCHS and MECS.

It is known that the introduction of cavities in the MCHS could possibly enhance its thermal performance significantly (Steinke & Kandlikar, 2004). To validate this, the thermal and hydraulic performance of MECS is compared with the simple MCHS.

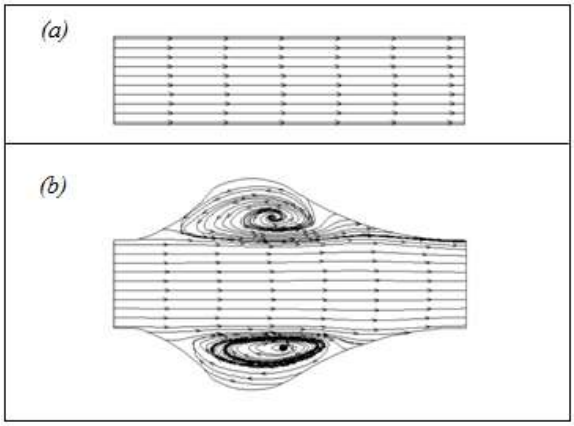

Figure 4.47: Streamlines of (a) simple MCHS (b) MECS.

As shown in Figure 4.47, the streamlines in the straight channel are continuous, while in the MECS, fluid in the mainstream egresses into the cavity region and recirculates before it re-enters into the mainstream region. The flow recirculation augments the fluid mixing and eventually intensifies the overall heat transfer. The pressure contour plot in Figure 4.48 illustrates that the static pressure of fluid in the simple channel reduces gradually along the flow direction. However, the pressure in the cavity vicinity of the MECS is slightly lower than its outer environs and stagnation occurs at the exit of the cavity (constriction section).

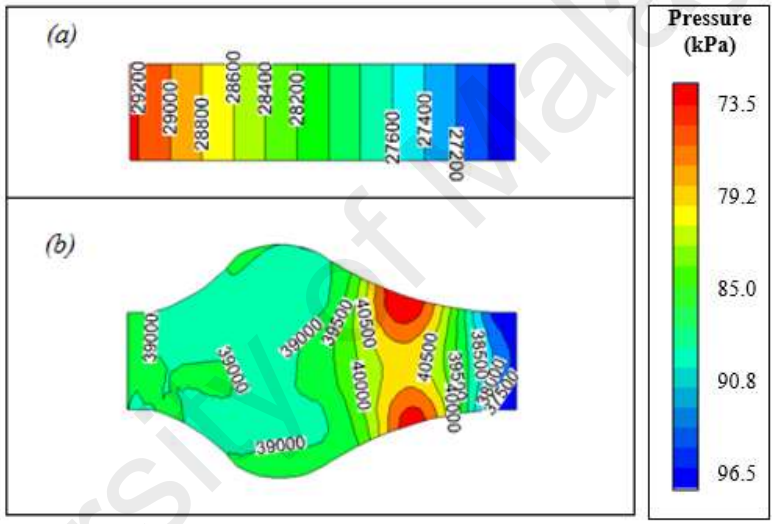

Figure 4.48: Pressure contour plots (Pa) of (a) simple MCHS, (b) MCHS with elliptical cavity.

There are a few phenomenon that occur in the cavity that affects the flow pressure significantly. (1) The fluid pressure reduces drastically when it enters the cavity region. However, as the fluid pressure reduces, some of the mainstream fluid slips over this region which reduces the heat transfer. Hence, the pressure stagnation provides a smooth surface that reduces the wall shear stress. In Figure 4.49, it can be seen that temperature is much lower, along with the constant cross sectional area and higher temperature in the cavity area. (2) The cooler region expands gradually, but not completely from the mainstream channel into the cavity region.

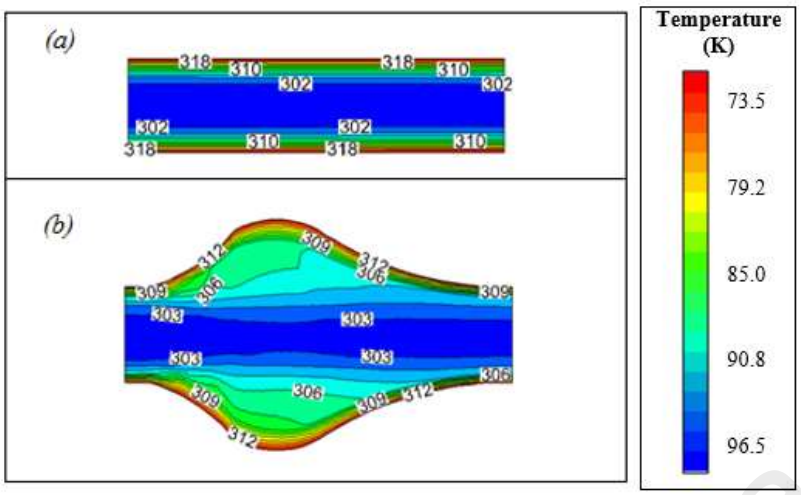

Figure 4.49: Isotherms (K) of (a) simple MCHS, (b) MCHS with elliptical cavity.

Such temperature distribution suggests that improvement in the convective heat transfer is due to the expansion of the flow field and the diversion of the mainstream fluid into the cavity area. (3) The flow agitation, together with expanded fluid-solid interface has improved the heat transfer performance significantly.

This improvement can be further enhanced by selecting pertinent numbers of cavity and geometrical parameters of the cavity. For this purpose, dimensionless parameters were established for the expediency of analysis. Numbers of cavities on both sides of the channel is represented as *n*. Distance between cavities (*p*) is determined from $p = \frac{L}{n-1}$, where *L* is the length of the MCHS. The integer value is fixed as distance between the cavities. The floats were distributed equally at the entry and exit of the channel. The size of the cavity is characterized by its length and depth. The corresponding dimensionless parameter for length and depth are defined as $\alpha = \frac{a}{W}$ and $\beta = \frac{a}{b}$, where '*a*' and '*b*' are the total length and depth of the cavity respectively. The dimensionless parameter expansion length and its radius are expressed as $\gamma = \frac{c}{a}$ and

$r_c = \frac{r_1}{c}$ respectively. The dimensionless parameters for the middle curvature and its radius are defined as $\delta = \frac{d}{c}$ and $r_d = \frac{b}{r_2}$. Contraction radius with respect to its length is presented as $R = \frac{r_3}{e}$ where $e = a - (c + d)$. The contraction length '*e*' is dependent on both, the expansion length (*c*) and the middle length (*d*). Thus, if '*c*' and '*d*' are fixed at a certain value, the size of the cavity will directly influence the expansion length and its radius.

4.6.2 MCHS Performance at Various *n* and Flow Directions

The variation of the number of cavities '*n*' is analyzed while setting the dimensionless parameters at α=3.5, β=2, γ=0.25, δ=1 *R*=2, r_c=2 and r_d=1. Concurrent with this analysis, the effect of the flow direction with cavities are also studied. The configuration of the flow direction is defined by *Case A* and *Case B* and the boundary conditions associated with these cases are explained in Section 3.1.

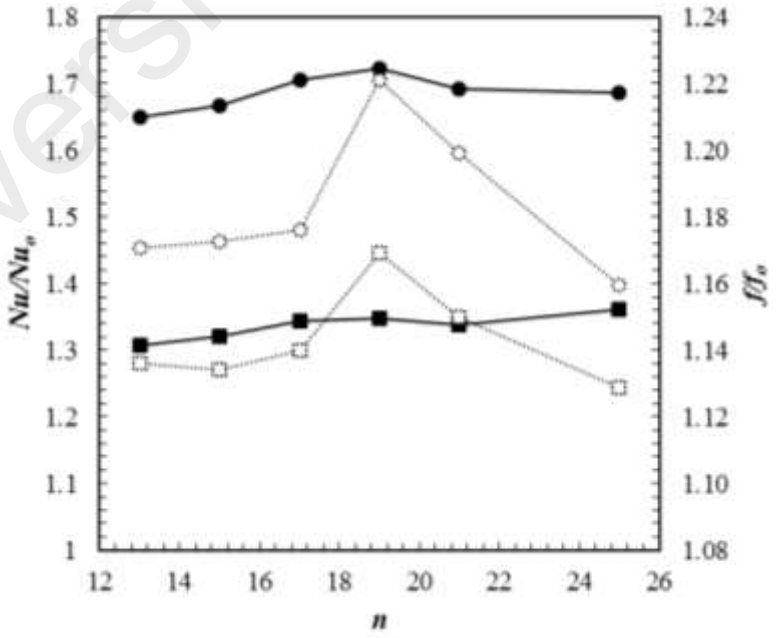

Figure 4.50: Variation of Nu/Nu_0 and f/f_o with *n* at different flow conditions.

Figure 4.50 shows that Nu/Nu_0 increases slightly as it increases from n=15 to 19, followed by a minor fluctuation from n=19 to 25. The thermal enhancement is significantly higher in *Case A* compared to *Case B* even though the proclivity of the enhancement with the variation of numbers of cavities for both cases are loosely similar. This suggests that the sudden expansion and gradual constriction in the flow field can enrich the thermal performance greatly. On the other side, proliferation of f/f_o is more vigorous than Nu/Nu_0 from n=13 to n=19, but decreases drastically from n=19 to n=25. It is also observed that f/f_o reaches its highest at n=19, where in *Case A*, f/f_o is very close to Nu/Nu_0 and for *Case B*, f/f_o overlaps and becomes higher than Nu/Nu_o. For this reason, the highest η for *Case A* is observed at n=17, unlike Nu/Nu_0 where the highest value is observed at n=19.

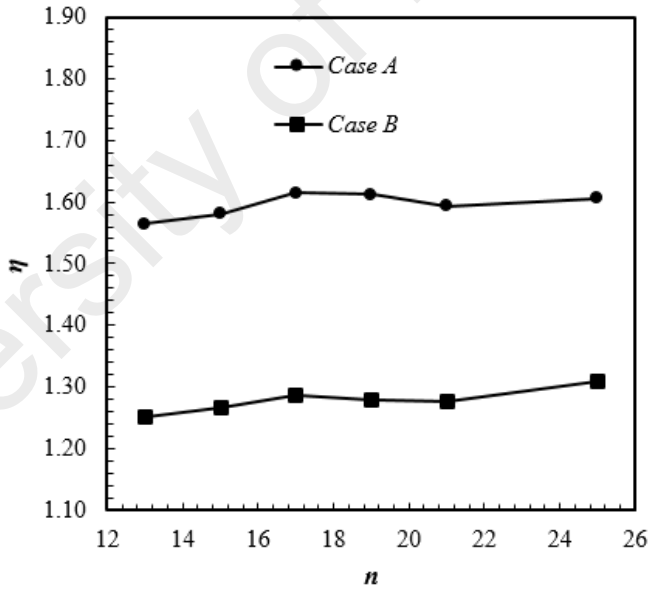

Figure 4.51: Variation of η with *n* at different flow conditions.

The reason behind this trend is because at a lower value of *n*, the cavities are apart from each other by very large distance. Hence, the thermal boundary layer grows to a fully-developed condition after the cavity remains in this condition for a longer distance until the next cavity. Consequently, the thermal performance does not increase too much. When *n* increases, the rupture and development boundary become more frequent

which results in a higher η. Furthermore, more cavities in the MCHS produce a more chaotic advection in the MCHS that contributes in a higher heat transfer performance. When *n* exceeds the optimal value, the boundary layer is disrupted too much until the layer is not reaching the fully developed condition which worsens the thermal performance. The highest performance in this case is observed at *n*=17, where η increases up to 1.62, as shown in Figure 4.51.

4.6.3 MCHS Performance at Various α and R

The variation of α at different *R* and their effects on the thermal and flow performance is studied. With *n*=17 and flow direction as in *Case A* (the best configuration obtained from the previous analysis), the remaining parameters were randomly fixed at γ=0.25, δ=1, r_c=2 and r_d =1. It is known that α is the ratio of the length of the cavity, respective to the overall length. Since β (the depth of the cavity) is fixed at 2, growth of α directly represents enlargement of the cavity. The result shows that Nu/Nu_0 and f/f_o increasing drastically with the increase of α from 0.5 to 4.0, as shown in Figure 4.52.

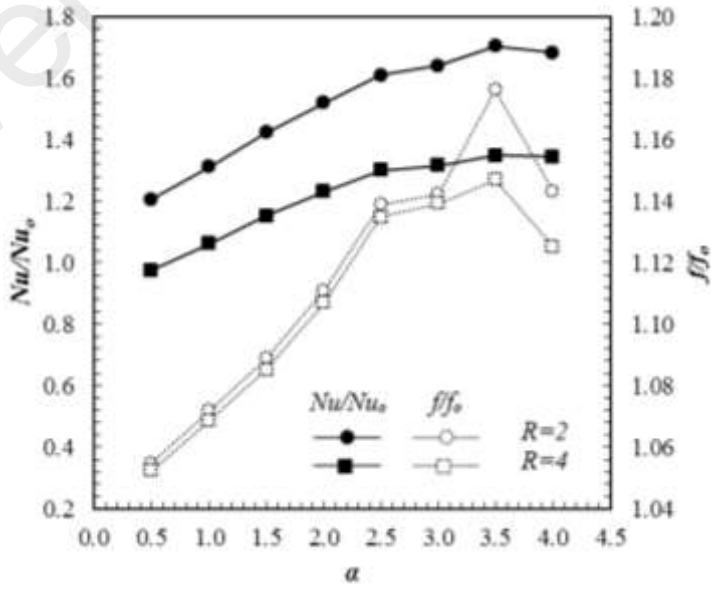

Figure 4.52: Variation of Nu/Nu_0 and f/f_o with α at different *R*.

The increase of f/f_o is much more drastic compared to Nu/Nu_o until α=2.5. This rise then becomes moderate and finally drops slightly at α=4.0. The significance of Nu/Nu_o is much higher for all 'α', even though the increase of f/f_o is drastic except for *R*=2 at α=3.5.

Proportionately, η increases significantly until α=2.5 and continues to increase slightly after that. It should also be noted that the reduction of radius '*R'* improves η significantly. This suggests that an elliptical cavity with a sharper radius can improve the thermal performance more effectively. Eventually, η reaches up to 1.62 at α=3.5, as shown in Figure 4.53.

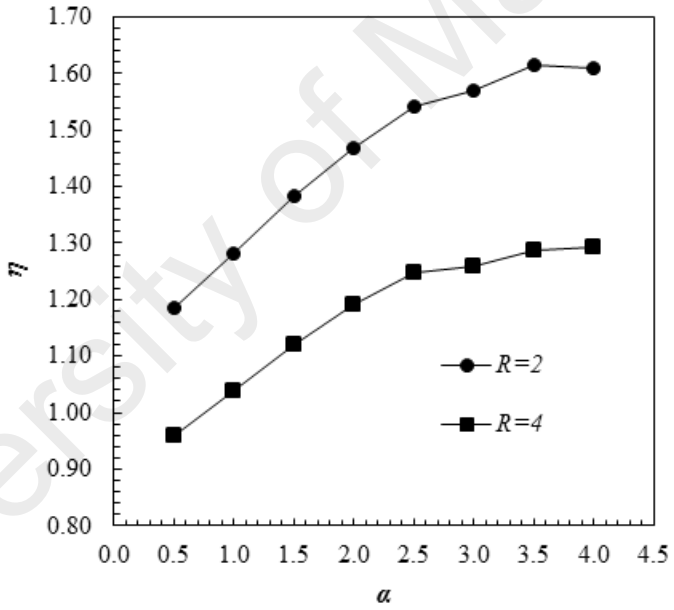

Figure 4.53: Variation of η with α at different *R*.

Streamlines in Figure 4.54(a) show an obvious difference between the two cavities where huge vortices were observed at α=3.5, *R*=2, whereas no changes were observed in the flow at α=0.5, *R*=4. Vortices completely occupy the cavity area according to the shape of the cavity. The pressure contour plot in Figure 4.40(b) shows a slight pressure drop in the central of the vortices. Moreover, pressure stagnations are formed at the exit of the cavities. The isotherm in Figure 4.54(a) shows a uniform temperature distribution

in the cavity area that explains the reasons for the enormous increment in heat transfer at α=3.5, *R*=2, whereas at α=0.5, *R*=4, there is no visible effect observed in the cavity. In other words, the thermal and flow fields in α=0.5, *R*=4 is similar to the channel without cavities. In fact, the drastic reduction in the cavity size worsens the heat transfer performance of the MCHS, as observed in α=0.5, *R*=4, where Nu/Nu_0 is smaller than 1.

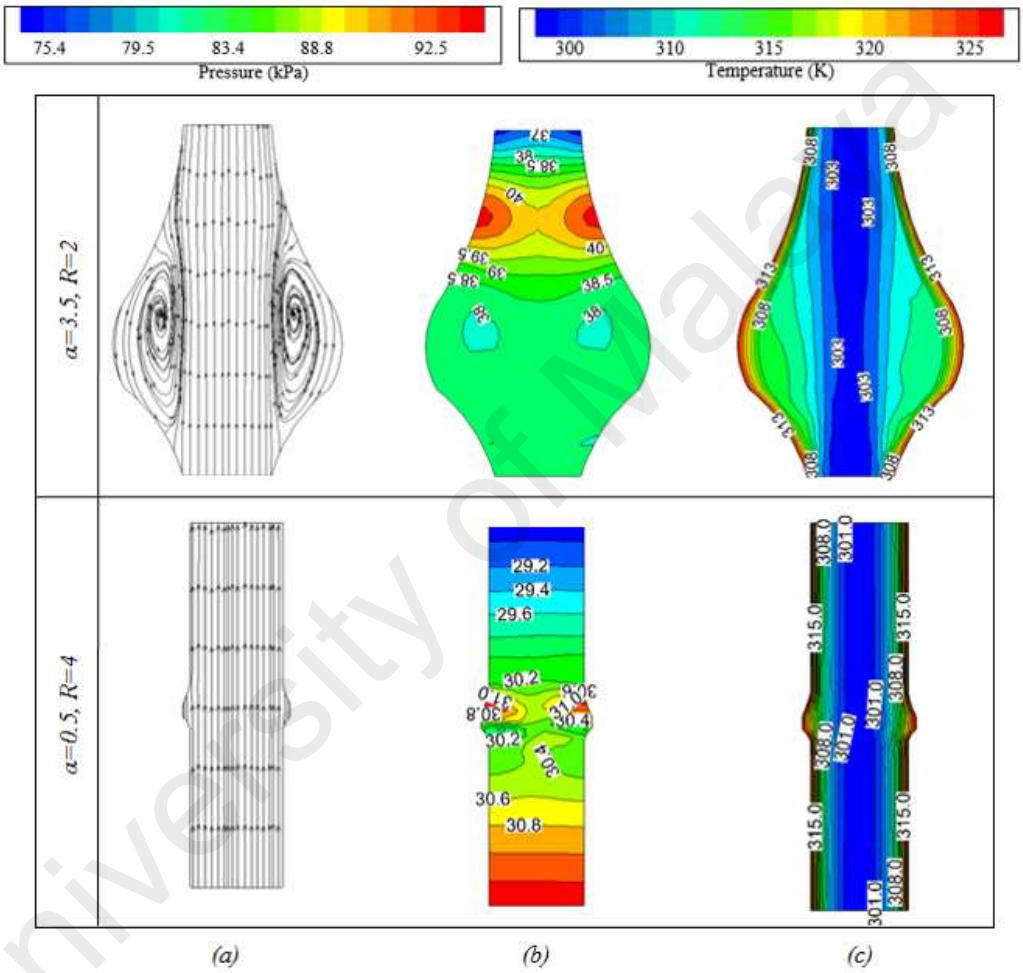

Figure 4.54: (a) Streamlines, (b) pressure contour plot (Pa), and (b) isotherms (K) at α=0.5 and α=3.5.

4.6.4 MCHS Performance at various γ and r_c

The effect of γ and r_c are studied while maintaining other parameters at *Case A*, *n*=17, α=3.5, γ=2, *R*=2 and r_d=1. Since 'δ' is fixed at 1, the middle length varies correspondingly with the entrance length. A significant ascension is observed in Nu/Nu_0 from γ=0.10 to 0.15 for r_c=2.0, as well as r_c=3.0 except for r_c=2.0, where its acclivity is marginally higher as perceived in Figure 4.55. As for r_c=2.0, this inclination is followed

by a small increase until γ=0.25 and trifling decreases through γ=0.40. Conversely, for r_c=3.0, Nu/Nu_0 dwindles perpetually from γ=0.15 down to γ=0.40.

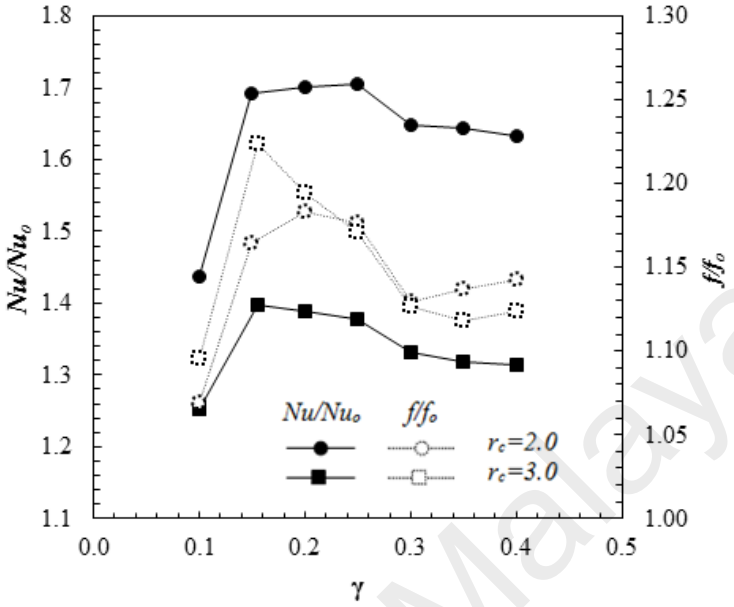

Figure 4.55: Variation of Nu/Nu_0 and f/f_o with γ at different r_c.

On the other hand, f/f_o intensifies noticeably from γ=0.10 to 0.15 and subsides tenuously until γ=0.40 for both radiuses. Due to these facts, η augments radically from γ=0.10 to γ=0.15 and the performance intrinsically weakens until γ=0.40, as shown in Figure 4.56.

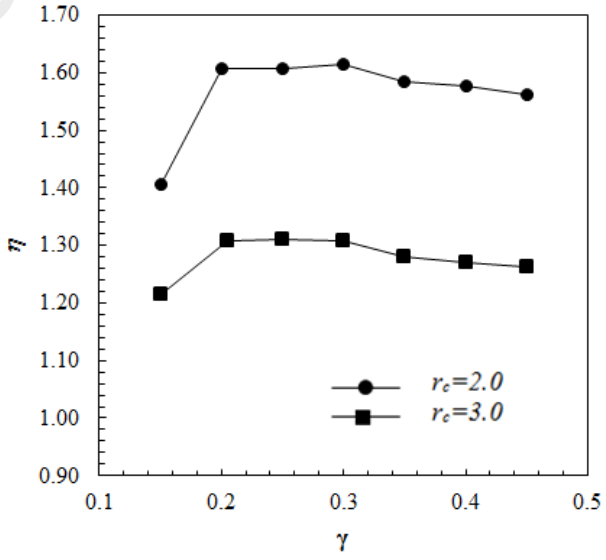

Figure 4.56: Variation of η with γ at different r_c.

Figure 4.57(a) shows that the streamlines at γ=0.25, r_c=2.0 are occupied with larger vortices that result in a higher thermal performance compared to γ=0.10, r_c=3.0. Pressure distribution in γ=0.25 (blueish) is much higher compared to γ=0.10 (greenish) which implies that the pressure loss in the former is much lesser than the latter as shown in Figure 4.57(b).

Isotherms in Figure 4.57(c) illustrates evenly distributed temperatures in γ=0.25 that proposes a higher heat transfer rate. It can be seen that MECS with γ=0.10, r_c=3.0 that the fluid in the cavity remains hotter (yellow-greenish) and does not mix with the colder mainstream fluid. Thus, it can be inferred that altering the cavity shape too narrow will result in weak fluid mixing and heat transfer.

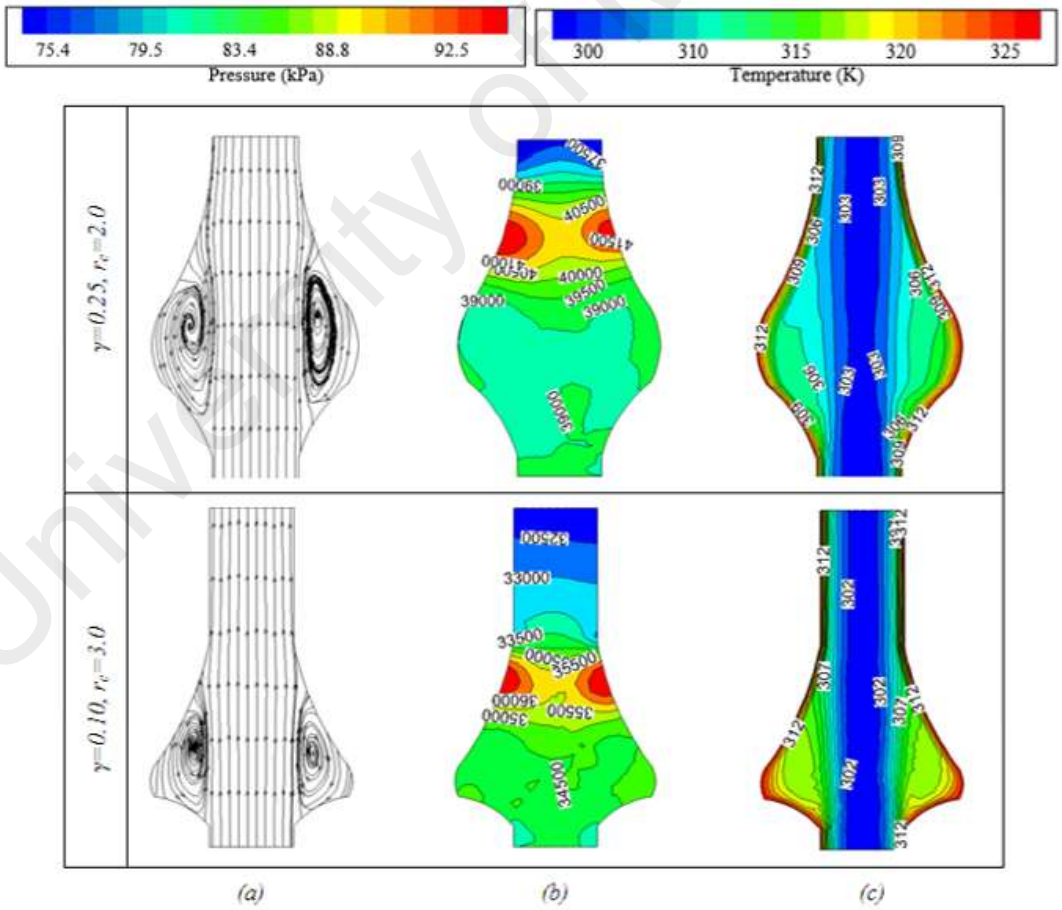

Figure 4.57: (a) Streamlines, (b) pressure contour plot (Pa), and (b) isotherms (K) at γ=0.25, r_c =2.0 and γ=0.10, r_c=3.0.

Cavities require adequate space, especially at the entry region for the mainstream fluid to divert and circulate. This is essential to achieve a virtuous heat transfer augmentation. Enlargement in the size of vortices also improves the convection heat transfer of the working fluid. It has to also be highlighted that the escalation of the entrance length beyond its optimum stature will leave the shape of the vortices distorted. This makes the fluid circulation indistinct even though the size of the vortices is large. Due to this reason, the fluid mixing and heat transfer performance is waned.

4.6.5 MCHS Performance at Various δ and r_d

The flow and heat transfer performance of the MECS are studied with alterations of δ and *rd* while keeping the flow condition at *Case A* and other parameters at *n*=17, α=3.5, β=2, γ=0.25, *R*=2 and r_c=2. As presented in Figure 4.58, Nu/Nu_o augments noticeably from δ=0.25 to 0.50 in both, r_d=1.0 and 1.5.

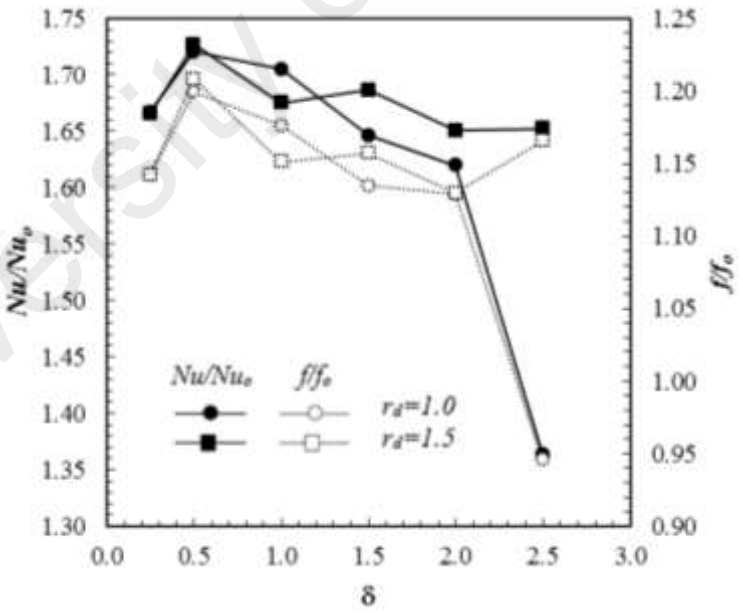

Figure 4.58: Variation of Nu/Nu_0 and f/f_o with δ at different r_d.

This is followed by a progressive decline from δ=0.50 to 2.5 Nu/Nu_0 with some oscillations except for r_d=1.0, with a sudden descent from δ=2.0 to 2.5. This trend is comparable with f/f_o except for r_d=1.5 where f/f_o intensifies from δ=2.0 to 2.5. Thus,

the inclination of η is also analogous with f/f_o and Nu/Nu_0 and the highest η of 1.62 is acquired at γ=0.5, as shown in Figure 4.59.

The streamlines in Figure 4.60(a) imply that the vortices are generated in both cavities at δ=0.5, r_d=1.5 and δ=2.5, r_d=1.0 where the former had the highest performance while latter had the lowest performance. Though the vortices are found in both cavities, these vortices that formed in δ=2.5, r_d=1.0 are distorted due to the bulbous shape of the cavity. As mentioned in the previous section, such fluid circulation does not enhance the fluid mixing significantly. Therefore, the overall enhancement is diminished.

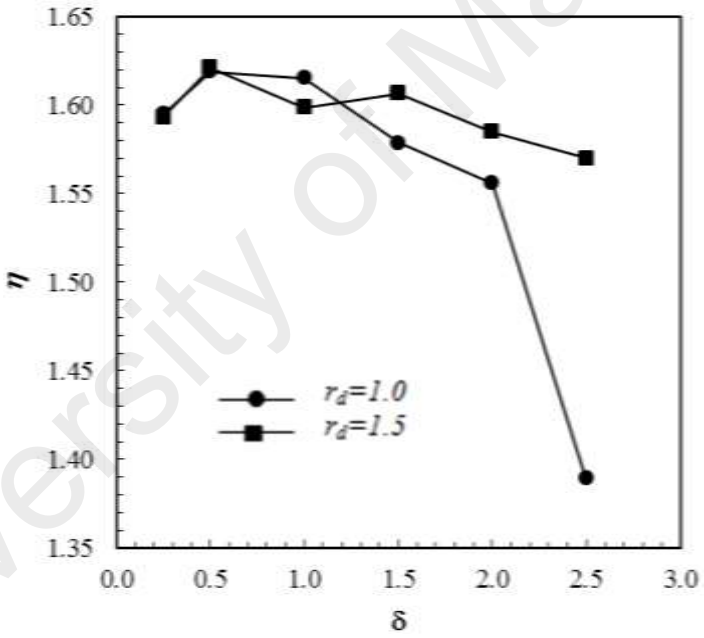

Figure 4.59: Variation of η with δ at Different r_d.

It is also found in Figure 4.60(b) that the pressure plot for δ=3.5 has a larger stagnation than δ=2.5. This has resulted in a higher result in a higher pressure drop. However, such large pressure loss does not affect the overall performance as the enormous thermal enhancement compensates this drawback.

Isotherms in Figure 4.60(c) show that most of colder fluid from the mainstream region is diverted into the cavity region in the MECS with δ=2.5. Whereas in δ=0.5, the

cold fluid remains in the mainstream region and a large portion of the cavity area is filled with hotter fluid with the temperature at a middle range (yellow-greenish). This suggests a very weak heat transfer occurring in that virtue, as discussed in the previous section.

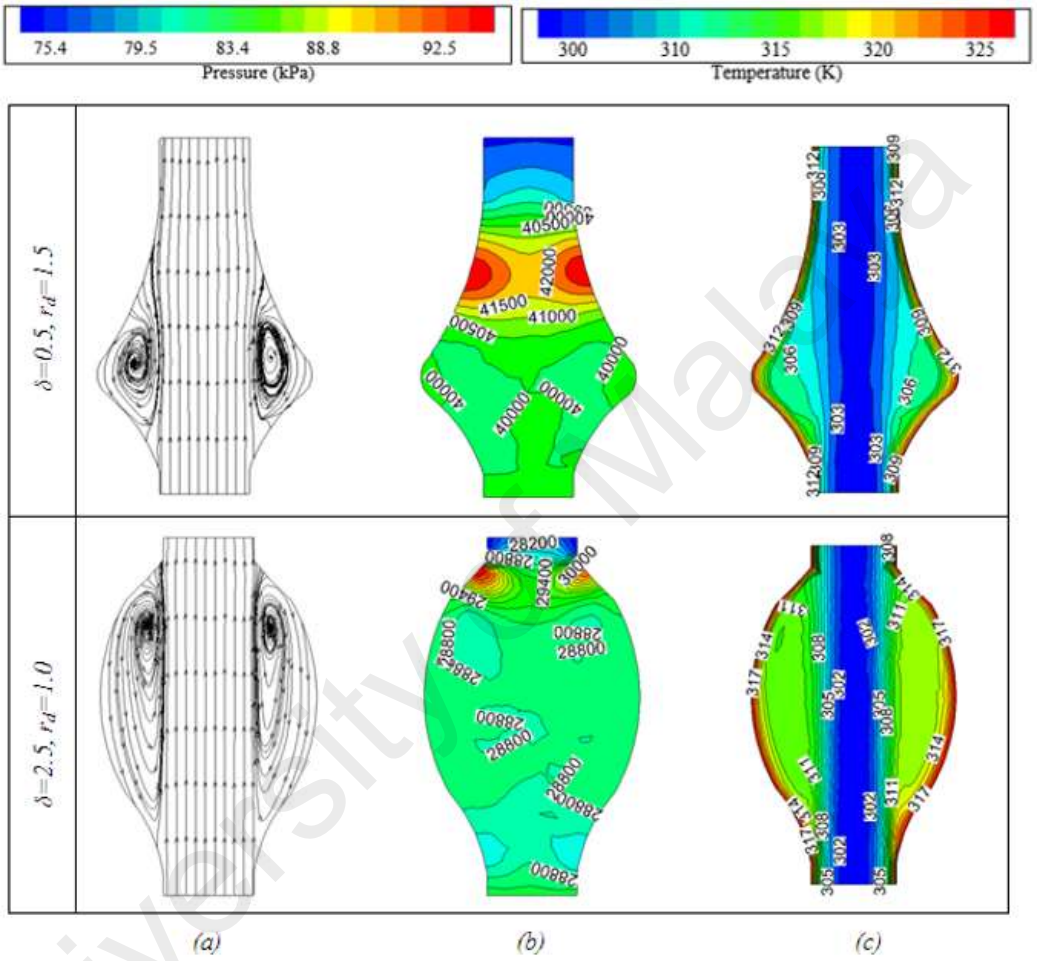

Figure 4.60: (a) Streamlines, (b) pressure contour plot (Pa), and (c) isotherms (K) at δ=0.5, r_d=1.5 and δ=2.5, r_d=1.0.

CHAPTER 5: CONCLUSION

5.1 Outline

Present work focuses on the thermal enhancement in a microchannel heat sink using the passive method. Different types of passive enhancements were studied such as the secondary passage, micromixer, periodic constriction, re-entrant cavities, and obstruction.

5.2 Conclusion

Firstly, the microchannel heat sink with a secondary passage which consisted of various geometrical configurations was studied. Thermal performance enhances with the increase of the width of the secondary passage, reduction in the length of the wall between the slated passage, and an increase in number of the secondary slanted passage. Contrary from the normal phenomenon, the thermal enhancement for the present study was accompanied by a reduced pressure drop. Therefore, the overall performance enhancement became higher than the thermal enhancement. This fact has multiplied the benefits of introducing the secondary passage in the microchannel heat sink.

Secondly, the effect of the micromixer (MTM) in the microchannel heat sink was analyzed. The aim of this study was to obtain the appropriate flow rate, micromixer angle, and its size in order to achieve the highest thermal enhancement possible without additional pressure drop. Similar to the previous case, improvement in heat transfer in this study also comes with a reduction in pressure drop. This is a double winning factor that would be very useful for researchers and heat transfer engineers in designing thermal solutions.

The third study consisted of an investigation of a forced convection of water in the microchannel with shield-shaped re-entrant obstruction at various flow velocities using a different substrate material. The results showed that introduction of the re-entrant

obstruction can enhance the overall heat transfer and effectiveness of the MCHS. The MCHS with re-entrant obstruction built in silicon substrate outperformed the aluminum MCHS. This is because the conduction heat transfer is dominant in a simple MCHS, but convection heat transfer enhances significantly in an interrupted MCHS and becomes the main heat transfer medium.

The effect of periodic elliptical-shaped constriction was studied at various flow conditions. Introduction of the periodical constrictions in the microchannel heat sink results in a significant thermal enhancement, together with a large pressure drop. Furthermore, the Reynolds number also influences its flow and the thermal characteristic significantly. It is also verified from the pressure contour plot that the jet and throttling effect that occurred in the constriction region resulted in the great heat transfer enhancement together with a drastic pressure drop.

Finally, the numerical simulation was conducted on the MCHS with an elliptical cavity to study its conjugate heat transfer performance. The effect of the number of cavities, flow direction and the geometrical parameters of the cavity on the flow and thermal field was studied. Seemingly, the variation of the geometrical parameter of cavity has more influence on the enhancement of the performance compared to the numbers of the cavities. It was also found that intensity of the vortex in the cavity is more assertive compared to its size.

From all the five enhancement methods studied, the MCHS with the secondary channel and the micro mixer appears to have the highest potential due to the significant enhancement in thermal performance, combined with a reduced pressure drop compared to the simple MCHS. On the other hand, the MCHS with cavity showed a great improvement in thermal performance with a negligible pressure drop. These facts

suggest that these three methods are highly feasible for implementation in practical applications.

5.3 Future Work

The findings of the present work can be directly implemented in on-chip cooling application. For instance, this technology can be also implemented for cooling of server rack in the data center. For initial stage, a hybrid air/liquid cooling can be implemented where the electronic components that has the highest heat dissipation will be liquid cooled.

While optimizing the air flow path within servers and the server rack in both natural and forced convection, the water side will be improved using optimization suggested in the present work i.e. optimizing the shape, orientation and layout of passive heat sinks. The liquid flow management at the rack level could significantly reduce the energy cost incurred from the air side due to the fan and duct sizing, resulting in guidelines to achieve an efficient air-water thermal management in data centers.

REFERENCES

Abouali, O., & Baghernezhad, N. (2010). Numerical Investigation of Heat Transfer Enhancement in a Microchannel With Grooved Surfaces. *Journal of Heat Transfer, 132*(4), 041005-041005. doi: 10.1115/1.4000862

Adams, T. M., Abdel-Khalik, S. I., Jeter, S. M., & Qureshi, Z. H. (1998). An experimental investigation of single-phase forced convection in microchannels. *International Journal of Heat and Mass Transfer, 41*(6–7), 851-857. doi: http://dx.doi.org/10.1016/S0017-9310(97)00180-4

Agarwal, A., Bandhauer, T. M., & Garimella, S. (2010). Measurement and modeling of condensation heat transfer in non-circular microchannels. *International Journal of Refrigeration, 33*(6), 1169-1179.

Alam, A., & Kim, K.-Y. (2012). Analysis of mixing in a curved microchannel with rectangular grooves. *Chemical Engineering Journal, 181*, 708-716.

Ansari, D., Husain, A., & Kwang-Yong, K. (2010). Multiobjective Optimization of a Grooved Micro-Channel Heat Sink. *Components and Packaging Technologies, IEEE Transactions on, 33*(4), 767-776. doi: 10.1109/tcapt.2010.2070874

Ansari, M. A., & Kim, K.-Y. (2007). Shape optimization of a micromixer with staggered herringbone groove. *Chemical Engineering Science, 62*(23), 6687-6695.

Balasubramanian, K., Lee, P., Jin, L., Chou, S., Teo, C., & Gao, S. (2011). Experimental investigations of flow boiling heat transfer and pressure drop in straight and expanding microchannels–A comparative study. *International Journal of Thermal Sciences, 50*(12), 2413-2421.

Balasubramanian, P., & Kandlikar, S. G. (2005). Experimental study of flow patterns, pressure drop, and flow instabilities in parallel rectangular minichannels. *Heat Transfer Engineering, 26*(3), 20-27.

Barba, A., Musi, B., & Spiga, M. (2006). Performance of a polymeric heat sink with circular microchannels. *Applied Thermal Engineering, 26*(8–9), 787-794. doi: http://dx.doi.org/10.1016/j.applthermaleng.2005.10.015

Chai, L., Xia, G., Wang, L., Zhou, M., & Cui, Z. (2013). Heat transfer enhancement in microchannel heat sinks with periodic expansion–constriction cross-sections. *International Journal of Heat and Mass Transfer, 62*(0), 741-751. doi: http://dx.doi.org/10.1016/j.ijheatmasstransfer.2013.03.045

Chai, L., Xia, G., Zhou, M., & Li, J. (2011). Numerical simulation of fluid flow and heat transfer in a microchannel heat sink with offset fan-shaped reentrant cavities in sidewall. *International Communications in Heat and Mass Transfer, 38*(5), 577-584. doi: http://dx.doi.org/10.1016/j.icheatmasstransfer.2010.12.037

Chai, L., Xia, G., Zhou, M., Li, J., & Qi, J. (2013). Optimum thermal design of interrupted microchannel heat sink with rectangular ribs in the transverse

microchambers. *Applied Thermal Engineering, 51*(1–2), 880-889. doi: http://dx.doi.org/10.1016/j.applthermaleng.2012.10.037

Chen, Y., Zhang, C., Shi, M., & Wu, J. (2009). Three-dimensional numerical simulation of heat and fluid flow in noncircular microchannel heat sinks. *International Communications in Heat and Mass Transfer, 36*(9), 917-920. doi: 10.1016/j.icheatmasstransfer.2009.06.004

Cheng, Y. J. (2007). Numerical simulation of stacked microchannel heat sink with mixing-enhanced passive structure. *International Communications in Heat and Mass Transfer, 34*(3), 295-303. doi: http://dx.doi.org/10.1016/j.icheatmasstransfer.2006.12.007

Chu, J.-C., Teng, J.-T., & Greif, R. (2010). Experimental and numerical study on the flow characteristics in curved rectangular microchannels. *Applied Thermal Engineering, 30*(13), 1558-1566.

Colgan, E. G., Furman, B., Gaynes, A., Graham, W., LaBianca, N., Magerlein, J. H., . . . Zitz, J. (2005, 15-17 March 2005). *A practical implementation of silicon microchannel coolers for high power chips.* Paper presented at the Semiconductor Thermal Measurement and Management Symposium, 2005 IEEE Twenty First Annual IEEE.

Desrues, T., Marty, P., & Fourmigué, J. F. (2012). Numerical prediction of heat transfer and pressure drop in three-dimensional channels with alternated opposed ribs. *Applied Thermal Engineering, 45–46*(0), 52-63. doi: http://dx.doi.org/10.1016/j.applthermaleng.2012.03.013

Dharaiya, V. V., & Kandlikar, S. G. (2013). A numerical study on the effects of 2d structured sinusoidal elements on fluid flow and heat transfer at microscale. *International Journal of Heat and Mass Transfer, 57*(1), 190-201. doi: http://dx.doi.org/10.1016/j.ijheatmasstransfer.2012.10.004

Dogan, M., & Sivrioglu, M. (2009). Experimental investigation of mixed convection heat transfer from longitudinal fins in a horizontal rectangular channel: In natural convection dominated flow regimes. *Energy Conversion and Management, 50*(10), 2513-2521. doi: http://dx.doi.org/10.1016/j.enconman.2009.05.027

Fan, Y., Lee, P. S., & Chua, B. W. (2014). Investigation on the influence of edge effect on flow and temperature uniformities in cylindrical oblique-finned minichannel array. *International Journal of Heat and Mass Transfer, 70*, 651-663.

Fan, Y., Lee, P. S., Jin, L.-W., & Chua, B. W. (2013). A simulation and experimental study of fluid flow and heat transfer on cylindrical oblique-finned heat sink. *International Journal of Heat and Mass Transfer, 61*(0), 62-72. doi: http://dx.doi.org/10.1016/j.ijheatmasstransfer.2013.01.075

Fan, Y., Lee, P. S., Jin, L.-W., & Chua, B. W. (2014). Experimental investigation on heat transfer and pressure drop of a novel cylindrical oblique fin heat sink. *International Journal of Thermal Sciences, 76*, 1-10.

Fan, Y., Lee, P. S., Jin, L., & Chua, B. W. (2011). *Numerical simulations of forced convection in novel cylindrical oblique-finned heat sink.* Paper presented at the Electronics Packaging Technology Conference (EPTC), 2011 IEEE 13th.

Fedorov, A. G., & Viskanta, R. (2000). Three-dimensional conjugate heat transfer in the microchannel heat sink for electronic packaging. *International Journal of Heat and Mass Transfer, 43*(3), 399-415.

Foong, A. J. L., Ramesh, N., & Chandratilleke, T. T. (2009). Laminar convective heat transfer in a microchannel with internal longitudinal fins. *International Journal of Thermal Sciences, 48*(10), 1908-1913. doi: http://dx.doi.org/10.1016/j.ijthermalsci.2009.02.015

Gamrat, G., Favre-Marinet, M., & Asendrych, D. (2005). Conduction and entrance effects on laminar liquid flow and heat transfer in rectangular microchannels. *International Journal of Heat and Mass Transfer, 48*(14), 2943-2954. doi: http://dx.doi.org/10.1016/j.ijheatmasstransfer.2004.10.006

Garimella, S. V. (2005). *Transport in mesoscale cooling systems.* Paper presented at the ASME 2005 Fluids Engineering Division Summer Meeting.

Garimella, S. V. (2006). Advances in mesoscale thermal management technologies for microelectronics. *Microelectronics Journal, 37*(11), 1165-1185.

Garimella, S. V., & Singhal, V. (2004). Single-phase flow and heat transport and pumping considerations in microchannel heat sinks. *Heat Transfer Engineering, 25*(1), 15-25.

Greiner, M. (1991). An experimental investigation of resonant heat transfer enhancement in grooved channels. *International Journal of Heat and Mass Transfer, 34*(6), 1383-1391.

Greiner, M., Faulkner, R., Van, V., Tufo, H., & Fischer, P. (2000). Simulations of three-dimensional flow and augmented heat transfer in a symmetrically grooved channel. *Journal of Heat Transfer, 122*(4), 653-660.

Hadjiconstantinou, N. G., & Simek, O. (2002). Constant-wall-temperature Nusselt number in micro and nano-channels. *Journal of Heat Transfer, 124*(2), 356-364.

Herman, C., & Kang, E. (2002). Heat transfer enhancement in a grooved channel with curved vanes. *International Journal of Heat and Mass Transfer, 45*(18), 3741-3757. doi: http://dx.doi.org/10.1016/S0017-9310(02)00092-3

Hong, F., & Cheng, P. (2009). Three dimensional numerical analyses and optimization of offset strip-fin microchannel heat sinks. *International Communications in Heat and Mass Transfer, 36*(7), 651-656. doi: http://dx.doi.org/10.1016/j.icheatmasstransfer.2009.02.015

Hung, T.-C., Yan, W.-M., Wang, X.-D., & Chang, C.-Y. (2012). Heat transfer enhancement in microchannel heat sinks using nanofluids. *International Journal of Heat and Mass Transfer, 55*(9), 2559-2570.

Hung, Y.-H., Teng, T.-P., Teng, T.-C., & Chen, J.-H. (2012). Assessment of heat dissipation performance for nanofluid. *Applied Thermal Engineering, 32*, 132-140.

Hwang, H.-J., & Simon Song, S. (2008). The effects of grooves on the flow rate in a microchannel. *Biochip J, 2*, 123-126.

Jang, S. P., & Choi, S. U. (2006). Cooling performance of a microchannel heat sink with nanofluids. *Applied Thermal Engineering, 26*(17), 2457-2463.

Judy, J., Maynes, D., & Webb, B. (2002). Characterization of frictional pressure drop for liquid flows through microchannels. *International Journal of Heat and Mass Transfer, 45*(17), 3477-3489.

Kalteh, M., Abbassi, A., Saffar-Avval, M., & Harting, J. (2011). Eulerian–Eulerian two-phase numerical simulation of nanofluid laminar forced convection in a microchannel. *International Journal of Heat and Fluid Flow, 32*(1), 107-116.

Kandlikar, S. G. (2002). Fundamental issues related to flow boiling in minichannels and microchannels. *Experimental Thermal and Fluid Science, 26*(2), 389-407.

Kandlikar, S. G. (2006). Chapter 3 - Single-phase liquid flow in minichannels and microchannels. In S. G. Kandlikar, S. Garimella, D. Li, S. Colin, & M. R. King (Eds.), *Heat Transfer and Fluid Flow in Minichannels and Microchannels* (pp. 87-136). Oxford: Elsevier Science Ltd.

Kandlikar, S. G., Steinke, M. E., & Balasubramanian, P. (2002). *Single-phase flow characteristics and effect of dissolved gases on heat transfer near saturation conditions in microchannels*. Paper presented at the ASME 2002 International Mechanical Engineering Congress and Exposition.

Khan, A. A., Kim, S.-M., & Kim, K.-Y. (2015). Multi-objective optimization of an inverse trapezoidal shaped microchannel. *Heat Transfer Engineering*(just-accepted), 00-00.

Korichi, A., & Oufer, L. (2007). Heat transfer enhancement in oscillatory flow in channel with periodically upper and lower walls mounted obstacles. *International Journal of Heat and Fluid Flow, 28*(5), 1003-1012. doi: http://dx.doi.org/10.1016/j.ijheatfluidflow.2006.11.002

Kumar, A., Saini, R. P., & Saini, J. S. (2012). Experimental investigation on heat transfer and fluid flow characteristics of air flow in a rectangular duct with Multi v-shaped rib with gap roughness on the heated plate. *Solar Energy, 86*(6), 1733-1749. doi: http://dx.doi.org/10.1016/j.solener.2012.03.014

Kuppusamy, N. R., Mohammed, H. A., & Lim, C. W. (2013). Numerical investigation of trapezoidal grooved microchannel heat sink using nanofluids. *Thermochimica Acta, 573*(0), 39-56. doi: http://dx.doi.org/10.1016/j.tca.2013.09.011

Kuppusamy, N. R., Mohammed, H. A., & Lim, C. W. (2014). Thermal and hydraulic characteristics of nanofluid in a triangular grooved microchannel heat sink

(TGMCHS). *Applied Mathematics and Computation, 246*(0), 168-183. doi: http://dx.doi.org/10.1016/j.amc.2014.07.087

Lasance, C. J., & Simons, R. E. (2005). Advances in high-performance cooling for electronics. *Electronics Cooling, 11*(4).

Lee, J., & Mudawar, I. (2007). Assessment of the effectiveness of nanofluids for single-phase and two-phase heat transfer in micro-channels. *International Journal of Heat and Mass Transfer, 50*(3), 452-463.

Lee, P.-S., & Teo, C.-J. (2008). *Heat transfer enhancement in microchannels incorporating slanted grooves.* Paper presented at the ASME 2008 First International Conference on Micro/Nanoscale Heat Transfer.

Lee, Y.-J., Lee, P.-S., & Chou, S.-K. (2009). *Enhanced microchannel heat sinks using oblique fins.* Paper presented at the ASME 2009 InterPACK Conference collocated with the ASME 2009 Summer Heat Transfer Conference and the ASME 2009 3rd International Conference on Energy Sustainability.

Lee, Y. J., Lee, P. S., & Chou, S. K. (2012). Enhanced Thermal Transport in Microchannel Using Oblique Fins. *Journal of Heat Transfer, 134*(10), 101901-101901. doi: 10.1115/1.4006843

Leng, C., Wang, X.-D., Wang, T.-H., & Yan, W.-M. (2015a). Multi-parameter optimization of flow and heat transfer for a novel double-layered microchannel heat sink. *International Journal of Heat and Mass Transfer, 84*, 359-369.

Leng, C., Wang, X.-D., Wang, T.-H., & Yan, W.-M. (2015b). Optimization of thermal resistance and bottom wall temperature uniformity for double-layered microchannel heat sink. *Energy Conversion and Management, 93*, 141-150.

Li, B., Feng, B., He, Y.-L., & Tao, W.-Q. (2006). Experimental study on friction factor and numerical simulation on flow and heat transfer in an alternating elliptical axis tube. *Applied Thermal Engineering, 26*(17–18), 2336-2344. doi: http://dx.doi.org/10.1016/j.applthermaleng.2006.03.001

Liu, D., & Garimella, S. V. (2005). Analysis and optimization of the thermal performance of microchannel heat sinks. *International Journal of Numerical Methods for Heat & Fluid Flow, 15*(1), 7-26.

Liu, J.-T., Peng, X.-F., & Yan, W.-M. (2007). Numerical study of fluid flow and heat transfer in microchannel cooling passages. *International Journal of Heat and Mass Transfer, 50*(9–10), 1855-1864. doi: http://dx.doi.org/10.1016/j.ijheatmasstransfer.2006.10.004

Liu, R. H., Stremler, M. A., Sharp, K. V., Olsen, M. G., Santiago, J. G., Adrian, R. J., . . . Beebe, D. J. (2000). Passive mixing in a three-dimensional serpentine microchannel. *Microelectromechanical Systems, Journal of, 9*(2), 190-197.

Liu, Y., Cui, J., Jiang, Y. X., & Li, W. Z. (2011). A numerical study on heat transfer performance of microchannels with different surface microstructures. *Applied*

Thermal Engineering, 31(5), 921-931. doi: http://dx.doi.org/10.1016/j.applthermaleng.2010.11.015

Ma, L.-D., Li, Z.-Y., & Tao, W.-Q. (2007). Experimental verification of the field synergy principle. *International Communications in Heat and Mass Transfer, 34*(3), 269-276. doi: http://dx.doi.org/10.1016/j.icheatmasstransfer.2006.11.008

McGarry, M., Campo, A., & Hitt, D. L. (2004). NUMERICAL SIMULATIONS OF HEAT AND FLUID FLOW IN GROOVED CHANNELS WITH CURVED VANES. *Numerical Heat Transfer, Part A: Applications, 46*(1), 41-54. doi: 10.1080/10407780490457653

McHale, J. P., & Garimella, S. V. (2010). Heat transfer in trapezoidal microchannels of various aspect ratios. *International Journal of Heat and Mass Transfer, 53*(1–3), 365-375. doi: http://dx.doi.org/10.1016/j.ijheatmasstransfer.2009.09.020

Mesalhy, O. M., Abdel Aziz, S. S., & El-Sayed, M. M. (2010). Flow and heat transfer over shallow cavities. *International Journal of Thermal Sciences, 49*(3), 514-521. doi: http://dx.doi.org/10.1016/j.ijthermalsci.2009.09.007

Mohiuddin Mala, G., & Li, D. (1999). Flow characteristics of water in microtubes. *International Journal of Heat and Fluid Flow, 20*(2), 142-148. doi: http://dx.doi.org/10.1016/S0142-727X(98)10043-7

Moore, G. (1998). Cramming More Components Onto Integrated Circuits. *PROCEEDINGS OF THE IEEE, 86*(1), 82-85.

Morini, G. L. (2004). Single-phase convective heat transfer in microchannels: a review of experimental results. *International Journal of Thermal Sciences, 43*(7), 631-651. doi: http://dx.doi.org/10.1016/j.ijthermalsci.2004.01.003

Muzychka, Y. S. (2007). Constructal multi-scale design of compact micro-tube heat sinks and heat exchangers. *International Journal of Thermal Sciences, 46*(3), 245-252. doi: http://dx.doi.org/10.1016/j.ijthermalsci.2006.05.002

Nonino, C., Savino, S., Del Giudice, S., & Mansutti, L. (2009). Conjugate forced convection and heat conduction in circular microchannels. *International Journal of Heat and Fluid Flow, 30*(5), 823-830. doi: http://dx.doi.org/10.1016/j.ijheatfluidflow.2009.03.009

Owhaib, W., & Palm, B. (2004). Experimental investigation of single-phase convective heat transfer in circular microchannels. *Experimental Thermal and Fluid Science, 28*(2), 105-110.

Peng, X. F., & Peterson, G. P. (1996). Convective heat transfer and flow friction for water flow in microchannel structures. *International Journal of Heat and Mass Transfer, 39*(12), 2599-2608. doi: http://dx.doi.org/10.1016/0017-9310(95)00327-4

Phillips, R. J. (1988). Microchannel heat sinks. *Lincoln Laboratory Journal, 1*, 31-48.

Phillips, R. J. (1990). Microchannel heat sinks. *Advances in thermal modeling of electronic components and systems, 2*, 109-184.

Promvonge, P., Sripattanapipat, S., & Kwankaomeng, S. (2010). Laminar periodic flow and heat transfer in square channel with 45° inline baffles on two opposite walls. *International Journal of Thermal Sciences, 49*(6), 963-975. doi: http://dx.doi.org/10.1016/j.ijthermalsci.2010.01.005

Promvonge, P., & Thianpong, C. (2008). Thermal performance assessment of turbulent channel flows over different shaped ribs. *International Communications in Heat and Mass Transfer, 35*(10), 1327-1334. doi: http://dx.doi.org/10.1016/j.icheatmasstransfer.2008.07.016

Qu, W., Mala, G. M., & Li, D. (2000). Heat transfer for water flow in trapezoidal silicon microchannels. *International Journal of Heat and Mass Transfer, 43*(21), 3925-3936. doi: http://dx.doi.org/10.1016/S0017-9310(00)00045-4

Qu, W., & Mudawar, I. (2002a). Analysis of three-dimensional heat transfer in micro-channel heat sinks. *International Journal of Heat and Mass Transfer, 45*(19), 3973-3985.

Qu, W., & Mudawar, I. (2002b). Experimental and numerical study of pressure drop and heat transfer in a single-phase micro-channel heat sink. *International Journal of Heat and Mass Transfer, 45*(12), 2549-2565. doi: http://dx.doi.org/10.1016/S0017-9310(01)00337-4

Rahman, M. M., & Gui, F. (1993). *Experimental measurements of fluid flow and heat transfer in microchannel cooling passages in a chip substrate.* Paper presented at the The ASME International Electronics Packaging Conference, Binghamton, NY, USA, 09/29-10/02/93.

Rosa, P., Karayiannis, T. G., & Collins, M. W. (2009). Single-phase heat transfer in microchannels: The importance of scaling effects. *Applied Thermal Engineering, 29*(17–18), 3447-3468. doi: http://dx.doi.org/10.1016/j.applthermaleng.2009.05.015

Ryu, J., Choi, D., & Kim, S. (2002). Numerical optimization of the thermal performance of a microchannel heat sink. *International Journal of Heat and Mass Transfer, 45*(13), 2823-2827.

San, J.-Y., & Huang, W.-C. (2006). Heat transfer enhancement of transverse ribs in circular tubes with consideration of entrance effect. *International Journal of Heat and Mass Transfer, 49*(17–18), 2965-2971. doi: http://dx.doi.org/10.1016/j.ijheatmasstransfer.2006.01.046

Sobhan, C. B., & Garimella, S. V. (2001). A COMPARATIVE ANALYSIS OF STUDIES ON HEAT TRANSFER AND FLUID FLOW IN MICROCHANNELS. *Microscale Thermophysical Engineering, 5*(4), 293-311. doi: 10.1080/10893950152646759

Sohel, M., Saidur, R., Sabri, M. F. M., Kamalisarvestani, M., Elias, M., & Ijam, A. (2013). Investigating the heat transfer performance and thermophysical

properties of nanofluids in a circular micro-channel. *International Communications in Heat and Mass Transfer, 42*, 75-81.

Steinke, M. E., & Kandlikar, S. G. (2004). *Single-phase heat transfer enhancement techniques in microchannel and minichannel flows.* Paper presented at the ASME 2004 2nd International Conference on Microchannels and Minichannels.

Steinke, M. E., & Kandlikar, S. G. (2005). *Single-phase liquid friction factors in microchannels.* Paper presented at the ASME 3rd International Conference on Microchannels and Minichannels.

Steinke, M. E., & Kandlikar, S. G. (2006). *Single-phase liquid heat transfer in plain and enhanced microchannels.* Paper presented at the ASME 4th International Conference on Nanochannels, Microchannels, and Minichannels.

Suh, J.-S., Greif, R., & Grigoropoulos, C. P. (2001). Friction in micro-channel flows of a liquid and vapor in trapezoidal and sinusoidal grooves. *International Journal of Heat and Mass Transfer, 44*(16), 3103-3109. doi: http://dx.doi.org/10.1016/S0017-9310(00)00331-8

Sui, Y., Teo, C. J., Lee, P. S., Chew, Y. T., & Shu, C. (2010). Fluid flow and heat transfer in wavy microchannels. *International Journal of Heat and Mass Transfer, 53*(13–14), 2760-2772. doi: http://dx.doi.org/10.1016/j.ijheatmasstransfer.2010.02.022

Tao, W. Q., He, Y. L., Wang, Q. W., Qu, Z. G., & Song, F. Q. (2002). A unified analysis on enhancing single phase convective heat transfer with field synergy principle. *International Journal of Heat and Mass Transfer, 45*(24), 4871-4879. doi: http://dx.doi.org/10.1016/S0017-9310(02)00173-4

Torresola, J., Chiu, C.-P., Chrysler, G., Grannes, D., Mahajan, R., Prasher, R., & Watwe, A. (2005). Density factor approach to representing impact of die power maps on thermal management. *IEEE Transactions on advanced packaging, 28*(4), 659-664.

Tuckerman, D. B., & Pease, R. (1981). High-performance heat sinking for VLSI. *Electron Device Letters, IEEE, 2*(5), 126-129.

Weisberg, A., Bau, H. H., & Zemel, J. (1992). Analysis of microchannels for integrated cooling. *International Journal of Heat and Mass Transfer, 35*(10), 2465-2474.

Wing Yin, L., Man, W., & Zohar, Y. (2002). Pressure loss in constriction microchannels. *Microelectromechanical Systems, Journal of, 11*(3), 236-244. doi: 10.1109/JMEMS.2002.1007402

Wu, H., & Cheng, P. (2003). An experimental study of convective heat transfer in silicon microchannels with different surface conditions. *International Journal of Heat and Mass Transfer, 46*(14), 2547-2556.

Xi, Y., Yu, J., Xie, Y., & Gao, H. (2010). Single-phase flow and heat transfer in swirl microchannels. *Experimental Thermal and Fluid Science, 34*(8), 1309-1315.

Xia, G., Chai, L., Wang, H., Zhou, M., & Cui, Z. (2011). Optimum thermal design of microchannel heat sink with triangular reentrant cavities. *Applied Thermal Engineering, 31*(6–7), 1208-1219. doi: http://dx.doi.org/10.1016/j.applthermaleng.2010.12.022

Xia, G., Chai, L., Zhou, M., & Wang, H. (2011). Effects of structural parameters on fluid flow and heat transfer in a microchannel with aligned fan-shaped reentrant cavities. *International Journal of Thermal Sciences, 50*(3), 411-419. doi: http://dx.doi.org/10.1016/j.ijthermalsci.2010.08.009

Xia, G., Zhai, Y., & Cui, Z. (2013). Numerical investigation of thermal enhancement in a micro heat sink with fan-shaped reentrant cavities and internal ribs. *Applied Thermal Engineering, 58*(1–2), 52-60. doi: http://dx.doi.org/10.1016/j.applthermaleng.2013.04.005

Xu, B., Ooti, K., Wong, N., & Choi, W. (2000). Experimental investigation of flow friction for liquid flow in microchannels. *International Communications in Heat and Mass Transfer, 27*(8), 1165-1176.

Xu, J., Song, Y., Zhang, W., Zhang, H., & Gan, Y. (2008). Numerical simulations of interrupted and conventional microchannel heat sinks. *International Journal of Heat and Mass Transfer, 51*(25–26), 5906-5917. doi: http://dx.doi.org/10.1016/j.ijheatmasstransfer.2008.05.003

Xu, J. L., Gan, Y. H., Zhang, D. C., & Li, X. H. (2005). Microscale heat transfer enhancement using thermal boundary layer redeveloping concept. *International Journal of Heat and Mass Transfer, 48*(9), 1662-1674. doi: http://dx.doi.org/10.1016/j.ijheatmasstransfer.2004.12.008

Yang, C.-Y., & Lin, T.-Y. (2007). Heat transfer characteristics of water flow in microtubes. *Experimental Thermal and Fluid Science, 32*(2), 432-439.

Yong, H., Yong Jiun, L., & Xiaowu, Z. (2013). Trapezoidal Microchannel Heat Sink With Pressure-Driven and Electro-Osmotic Flows for Microelectronic Cooling. *Components, Packaging and Manufacturing Technology, IEEE Transactions on, 3*(11), 1851-1858. doi: 10.1109/TCPMT.2013.2272478

Yuki, K., & Suzuki, K. (2011). Applicability of Minichannel Cooling Fins to the Next Generation Power Devices as a Single-Phase-Flow Heat Transfer Device. *Transactions of The Japan Institute of Electronics Packaging, 4*(1), 52-60.

Zhai, Y. L., Xia, G. D., Liu, X. F., & Li, Y. F. (2014). Heat transfer in the microchannels with fan-shaped reentrant cavities and different ribs based on field synergy principle and entropy generation analysis. *International Journal of Heat and Mass Transfer, 68*(0), 224-233. doi: http://dx.doi.org/10.1016/j.ijheatmasstransfer.2013.08.086

LIST OF PUBLICATIONS AND PAPERS PRESENTED

N.R. Kuppusamy, R. Saidur, N.N.N. Ghazali , H.A. Mohammed, Numerical Study of Thermal Enhancement in Microchannel Heat Sink with Secondary Flow, International Journal of Heat and Mass Transfer 78 (2014) 216 223. doi: 10.1016/j.ijheatmasstransfer.2014.06.072 (ISI-Cited Publication)

Navin Raja Kuppusamy, N.N.N. Ghazali, R. Saidur, Optimum Design of Triangular Shaped Micromixer in Microchannel Heat Sink, International Journal of Heat and Mass Transfer, 2015. doi:10.1016/j.ijheatmasstransfer.2015.07.088 (ISI-Cited Publication)

N. R. Kuppusamy, N.N.N. Ghazali, R. Saidur, M.A. Omar Awang, H. A. Mohammed, "Heat Transfer Enhancement in a Microchannel Heat Sink with Trapezoidal Cavities on the Side Walls", Applied Mechanics and Materials, Vol. 819, pp. 127-131, 2016